Study on Subsurface Water Discharge and Sediment Yield Interaction, and the Mechanism of Subsurface Hydraulic Erosion at Head Water Slopes

by

TERAJIMA, Tomomi[1]

Summary : The basin ecosystems from the up- to down-stream areas link and interact not only within the same drainage networks but also into adjacent basins. Thus, from the numerous aspects on water management, disaster prevention, and fluvial or sea ecosystem conservation, subsurface water discharge and sediment production in head waters must threaten directly the human lives residing chiefly in down stream areas. In order to mitigate the catastrophic phenomena in residential areas, forests are widely expected to give full roles to the ability for the water and soil conservation. Human activities, however, are reducing the function of water and soil conservation in forests. Quantitative studies for the practical hydrogeomorphic processes occurring in forests, such as the interaction between water discharge and sediment movement, provide an adequate watershed management to increase the function of water and soil conservation of forests. In this study, subsurface water discharge and coarse- and fine-grained sediment production resulting from subsurface water flow were measured in two forested drainages to obtain the fundamental aspects relevant to watershed management. Quantitative results and interactions between subsurface water discharge and sediment production derived both the mechanisms of subsurface hydraulic erosion in non-uniform soils of slopes and the preventive measures for forest devastation with sediment movement, being represented by shallow land-slides and/or debris flows, under unsteady state hydraulic conditions in subsurface water flow regimes. The knowledge obtained in this study must supply the effective understandings for turbid water discharge from forested head waters. In addition, this study provides the information on valley development through coarse-grained sediment discharge at slopes, subsequently to the release of fine-grained sediment, and on the head slope evolution resulting from subsurface hydraulic erosion.

Introduction

Recent artificial alterations of land surfaces around headwaters, such as the tree felling, resort construction, and residential developments, often bring environmental calamity to down stream areas ; for example, through floods or marsh destruction by sediment deposition.　Based on perspectives in the recent environment conservation, drastic environmental changes in basins require the resolution of numerous social issues regarding people's lives and productive environment, and the conservation of natural ecosystems.

Water and sediment discharge in headwaters commonly and immediately affects down stream areas where human activities occur.　Thus, significant themes such as "Natural disaster and forest devastation caused by landslide and debris flow", "Devastation of basin ecosystems resulting from turbid water discharges", and "Water quality and amount for human use" have to be considered in the estimation of the water and soil conservation mechanisms of forests surrounding headwaters.　The author, however, believes that a sufficient number of reasonable suggestions have not been made resolve these issues from the aspects based on the water and soil conservation.　This is because many researchers have conducted individual studies to clarify the water and soil conservation mechanisms of forests, but, they have seldom focused on the interaction between the water cycle and geomorphic processes.　Thus, an understanding of the hydrogeomorphic mechanism in headwaters with interactive aspects is essential for obtaining valuable information related to the water and soil conservation mechanisms of forests.

In humid and temperate regions, where forests cover most slope surfaces, rainfall infiltrates mostly into soils and overland flow is rarely produced except in the case of artificially altered land surfaces (DUNNE and BLACK, 1970).　Thus, most rainfall supplied to slopes flows out to streams via subsurface routes in slopes.　Ultimately, subsurface water flow controls mainly the stream water quality and provides topographic changes through shallow landslides, debris flows, slope depressions, and initiations of rills and gullies (e.g., TANAKA, 1956 ; PIERSON, 1983 ; SIDLE and SWANSTON, 1986 ; SWANSTON et al., 1989 ; HIGGINS and COATES, 1990).　That is, subsurface water discharge affects significantly the geomorphic processes in forested head slopes.　Accordingly, a consideration for the relationship between subsurface water movement and sediment production caused by subsurface water flow is indispensable to quantify the function of the water and soil conservation of forests.　The importance of subsurface water discharge on topographic changes at forested head slopes has long been indicated, but only a few studies have focused quantitatively on subsurface hydraulic erosion on slopes.

In this study, the author observed subsurface water flows and sediment discharges in two

drainages composed of the similar soil structure, and tried to understand quantitatively the process of subsurface hydraulic erosion, which is the main geomorphic process in humid and temperate region.

This article was supplemented and modified from a doctoral dissertation of Hokkaido University, whose title is : "Study on characteristics of subsurface water flow and sediment production on head slopes and on the mechanism of subsurface hydraulic erosion".

1. Methodology

1. 1 Water and sediment movement in slopes

Figure 1 shows the relationship between the water movement and sediment discharge in headwaters. Topographic changes caused by subsurface water flow often occur in valley heads, so that many researchers have long focused on headwaters as one of the most suitable places to understand the implication between water and sediment discharge (e.g., TSUKAMOTO, 1973 ; SHINDO, 1983, 1984 ; DETRICH and DUNNE, 1993). This sediment movement is classified into either "Direct changes in slope surfaces resulting from shallow landslides and rill-gully erosion" or "Indirect topographic changes resulting from seepage erosion caused by subsurface water discharge". These have to be considered sufficiently from the geomorphological aspects related to valley development by the agent of water flow and sediment production because of their influence on the expansion of stream networks in mountainous areas. Simultaneously, sediment movement in head waters must be considered in terms of disaster prevention, forest devastation, turbid water discharge, and the damage to human lives and property.

Permeability of soils is usually higher than rainfall intensity in humid and temperate forested slopes, and most rain infiltrates into soils (TSUKAMOTO and OTA,1985). Hortonian overland flow is seldom observed in forested slopes except on volcanic slopes where impermeable deposits occur. This suggests that forested slopes chiefly provide saturated overland flow rather than Hortonian overland flow (DUNNE and BLACK, 1970). However, since saturated overland flow on slopes also
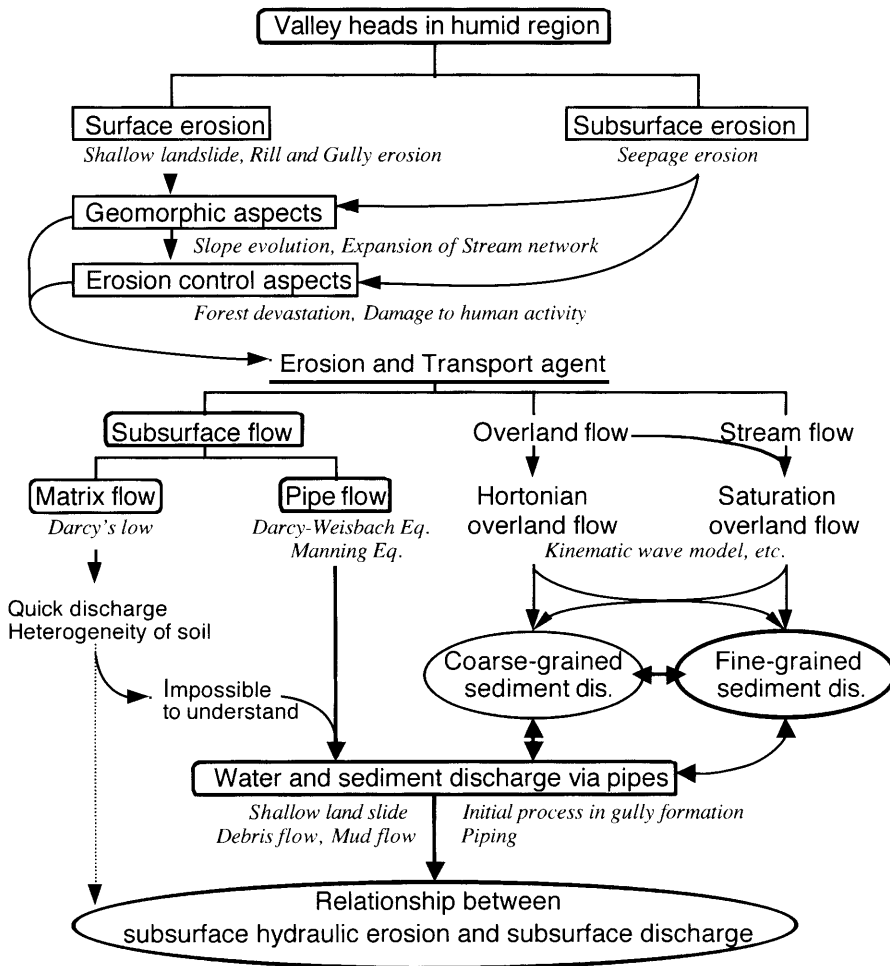
Fig. 1 Water and sediment discharge in headwaters.

results from heavy rains, subsurface water flow is usually the main component of discharge from slopes. Although erosion caused by surface water flow has commonly been considered in many hydrological fields, subsurface water flow has yet to be evaluated sufficiently as one of the significant agents for the erosion of slope soils and for turbid water discharge from slopes.

The mechanism of subsurface water flow has long been explained on the basis of matrix flow according to DARCY's law. However, the flow mechanics depending on DARCY's law rarely demonstrate a quick discharge of subsurface water flow from slopes, nor do they include the hydrological significance of the heterogeneity of forest soils. Water and sediment discharge via soil pipes, therefore, are important in the forest hydrology, initiation of gully formation, and the process of subsurface hydraulic erosion (e.g., JONES, 1971, 1978, 1987 ; NEWSON, 1976 ; BEVEN and GERMANN, 1982 ; SHINDO and SAKAI, 1983 ; KITAHARA et al., 1988, 1989, 1992 ; TSUKAMOTO et al., 1988 ; SWANSON et al., 1989 ; GARLAND and HUMPHREY, 1992 ; KITAHARA and NAKAI, 1992 ; KITAHARA et al., 1992 ; KITAHARA et al., 1994 ; ONDA, 1994). Accordingly, the interaction between the hydrological

Mechanism	**Mode**	**Process**
Fluidization	Piping	Seepage erosion Tunnel scour

Type of sediment transport

Boiling	Tunneling Channeling (piping in narrow sense)	Heaving
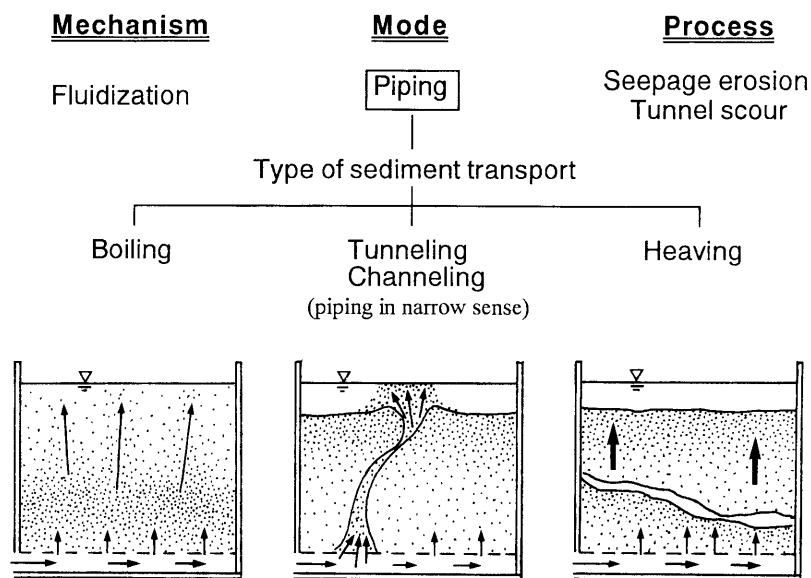
Fig. 2　Classification of piping phenomena.

and gemorphological processes through macro-pore drains at forested slopes is indispensable for evaluating water and sediment discharge from forested watersheds.

When the hydraulic gradient of subsurface water flow increases during heavy storms, piping flushes out more soils around soil pipes. This subsurface hydraulic erosion sometimes triggers shallow landslides if the erosion comes up to the upper part of slopes (TANAKA, 1956). Photo 1 shows subsurface water discharge from a macro-pore that resulted from piping at a landslide site. Piping is often responsible for slope collapses (KOBASHI, 1993), so the process of piping at slopes is commonly observed in valley heads including the area of stream flow generation and at the seepage faces of ephemeral subsurface water flows during heavy rain. Flush flood phenomena are the typical examples of piping, and both pipe-like holes observed at heads of rills and/or gullies (e.g., Photo 2) and spring points at the bottom of a valley deposit (e.g., Photo 3) may be evidence of soil wash out induced by piping which occurred in the past.

Piping is classified into three types, such as boiling, tunneling, and heaving, depending on the difference in style of sediment movement, as shown in Figure 2. This difference in soil movement is mainly due to the cohesion and heterogeneity of soils as described in Chapter 4. Thus, from the aspect of the mechanism of sediment movement, that is the effect of pushing out of soil particles and/or soil clods by subsurface water flow, these all forms of sediment movement are thought as a synonym of piping. There is little knowledge which relates to changes in subsurface water flow behavior and sediment movement with piping for 1) relationship between subsurface hydraulic erosion and subsurface water discharge, and 2) forest devastation resulting from subsurface hydraulic erosion, has developed quantitatively in comparison to the knowledge on erosion by overland flow. This is due to the lack of precise data on water and sediment movement in slopes at shallow landslide initiation.

In contrast, subsurface water discharge from slopes creates turbid water discharge containding fine-grained particles of soils. Thus, water and sediment discharges in head waters directly

Table 1   Topography, geology, meteorology, and vegetation in the experimental watersheds.

	Watershed Area (km²)	Elevation (m)	Geology	Soil	Saturated Hydraulic Conductivity (ms⁻¹)	Mean Annual Temp. (°C)
Kitadani	0.02	340~380	Granodiolite	Decomposed granite	10^{-4}~10^{-6}	14
Jozankei	0.02	312~441	Quartzporphry	Sand and Gravel	10^{-3}~10^{-6}	7

	Annual Precipitation (mm)	Mean Annual Discharge (mm)	Vegetation	Wood Volume (m³ ha⁻¹)
Kitadani	1853	1004	Mixed Conifer-hardwood Forest in humid and warm temperate region (e.g. Japanese Red Pine and Hinoki Cypress)	277.5
Jozankei	1000	512	Mixed Conifer-hardwood Forest in cool temperate region (e.g. Todo Fir and Mizunara Oak)	175.0

affect the ecosystems in rivers, lakes, and seas, as well as the water management for quality conservation.   Accordingly, data on both the mechanism of water flow and the control for fine-grained particle discharge are recognized important environmental indices (SATO, 1987 ; MATSUNAGA, 1993).   Since the process of fine-grained particle discharge in subsurface water flow has been little known, the systematic and quantitative comprehension of the influence of fine-grained particle discharge in subsurface water flow on the watershed ecology in downstream areas is indispensable.   In addition, studies on fine-grained sediment discharge have been conducted chiefly in relatively large watersheds, containing the streams of at least the third or forth order.   Even though we can easily identify the source of the sediment, studies in small drainages, including the streams below first order, have scarcely been conducted except for the studies of SAKAMOTO et al. (1992, 1993a, 1993b, 1994, 1996).   A few researchers have focused on quantitative descriptions of subsurface hydraulic erosion at slopes (e.g., Jones,1987).   However, we have not yet procured complete knowledge about the role of subsurface water flow on fine-grained sediment discharge and resultant turbid water discharge from slopes, and efficient indices have not yet been proposed for the preferable forest management associated with sediment discharge.

1. 2   Observation sites

   Table 1 shows the geological, geomorphic, and climatic characteristics of two drainage areas examined in this study.   The watershed are respectively located in a humid and a cool temperate region with considerable differences in mean annual temperature, annual precipitation, annual discharge, and vegetation.   However, the watershed are similar in their geology (felsic igneous or metamorphic rocks), in their regolith constructed of sandy soil materials, and in the saturated hydraulic conductivity of their soils.

1. 2. 1   Kitadani Watershed in Aichi Prefecture, central Japan

   Figures 3 and 4 (after YAMAGUCHI, 1963) show the Kitadani Watershed where coarse-grained sediment discharge from a soil pipe and a topographic change in a slope with piping were observed.   The watershed is in the Akatsu Experimental Forest of Tokyo University (35° N, 137° E).   The small drainage area containing the first order stream (Fig. 4) is focused on in this study.   The Kitadani watershed with an area of 0.02 km² (2.0 ha) and a relief of 40 m with a
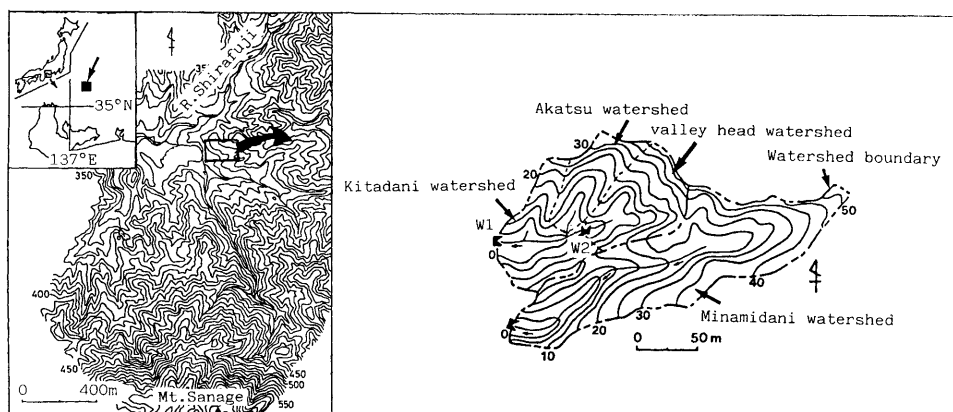
Fig. 3　Location and topography of the Kitadani Watershed.
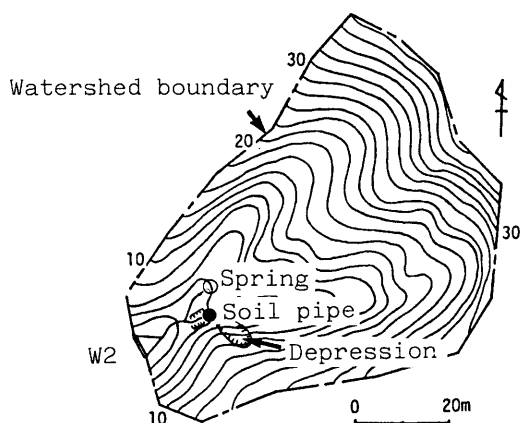
Fig. 4　Valley head in the Kitadani Watershed (see Photo 5).

minimum elevation of 340 m at the W1-weir, is one of the head waters of the Shonai River which flows down to Ise Bay (Pacific Ocean).　The geology of the watershed is granodiolite intruded during the Cretaceous period (about 200 MY.B.P., NAKAI, 1970).　Both the cone penetration test and observation of soil profiles of trenches which were excavated on the ridges exposed the boundary between the decomposed granite and the basement rock at $N_{10}=40$.　The Kitadani Watershed is located in a humid and temperate region.　The ambient forests are the coniferous trees of Japanese Red Pine (*Pinus densiflora* Sieb. et Zucc.), Hinoki Cypress (*Chanaecyparis obtusa* (Sieb. et Zucc.) Endlicher), and the broad-leaved trees of Konara (*Quercus serrata* Murray) typical in this area.　Thin organic horizons have developed on the slope and portions in the bare lands which are found on some ridges.

　　Table 2 shows the physical characteristics of the soil of the Akatsu Watershed (see Fig. 3) in the Kitadani Watershed, measured by undisturbed 100 cm³ soil cores.　The numbers at the right side of the hyphen on the sample name indicate the soil sampling depth (cm ; the number 0 represents the depth of 0 to 5 cm).　The moisture characteristic curves (*pF*-test, see Fig. 5) at the

Table 2 Physical properties of soil layer in the Akatsu Watershed.

Location of sampling	Sample name	N_{10} Value	Saturated hydraulic conductivity (m s^{-1})	Specific gravity	Porosity (%)	Field capacity (%)
Head floor	C2-0	5	6.7×10^{-4}	2.48	—	—
	C2-50	2	4.8×10^{-5}	2.59	38.3	13.5
	C2-100	2	5.6×10^{-6}	2.67	36.9	15.0
	C4-100	3	5.3×10^{-5}	—	—	—
Side slope	C8-0	1	4.5×10^{-4}	2.56	—	—
Crest slope	R6-10	10	5.4×10^{-4}	2.59	40.0	10.2
	R6-30	20	6.3×10^{-5}	2.60	36.8	8.3

The numbers at the right side of hyphen on sample name indicate the soil samplimg depth (cm).

Fig. 5 Moisture characteristic curves of soil layer distributed in the head floor and the crest slope in the Akatsu Watershed.

drainage stage provide the unsaturated hydraulic conductivity used in a numerical experiment which is described in Chapter 4. The field capacity of the soil is calculated from the saturated moisture content minus the content where the moisture characteristics curve in Figure 5 almost becomes perpendicular ($pF = 2.2$: 158.5 cm H$_2$O).

1. 2. 2 Jozankei Watershed in Hokkaido, northern Japan

Figure 6 shows the topography of the Jozankei Watershed (43° N, 141° E) where the mode of subsurface water discharge and fine-grained sediment yield were examined. The watershed is situated 20 km west of Sapporo and includes only one first order stream which is a tributary of the Otarunai River. The watershed has an area of about 0.02 km^2, a relief of 129 m with a minimum elevation of 312 m at the Wt-weir, an average slope gradient of 36.7 degrees, and an average stream bed gradient of 16 degrees. A perennial spring is located at a distance of 150 m down from the crest slope. The drainage area contributing to the spring is about 0.011 km^2, corresponding to 55 per cent of the total watershed area. The geology of the watershed is quartz porphyry intruded
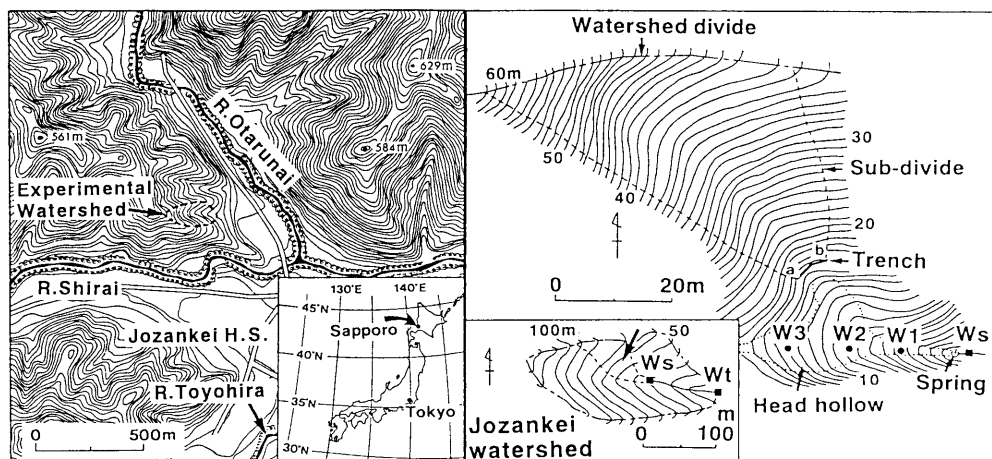
Fig. 6　Location and topography of the Jozankei Watershed (see Photo 3).

as a metamorphic rock during the Miocene period (20 MY.BP, GEOLOGICAL SURVEY OF HOKKAIDO, 1980). The surface layer of the slope consists of the weathering products of the basement rock (like decomposed granite). Vegetation in the watershed is a mixed conifer-hardwood forest typical of this cool-temperate region, composed mostly of Todo fir (*Abies sachalinensis* (Fr.Schmid.) Masters) and Mizunara oak (*Quercus mongolica* Fischer et Turcz.). The understory vegetation and organic matter that originated from the trees cover the surface of the watershed. The A_0-horizon is well developed. Ambient temperature at the drainage ranges from $-20°C$ in late January to $25°C$ in mid July, and the average annual temperature is 7 C. Annual precipitation is about 1000 mm, with snow contributing about 45 per cent. Maximum accumulated snow depth is typically 1.5 to 2 m in early March. Stream discharge measured at the Wt-weir decreases during the snow-accumulation season from late November to late March, since little melt water percolates from the bottom of the accumulated snow into the soil. There is usually considerable melt water starting in late March or early April. In June and July, it is drier because of reduced rainfall and melt water discharge. Subsurface water flow temperature measured at the spring in the Jozankei Watershed ranges from 0 C to 10 C. Pipe flow during storm runoffs occupies a maximum of 70 per cent of subsurface water discharge from the side slope between the weir Ws and Wt (KITAHARA and NAKAI, 1992 ; KITAHARA et al., 1994).

The head hollow in the valley head (see Fig. 6) is 30 m long, a maximum of 15 m wide, and 10 to 20° in inclination. The upper part of the hollow gradually continues to the side slope (30 to 40° in inclination). The rill (5 m long and 0.3 m deep), including no flow, runs between the spring and well W1. Figure 7 shows the schematic longitudinal soil profile of the head hollow along with values of saturation hydraulic conductivity (K_s) measured in 400 cm³ soil cores for the A-horizon, a relatively shallow sandy layer, and a middle clay-rich layer. The electrical conductivity measurement of subsurface water discharge at the spring was used to estimate flow velocity in order to get the hydraulic conductivity value for a lower sand after salt had been inserted into well W1.

The soil matrix consists mostly of particles with a diameter observed at the soil section of below 5 mm, corresponding to fine pebble. The maximum thickness of the soil layer is 3.6 m at well W3. The A-horizon ($K_s = 10^{-3} \, ms^{-1}$) is less than 0.3 m. The underlying sedimentary soil is
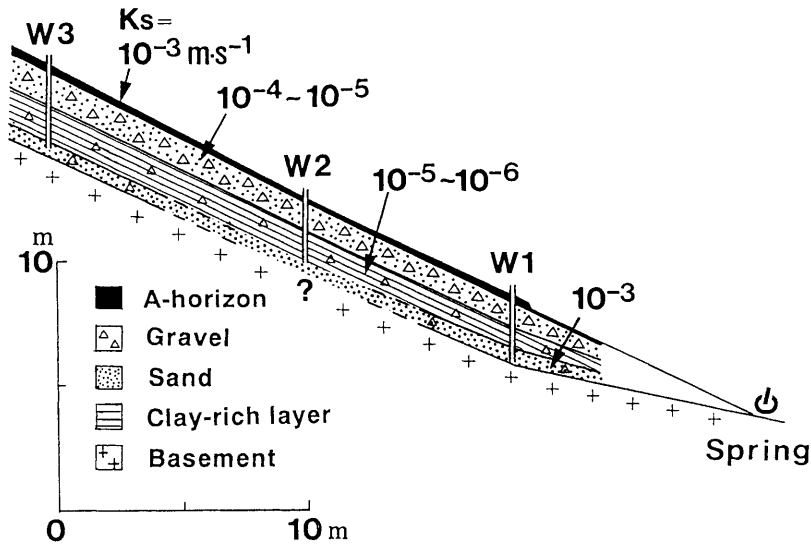
Fig. 7 Schematic longitudinal soil profiles of the head hollow in the Jozankei Watershed.

composed of three parts : (1) a relatively shallow sandy layer ($K_s=10^{-1}$ to 10^{-3} ms^{-1}) containing much angular gravel (about 0.2 m in diameter) ; (2) a middle clay-rich layer ($K_s=10^{-5}$ to 10^{-6} ms^{-1}) also containing much angular gravel (mostly below 0.2 m in diameter) ; and (3) a lower sandy layer ($K_s=10^{-3}$ ms^{-1}) with some angular gravel. These sediments are colluvial deposits from the side slope. The saturation hydraulic conductivity of the lower sandy layer is greater than that of the upper clay-rich soil. A more permeable zone, therefore, must be formed along the bottom of sedimentary soils (e.g., as reported by SHINDO, 1983 ; TERAJIMA and MOROTO, 1990 ; ASANO et al., 1993 ; and OKUNISHI et al., 1993). Subsurface water flow is sometimes converged at the bottom of head hollow soils and piping may be initiated at sites where the water level reaches a slope surface.

1.3 Research procedure

Figure 8 shows the flow chart of this study. Various hydrogeomorphic processes at channel heads provide the topographic diversity of heads and valley development (DIETRICH and DUNNE, 1993). Slope soil commonly piles up in the bottom of the valley following shallow landslides. This repeated geomorphic process brings about the formation of head hollows (TAMURA, 1987) by the creation of a relatively thick soil layer which retains a large capacity for water storage. Thus, surface flow rarely occurs at the head hollows in humid and forested drainages except in the case of heavy rainfall. Subsurface water discharge usually removes and redistributes the sediment in valley heads. This geomorphic process reveals that subsurface hydraulic erosion transforms the topography of valley heads in the long term, that is, it shows that subsurface water discharge from head hollows is a significant agent in valley development.

Sediment discharge in subsurface water flow signifies the following two erosion processes : 1) Sediment discharge with the creation of soil pipes (the formative process of soil pipes), and 2) Sediment discharge through soil pipes (the effect of soil pipes on sediment discharge). However, both are the same hydraulic phenomenon in dynamic perspectives, that is sediment discharge resulted form flushing out from soil matrices to preferential pathways (i.e., macro-pores) by seepage force. Coarse- and fine-grained sediments are defined in this study as "soil particles

```
        ┌────────────────────┐
        │   Water cycle      │
        │      and           │ ──────▶ [ Slope ]
        │ topographic change │
        └────────────────────┘
```

Subsurface hydraulic erosion

Subsurface discharge and sediment production (Chapter 2)

[Observation]

Analysis of subsurface discharge from the head hollow (Chapter 3)
— *Function of pipes for subsurface discharge* —

[Experiment on pipe flow]

Process of coarse-grained sediment production (Chapter 4)
— *Process of pipe formation* —

[Numerical simulation and liquefaction experiment]

Process of fine-grained sediment production (Chapter 5)
— *Function of pipes for subsurface sediment yield* —

[Measurement of subsurface flow and sediment yield]

Relationship between subsurface discharge and sediment yield in
subsurface hydraulic erosion (Chapter 6)
— *Water and sediment interaction, subsurface hydraulic erosion
and conservation for watershed environment* —

[Comprehensive discussion]

[Quantitative comprehension of subsurface hydraulic erosion]

Fig. 8   Flow-chart of this study.

being estimated visually as over 0.1 mm in diameter" and "wash load ranging from 0.1 to 0.001 mm in diameter", respectively.

In addition, fine-grained sediment is an adequate indicator for observations and analyses of the interaction between subsurface water discharge and sediment movement, because :

(1)   Fine-grained sediment discharge represents the initial stage of subsurface hydraulic erosion, because turbid subsurface water containing fine-grained sediment is known to flow out from slopes before a landslide initiation (SASSA, 1984).   Furthermore, movement of fine-grained sedi-

ment from the soil surface preceded movement of sand particles by several minutes in a hydraulic experiment related to liquefaction (in Chapter 4).

(2) Fine-grained particles are the primary source of sediment in typical subsurface water flows from valley heads ; movement of bed load materials may be initiated after extensive flushing of fine sediment from a soil matrix (i.e., suspended sediment).

1. 4 Observation method

1. 4. 1 Subsurface water discharge

Observations were conducted in the Jozankei Watershed from September 1993 to May 1995. All observations of subsurface water discharge were discontinued at the Ws-weir during the winter season between December and mid-March, because there was no suspended sediment yield ; this was a result of low subsurface water discharge due to accumulated snow. Instrumentation within the drainage is shown in Figure 6. A 60° V-notch weir (Ws) was installed at 3 m below the spring and automatically measured water discharge from the head hollow. The rain gauge (0.5 mm per pulse) registered precipitation at 10 min intervals out side the forest at a point of 20 m east of the Wt-weir. Potentiometers automatically recorded shallow groundwater level at 10 min intervals in three wells (W1-W3) having depths of 2.6, 2.5, and 3.3 m respectively. The bottom of the W1-well reaches the basement rock.

1. 4. 2 Sediment discharge

The coarse-grained sediment yield was observed in the Kitadani Watershed where a piping phenomenon occurred during the heavy rain on 25 September 1988 with total rainfall of 220 mm and maximum one-hour rainfall intensity of 70 mm from 12 : 00 to 13 : 00. The W2-weir (see Figs. 3, 4 and Photo 4) measured water discharge from the valley head. The sediment deposited in the W2-weir after the piping provided the approximate amount for sediment from the subsurface portion of the slope.

On the other hand, manual and automatic water sampling at the spring in the Jozankei Watershed collected fine-grained sediment in subsurface water flow during the heavy rainfalls from September 1993 to November 1994. During the observation period, the author observed eight storms accompanied by fine-grained sediment yield in subsurface water flow (see Tables 6 and 7 in Chapter 5 for details of the storms). Manual sampling required intervals of 15 to 60 min to collect water during storm runoffs, and an automatic water sampling system (ISCO, model 2700) enabled observation at night. Sediment with particle diameter of less than 0.1 mm flows down mostly as wash load (EGASHIRA and ASHIDA, 1981). Consequently, when the particles of less than 0.1 mm in diameter were eroded, they are certainly transported from the subsurface portion to the spring by subsurface water flow unless they were trapped in the drainage networks of the sedimentary soil.

The following method was used to determine the fine-grained sediment concentration (Fg.S. C.) in subsurface water flow : The water samples were first passed through a 0.106 mm screen and then strained in a 0.001 mm glass fiber filter (Whatman, GF/B). The desiccation of the residual matter on the glass fiber filters required heating for 24 hours at 80°C. Organic matter was then removed from the desiccated sediments by ashing for 30 minutes at 550 C in an electric furnace. The particle size of the remaining fine-grained sediments ranged from 0.001 to 0.106 mm, corresponding to clay to fine sand. Multiplying the subsurface water discharge by Fg.S.C. produced fine-grained sediment flux (Fg.S. Flux).

2. Subsurface water discharge and sediment production

2.1 Subsurface water discharge from a head hollow

Shallow groundwater level in well W1 of the Jozankei Watershed strongly affects water movement in the head hollow. For instance, the generation of saturated overland flow in the head hollow is affected because well W1 is located at the head of the rill being formed between W1 and the spring. The water level in well W1 must eventually reflect the upper boundary of subsurface water flow in the valley head. Accordingly, well W1 better reveals the relationship between the shallow groundwater level in the head hollow and subsurface water discharge from the spring than the other two wells (W2 and W3). In addition, well W1 had uninterrupted records of the shallow groundwater level in the head hollow during the observation period. Because of these reasons, the author focused on the measurement of the shallow groundwater level in well W1 to understand the subsurface water discharge regime in the head hollow.

Figure 9 shows changes in subsurface water discharges and shallow groundwater levels from 12 April to 13 May 1994. Maximum snow depth was 1.9 m near well W1. Water equivalents of the snow pack on 8 March (prior to the melt season) were 450, 430, and 330 mm in a bare plot, the deciduous forest, and the coniferous forest within the drainage, respectively. Bulk densities of the accumulated snow in these three plots were 0.32, 0.31, and 0.33 $g \cdot cm^{-3}$, respectively. Melt water generated the maximum groundwater level on 16 April and a similar peak on 5 May. One weir, buried by a snow avalanche, did not operate on 5 May. A similar interruption for the measurement of groundwater level from 24 to 27 April was also attributed to a snow avalanche.

Subsurface water discharge and the shallow groundwater level clearly showed diurnal variations which coincided in time. These same temporal trends were observed during the subsequent storms on 27 May and 16 September. Because of these consistent data trends, the relation between subsurface water discharge and the shallow groundwater level can be easily analyzed for the same time periods. Hydraulic head gradient in this case is given by :

$$i_{(W1)} = h_{(W1)} \, l_{(W1)}^{-1} \tag{1}$$

where $i_{(W1)}$ is the hydraulic head gradient between the spring and well W1, $h_{(W1)}$ is the groundwater height (m) in well W1 based on the level at the spring, and $l_{(W1)}$ is the horizontal distance between the spring and well W1 (9.37 m).

Figure 10 shows the relationship between $i_{(W1)}$ and subsurface water discharge. Some curvilinear correlations occur in Figure 10, so that the relationship between $i_{(W1)}$ and subsurface water discharge is expressed as

$$Q_t = \alpha \, i_{(W1)}^{a} + \beta \tag{2}$$

where Q_t is the total subsurface water discharge (ls^{-1}), a is the constant depending on the shape of the correlation curves in Figure 10, and α and β are the coefficients.

2.1.1 Subsurface water flow during low flows

Figure 10d shows that the $i_{(W1)} - Q_t$ relation in eq. (2) represents a linear correlation with the correlation coefficient (r) of 0.985 and $a=1$ ($\alpha = 3.165$, $\beta = -0.722$) in $i_{(W1)} \leqq 0.233$ (shallow groundwater level on the basement rock was below 0.07 m). Therefore, these low flows must originate from matrix flow explicated by DARCY's law. If Q_t in eq. (2) is null, then $i_{(W1)}$ is 0.228, suggesting that $h_{(W1)}$ in eq. (1) is 2.14 m (i.e., 0.03 m above the basement rock). That is, no subsurface water discharge is produced from the head hollow when the shallow groundwater level is consistent

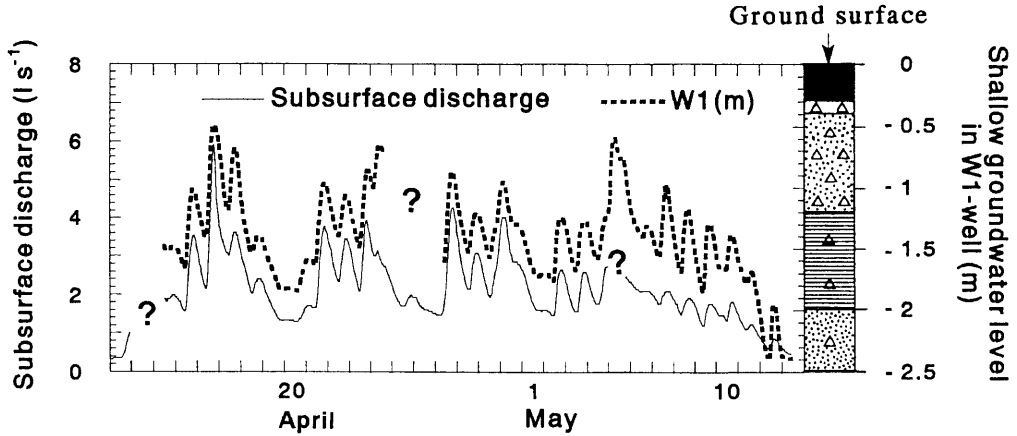Fig. 9   Changes in subsurface discharge and shallow groundwater level in well W1 during meltwater discharge in 1994.
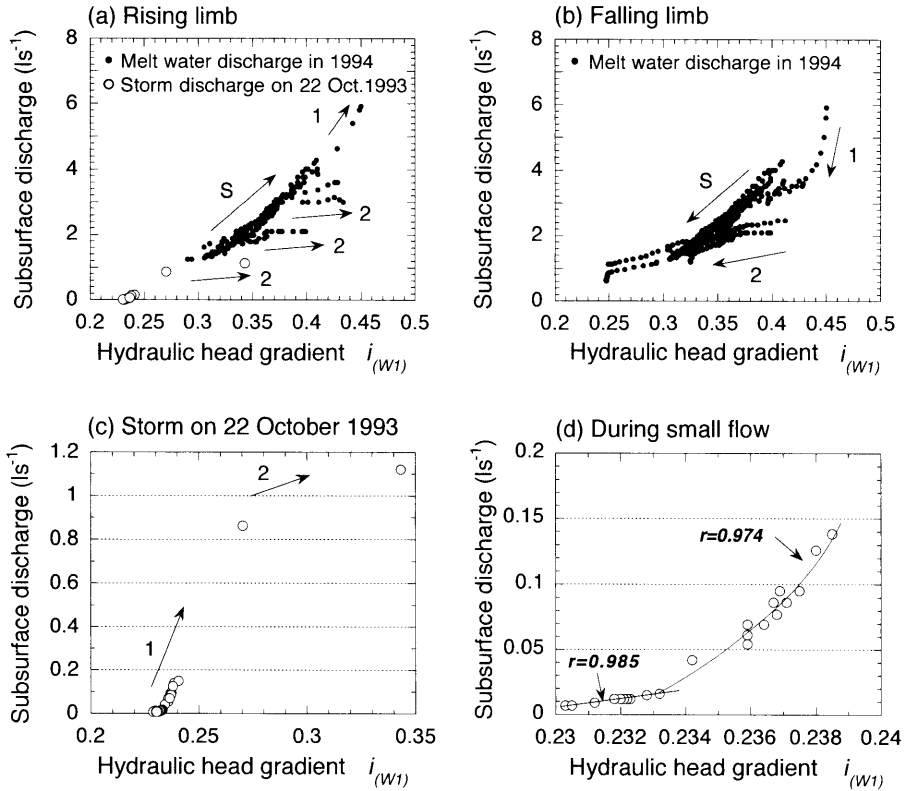
Fig. 10   Relationship between hydraulic head gradient and subsurface discharge.

with the level of the basement rock. Consequently, the discharge from the spring consists mostly not of groundwater discharge from the basement rock, but of subsurface water flow via the head hollow sediment.

2.1.2　Subsurface water discharge during runoff events

Figures 10(c) and 10(d) show that the $i_{(W1)}-Q_t$ relation reveals a slightly concave curvilinear correlation (Arrow 1) with the correlation coefficient (r) of 0.974 and $a=91.6$ ($\alpha=1.64$, $\beta=0$) in $0.233 \leqq i_{(W1)} \leqq 0.260$ (shallow groundwater level on the basement rock ranged from 0.07 to 0.33 m). Subsurface water discharge abruptly augmented with an increase in $i_{(W1)}$. In contrast, the $i_{(W1)} -Q_t$ relation represented the convex curvilinear correlation (Arrow 2) in $i_{(W1)} \geqq 0.26$. Furthermore, Figure 10(a) shows that when $i_{(W1)}$ exceeded 0.30, corresponding to shallow groundwater level of 0.7 m above the basement rock and to the upper level of the bottom sand layer, the $i_{W1}-Q_t$ relations exhibited the linear or slightly concave curvilinear correlations (Arrow S). However, under larger $i_{(W1)}$, the shapes of the correlation lines comprised the following two types during both the rising and falling limbs of the hydrograph : (1) an abrupt increase in subsurface water discharge by shifting for the prolongation (Arrow 1 in Fig. 10(a) ; $a > 1.0$) of the concave curvilinear correlation (the Arrow S), (2) a recession of the increasing rate of subsurface water flow (Arrow 2 in Fig. 10(a) ; $0 < a < 1.0$) with shifting into the lower portion of the concave curvilinear correlation (Arrow S).

2.1.3　Characteristics of subsurface water discharge

The following two aspects demonstrate the significance of pipe flow and the head hollow on subsurface water discharge from the spring : (1) Soil pipes must be the main route of subsurface water discharge, because subsurface water flow reaches the surface mostly from the soil pipes occurring near the spring, and the saturated area on the hollow expands only at overland flow generation ; (2) Peak subsurface water discharge from the side slope measured at the trench shown in Figure 6 accounted for a merely 10 per cent of subsurface water discharge from the spring, and no subsurface water discharge from the side slope occurred during the low flow at the spring. Thus, it was impossible for the small segment of the side slope between the spring and well W1 to create the abrupt increase in subsurface water discharge from the spring. Accordingly, both the variation in flow section area of subsurface water explained by DARCY's law (an expansion of the saturated zone) and the contribution of subsurface water flow from the side slope between the spring and well W1 could hardly account for the changes in mode of subsurface water discharge in $i_{(W1)} \geqq 0.233$ shown in Figure 10.

If the assumption that the subsurface water flow during the storms passed entirely through the soil matrix of the head hollow is correct, the Reynolds number derives the subsurface water flow regime during the larger hydraulic head gradient. Subsurface water flow via the soil matrix is classified by Reynolds number (R_e) into the following two states : (1) $R_e \leqq 10$, laminar flow ; (2) $R_e > 10$, turbulent flow. The Reynolds number for subsurface water flow is given by :

$$R_e = v d_s \nu^{-1} \tag{3}$$

where v is the mean velocity of matrix flow (in $m \cdot s^{-1}$, $v = K_s i$ where i is the hydraulic gradient), d_s is the soil particle diameter (in mm), and ν is the kinematic viscosity (in $m^2 \cdot s^{-1}$).

The soil profile observed at the excavation for the wells revealed that the soil matrix at the head hollow consisted mostly of particles whose diameter was below 5 mm, corresponding to fine pebble. Insertion of the following three parameters into eq.(3) gives the maximum R_e for subsurface water flow in the head hollow of the Jozankei Watershed : ① $0.495 \times 10^{-3} m \cdot s^{-1}$ of the maximum v ($10^{-3} m \cdot s^{-1}$ in maximum K_s and 0.495 in maximum $i_{(W1)}$), ② 5 mm of the maximum d_s (for the maximum diameter of fine pebble), and ③ $1.310 \times 10^{-6} m^2 \cdot s^{-1}$ of the minimum ν (for 10°C

corresponding to the maximum subsurface water flow temperature in the Jozankei Watershed). Consequently, the maximum R_e is 1.89, suggesting that subsurface water flow is almost laminar during a storm and consequently the curvilinear correlation in Figure 10 must be interpreted by DARCY's law.   However, the linear correlation in the relationship between the hydraulic head gradient and subsurface water discharge can be explained only by DARCY's law.   Accordingly, subsurface water flow indicating the curvilinear correlation in Figure 10 must be due not to Darcy's law but to some other kinematic law.

TANAKA *et al.* (1990) observed an abrupt increase in subsurface water discharge from a spring accompanied with an increase in shallow groundwater level in a steep mountain slope.   Thus, such abrupt increases in subsurface water discharge may be common in many valley heads and slopes.

2. 2   Coarse-grained sediment discharge with piping

A heavy rain totalling rainfall of 220 mm occurred in the Kitadani Watershed (see Fig. 3) from 23 to 25 September 1988.   The rain began at noon on 23 September and supplied a one-day amount of 191 mm on 25 September.   The peaks in rainfall intensity of over $20 \, mm \cdot h^{-1}$ occurred three times during this storm, with a maximum of 70 mm from 12 : 00 to 13 : 00 on 25 September.

During the storm, piping with the coarse-grained sediment discharge of $3 \, m^3$ (see Photo 4) occurred at a seepage zone in a valley head drain (see Fig. 4).   According to the observation in December 1988, the piping created a soil pipe of 0.25 m in initial outlet diameter, with a resultant depression of about 0.5 m deep, 3 m long, and 2 m wide at a slope (Photo 5).   The formation of the depression brought about the slope disturbance resulting from the fall and leaning of deciduous trees.   Coarse-grained sediment composed mostly of sandy materials (decomposed granite) was suddenly produced and the sediment discharge gradually increased as rainfall and stream flow increased after the sudden production of the sediment.

The direction of the soil pipe outlet was relatively ascending to the slope surface.   No erosion by overland flow took place between the down edge of the depression and the soil pipe.   Thus, the concentration of subsurface water flow to the seepage zone with the supply of heavy rain and the drastic rising of seepage force was the likely cause of the piping and sediment discharge.

A heavy rain of the same amount and intensity happened the next year (20 September 1989). Another sediment discharge of $3 \, m^3$ from the same soil pipe occurred and the diameter of the soil pipe increased from 0.25 to 0.5 m, and the depression was also deepened, from 0.5 to 1 m deep.

2. 3   Fine-grained sediment discharge in subsurface water flow

Figure 11 shows two typical cases of subsurface water discharge from the head hollow, changes in fine-grained sediment concentration (Fg.S.C., in $mg \cdot l^{-1}$) and flux (Fg.S.Flux, in $mg \cdot s^{-1}$) in subsurface water flow on 22 October, 1993 and 16 September, 1994.   Total rainfall and maximum rainfall intensity were 58 mm and $10.5 \, mm \cdot h^{-1}$ (from 12 : 00 to 13 : 00) during the October storm in 1993, and corresponding values were 68 mm and $14.5 \, mm \cdot h^{-1}$ (from 9 : 00 to 10 : 00) during the September storm in 1994.   Although these rainfall amounts were similar and they were large storms for Hokkaido, northern Japan, overland flow was generated in the rill only from 11 : 45 to 15 : 30 on 16 September, 1994 ; at this point, antecedent soil moisture, surmised from initial subsurface water discharge prior to the storm, was more than that on 22 October, 1993 (see Table 6 in Chapter 5 for initial subsurface water discharge prior to the storm).   The Fg.S.C.   and Fg.S. Flux preceded the peak in subsurface water discharge by several hours, except in the case of overland flow initiation on 16 September, 1994.   The maximum value of the Fg.S.Flux, however,
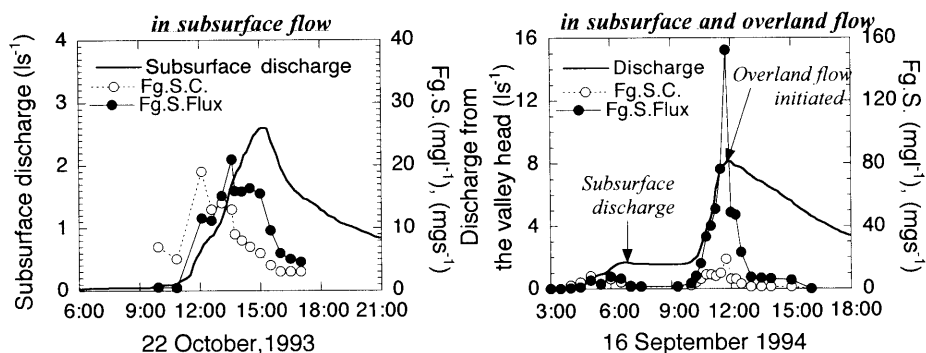
Fig. 11　Water discharge from the head hollow and changes in Fg.S.C. and Fg.S.Flux on
(a) 22 October, 1993 and (b) 16 September, 1994.
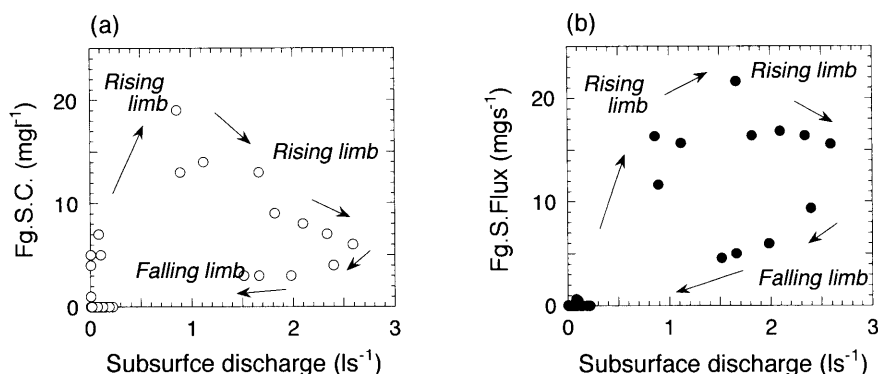
Fig. 12　Relationship between subsurface discharge and fine-grained sediment discharge
on 22 October, 1993.

occurred a short time before the peak in subsurface water discharge.

Figure 12 shows the relationships between subsurface water discharge, the Fg.S.C., and the Fg.S.Flux on 22 October, 1993. Although the Fg.S.C. and Fg.S.Flux conspicuously increased on the initial rising limb of the hydrograph, both decreased to approximately 1 to 1.5 $l \cdot s^{-1}$ of subsurface water discharge. The Fg.S.C. reduced notably to 0.3 times as much as its maximum concentration when subsurface water flow showed the peak discharge. During the falling limb of the hydrograph, both the Fg.S.C. and Fg.S.Flux were lower than during the rising limb. Consequently, they represented clockwise hysteresis loops for a one-storm event.

The above phenomena (sediment discharge prior to subsurface water flow and a clockwise hysteresis loop) were usually observed in the other six storms shown in Tables 6 and 7 in Chapter 5. The characteristics of fine-grained sediment discharge in subsurface water flow have something in common with observations in some rivers : for example, the observation in a small catchment in the United Kingdom by WALLING (1974) and the measurement of suspended sediment concentration in the forested basin of the Bankei River, near Sapporo, Japan, by KURASHIGE (1985).

In the Jozankei Watershed, the characteristics of fine-grained sediment discharge in stream flow were described by SAKAMOTO et al. (1993b,1994) : ① Fine-grained sediment concentration and

flux preceded the peak in stream discharge and exhibited clockwise hysteresis loops, (2) Fine-grained sediment flux correlated with stream discharge during the falling limb of the hydrograph, and ③ The time lags between peaks in stream discharge and fine-grained sediment were smaller than those in subsurface water discharge, as shown in Figure 11.

Thus, during the falling limb, the fine-grained sediment in subsurface water flow may also be evaluated from the change in subsurface water discharge. This is because, during the rising limb of the hydrograph, the fine-grained sediment discharge in subsurface water flow is not simply based on the change in subsurface water discharge.

3. An analysis of subsurface water discharge from the head hollow

3.1 Experiment on subsurface water discharge through a soil pipe

Matrix flow and macro-pore flow (i.e., pipe flow) primarily characterize the mechanism of subsurface water flow in the head slope of the Jozankei Watershed. The inability to apply DARCY's low to interpret the subsurface water flow regime from the head hollow (in Chapter 2, Section 2) and the existence of the permeability zone along the bottom of the head hollow sediment signifies the significance of pipe flow on the subsurface drainage system at the head hollow of the Jozankei Watershed. In addition, experiments on pipe flow provide the mode of subsurface water discharge for understanding the contribution of pipe flow to the subsurface water flow regime in the head hollow of the Jozankei Watershed, which is represented by the various curvilinear correlations as shown in Figure 10.

Figure 13 shows the devices used in the pipe flow experiment. The experimental box was constructed of a waterproofing plywood board and was fixed at 12.8°. Polyester felt materials, whose thickness of 1.2 mm and permeability of 1.0×10^{-3} m·s^{-1} nearly the same as the value of the experimental sand, were secured to the upper and lower faces of the soil block with wire meshes to insure the even distribution of water entry and to prevent erosion from the block faces. The box was filled with sand whose saturation hydraulic conductivity measured by a 400 cm^3 soil core was 1.1×10^{-3} m·s^{-1} with a bulk density of 1.5 t·m^{-3}. The sand was saturated by adjusting water levels at the top and bottom of the box. Water was then allowed to drain for 24 hours.

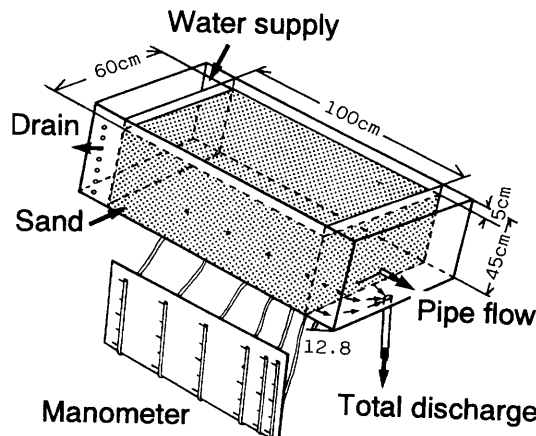Table 3 shows the characteristics of artificial pipes used in the experiment. Only one pipe

Fig. 13   Illustration of the experimental box related to pipe discharge.

Table 3　Lengths and diameters of the artificial pipes used in the experiment.

Drainage capacity	Small ←			→ Large
Length (m)	0.14	0.54	0.74	0.94
Inner diameter (mm)	9	9	13	13

was placed 0.05 m above the bottom and in the middle of a 0.6 m wide box. The pipe was oriented perpendicular to the slope counters, parallel to the side walls of the box. The combinations of pipe length and inner diameter (ID) shown in Table 3 represent the changes in the drainage capacity of the pipe. The long pipes have a high ability for concentrating subsurface water flow into the pipe, and the large diameter pipes have a high ability both for concentrating inflow and drainage from the pipes. These pipes were constructed from polyvinyl chloride (PVC) tubing, and drain holes (4 mm in diameter) were evenly spaced around the pipes at a density of 1.5 holes ·cm $^{-2}$ (open ratio is 75.4 per cent). Preliminary experiments exposed that the density of the drain holes beyond 0.4 holes·cm $^{-2}$ (the open ratio is 20.1 per cent) did not impede the amount of seepage flow from the soil matrix into the pipes. To prevent the drain holes of the pipe from clogging with sand and to ensure the even seepage distribution into the pipe, each pipe was wrapped with two layers of polyester felt materials.

During the experiment, water was supplied to the upper end of the box and pipe discharge (Q_p) and total discharge (Q_t : pipe discharge + matrix discharge) were measured separately at the lower end. Thus, matrix discharge (Q_m) is calculated as the difference in $Q_t - Q_p$.

Water level for six or seven hydraulic differences was given at the upper end of the box (h_u), and discharge without water level was created at the end of the box in order to measure the discharge from the box with the various differences in hydraulic head gradient under steady-state hydraulic conditions. Measurements were taken during the falling stage of discharge, because the experiment had to be performed under sufficiently steady hydraulic conditions to take account of the hysteresis phenomena of the soil moisture content during the rising and falling stages. A full flow condition in the pipes was artificially created at the initiation of the experiment. Six manometers (h_0, h_{10}, h_{20}, h_{40}, h_{60}, h_{80}) were installed at the following positions relative to the downslope end of the box : 0, 0.1, 0.2, 0.4, 0.6, and 0.8 m. Inlets of manometers were placed at the bottom and center of the experimental sand.

3.2　Results and discussion

3.2.1　Shallow groundwater

Figure 14 shows the relationship between the pressure head measured at the side and center of the experimental box when each pipe was placed. This preliminary experiment exhibited that the pressure head differences were negligible between the side and center of the box for the wide range of hydraulic conditions. Thus, two-dimensional analysis of the pressure head measurement is reasonable for such a small box used in this experiment.

Figure 15 shows the pressure head distributions measured at the center of the experimental sand for the lowest (9 mm ID and 14 cm long) and highest (13 mm ID and 94 cm long) drainage capacity of the pipes. The concave drawdown profiles in the pressure head were more remarkable at the upslope side in the highest drainage capacity of the pipe (b) than in the lowest one (a), and the pressure heads ran parallel to the pipes at the downslope side. These facts suggest that the larger drainage capacity of the pipe brought about sufficient effects on subsurface drainage
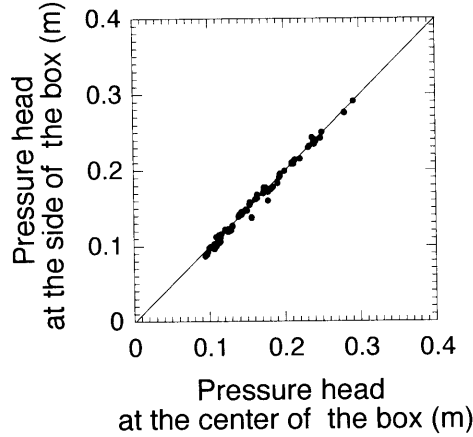
Fig. 14   Relationship between pressure heads at the center and the side of an experimental box when pipes having various drainage capacities were laid into the box.

(a) lp=0.14m,dp=9mm   **(b) lp=0.94m,dp=13mm**
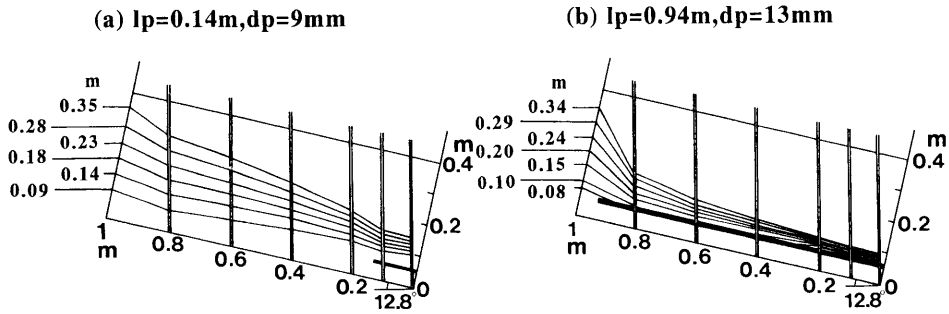
Fig. 15   Pressure head distributions along the center of the experimental box when the pipes of the smallest (a) and the largest drainage capacities (b), shown in Table 4, were laid.

via the pipe.

3. 2. 2   Mode of subsurface water discharge

The hydraulic head gradient $i_{(W1)}$ in the head hollow of the Jozankei Watershed was used for the subsurface water flow analysis on the basis of the shallow groundwater level in well W1 that recorded the highest water level during the observation.   Accordingly, since the upper end of the experimental box always showed the highest water level in the experiments, the hydraulic head gradient used in the experiment was defined as :

$$i_e = h_e(l_e \cdot \cos 12.8°\ )^{-1} \tag{4}$$

where i_e is the hydraulic head gradient used in the experiment ; and $h_e = h_u + l_e \cdot \sin 12.8° - h_0$ where h_u is the water depth (in m) in the up-slope end of the box, l_e is the length of the experimental sand (in m), and h_0 is the pressure head (in m) measured by the manometer installed at the center and down-slope end of the box.

The hydraulic head gradients in the head hollow of the Jozankei Watershed ($i_{(W1)}$) were

(a) l_p=0.14m, d_p=9mm

(b) l_p=0.94m, d_p=13mm
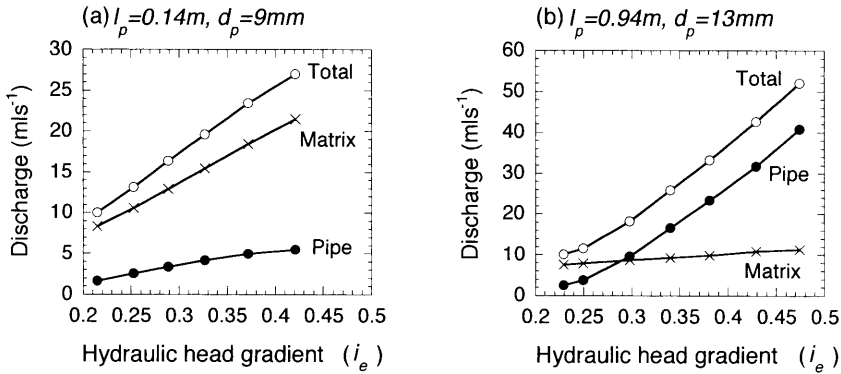
Fig. 16　Relationship between hydraulic head gradients and discharge when the pipes of the smallest (a) and the largest drainage capacity (b), shown in Table 3, were laid.

calculated for the down slope edge of the subsurface water body. In contrast, the hydraulic head gradient in the experiment (i_e) represented the average gradient of shallow groundwater in the box, and was calculated from the whole body from the up- to down-slope ends of shallow groundwater. Thus, in order to coordinate the results between the Jozankei Watershed and the experiment, the values from h_{20} to h_{80} were inserted into eq. (4) instead of h_u. The results emphasized the rationality to use h_u for the analysis in the experiment, for the following reasons : Only α in eq. (2) was varied with the change in the hydraulic head gradient (i_e) in the experiment for using h_{20} to h_{80} instead of h_u, and the coefficient a was not changeable in spite of being over 1.0 or not.

Figure 16 shows the relationship between the hydraulic head gradient (i_e), matrix discharge, pipe discharge, and total discharge for the minimum (a) and maximum (b) drainage capacity of the pipes. The scale in longitudinal axis is different in the two diagrams because of the clear description for each mode of discharge.

In the minimum drainage capacity of the pipe (Fig. 16 (a)), matrix flow correlated linearly with the hydraulic head gradient. The pipe discharge showed a convex curvilinear correlation in the $i_e - Q_t$ relation that conveyed the reduction of the increasing ratio of pipe discharge with the rising of hydraulic head gradient. For these reductions in pipe discharge, hydraulic experiments by KITAHARA (1989) and SIDLE *et al.* (1995) revealed that MANNING's equation or the DARCY-WEISBACH formula exhibited well the mechanism of these flows via a pipe under a full flow condition in the pipe. While matrix discharge strongly contributed to total discharge, the mode of total discharge showed a slightly convex curvilinear correlation which was influenced by pipe discharge.

In contrast, matrix discharge precisely correlated linearly with the hydraulic head gradient in the maximum drainage capacity of the pipe (Fig. 16 (b)), and controlled the total discharge in $i_e \lesssim$ 0.29 because of a larger matrix discharge than pipe discharge. Pipe discharge, however, showed a concave curvilinear correlation in the $i_e - Q_t$ relation in Figure 16 (b), and the total discharge also increased with an increase in the pipe discharge.

Despite the changes in the drainage capacity of the pipe, matrix discharge had a linear correlation with the hydraulic head gradient and eventually did not agree with subsurface water discharge representing the concave and convex curvilinear correlations shown in Figure 10.
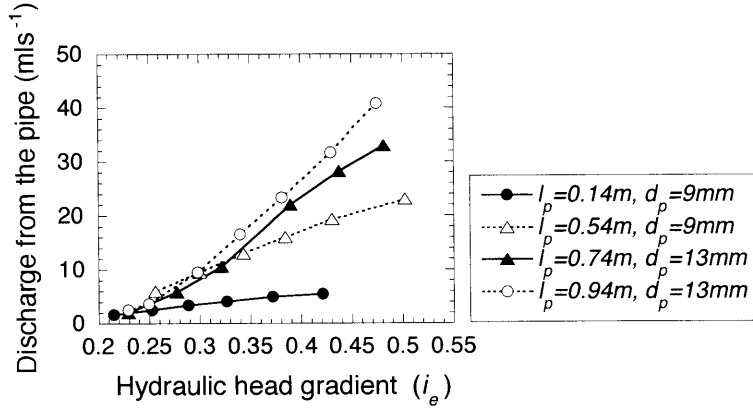
Fig. 17   Relationship between hydraulic head gradients and discharge from the pipes under full flow conditions at the initiation of the experiment.

Accordingly, the subsurface water flow regime in the head hollow of the Jozankei Watershed during the runoff events cannot be disclosed only from the hydraulic theory based on DARCY's law.   On the other hand, the pipe discharge well described the substantial regime of subsurface water discharge and intensively affected the mode of total discharge.   Thus, pipe flow must be a main cause of the change in flow style of the total discharge from the head hollow of the Jozankei Watershed.

Figure 17 shows the change in pipe discharge (Q_p) for the different drainage capacities of the pipes.   The $i_e - Q_p$ relation exhibited convex and concave curvilinear correlations for a wide range of drainage capacities.   These correlations seem to be the same as the change in subsurface water discharge shown in Figure 10a.   Consequently, the flow via the pipe, resulting from the difference in the drainage capacity of the pipe, created the convex and concave curvilinear correlations in Figure 10 and was the main reason for constructing the subsurface water discharge regime under the conditions of $a > 1$ and $0 < a < 1$ in eq. (2).   In addition, the shift from the concave (Arrow S) to convex (Arrow 2) curvilinear correlations occurred at different points on the concave line.   This is because the movement of fine-grained sediment, such as clogging and erosion, took place in the sedimentary soil : the various roles of the pipes for the subsurface water discharge regime were displayed through subsurface hydraulic erosion at all runoffs (refer to Chapter 6).

3. 2. 3   Relationship between pipe flow and hydraulic head gradient

As described in the previous section, earlier studies have commmonly regarded pipe flow as being under full flow condition, and used theories based on MANNING's equation or the DARCY-WEISBACH formula to interpret most of the subsurface water flow regime in drainage network systems resulting from pipe flow (KITAHARA, 1989 ; SIDLE et al., 1995).   This suggests that the increasing ratio of pipe discharge recedes with the rising of the hydraulic head gradient of pipe flow or subsurface water flow in soil matrices.

However, in the present experiment, pipe discharge suddenly increased with the rising of the hydraulic head gradient of subsurface water flow in the high drainage capacity of the pipe.   In order to understand the difference in the subsurface water discharge regime between high and low drainage capacities of the pipes, the relationship between i_e and Q_p was verified through
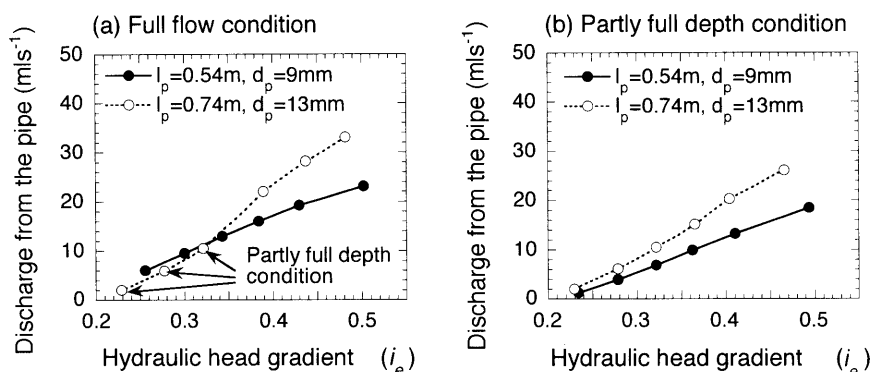
Fig. 18　Relationship between hydraulic head gradients and discharge from the pipes when the pipes of intermediate drainage capacity, shown in Table 3, were laid.

model experiments using the intermediate drainage capacities of pipes of 0.54 mm long and 9 mm ID and of 0.74 m long and 13 mm ID, shown in Table 3. The results are shown in Figure 18. The methodology for the creation of a full flow condition in the pipes was as follows : At the initiation of the experiment with water discharge from the pipe outlets, a thin vinyl tube was inserted into the pipes and then new water was supplied into the pipes through the tube. This method required the creation of a full flow condition in the pipes (of course, the vinyl tube was removed to measure the discharge). In contrast, air supplied through the tube into the pipes provided and subsequently maintained a partly full depth condition in the pipe.

Figures 18 (a) and 18 (b) show pipe discharge under the full flow condition and the partly full depth condition at the initiation of the experiment, respectively. Discharges from the pipes showed convex curvilinear correlations under the full flow condition (Fig. 18 (a)). Discharge from 0.74 m long, 13 mm ID pipe, however, changed to the partly full depth condition at $i_e \leqq 0.35$ and showed simultaneously a concave curvilinear correlation in $Q_p \leqq 15$ ml·s^{-1}. Thus, pipe discharge under the partly full depth condition at the initiation of the experiment may also have caused the same discharge regime representing the concave curvilinear correlation in the $i_e - Q_p$ relation.

Under the partly full depth condition at the initiation of the experiments (Fig.18b), discharge from 0.74 m long, 13 mm ID pipe exhibited a concave curvilinear correlation at $i_e \leqq 0.37$ ($Q_p \leqq 15 \sim 20$ ml·s^{-1}, that is, the opposite of what was under the full flow condition in $Q_p \geqq 20$ ml·s^{-1}), and discharge from the pipe of 0.54 m in length and 9 mm ID also showed a concave curvilinear correlation at $i_e \leqq 0.37$ ($Q_p \leqq 10$ ml·s^{-1}).

The curvilinear correlations in the experimental results may be contained within an error range because of the availability of a linear approximation for these relations. Supplemental experiments, repeated three or four times, revealed no transition of the shapes of the curvilinear correlations ($a < 1$ or $a \geqq 1$ in eq. (2)) with the relative standard deviation of 0 to 3.47% for the values shown in Figure 18 (b). Thus, the flow regime of $a > 1$ was obviously created under the partly full depth condition in the pipes.

In the relative high drainage capacity of the pipe, flow in the pipe with a small hydraulic head gradient was under the partly full depth condition and pipe discharge increased with $a > 1$ when the hydraulic head gradient rose. If the hydraulic head gradient rose more, a decrease in the

drainage capacity of the pipe resulting from an increase in seepage flow from the soil matrix into the pipe would promote the full flow condition in the pipe, and then MANNING's equation or the DARCY-WEISBACH formula, supporting the reduction of the increasing ratio of pipe discharge, would interpret the pipe flow mechanism as demonstrated in Figure 16(a). In other words, the hydraulic property expressed by MANNING's equation or the DARCY-WEISBACH formula (KITAHARA, 1989 ; SIDLE *et al.*, 1995) can only be applied to the pipe flow mechanism in the relatively low drainage capacity of the pipe and to the convex curvilinear correlations shown in Figures 16 (a) and 18(a).

From the above results, we can make the following conclusion from the simultaneous records of the concave and convex curvilinear correlations at one storm event in Figure 10c : Subsurface water via the soil pipes was mostly an open channel flow owing to the sufficient and optimum drainage capacity of soil pipes to shallow groundwater at the initial stage of runoff events. However, the relative reduction of drainage capacity of the soil pipes, resulting both from the continuity of rainfall and the rising of the hydraulic head gradient, converted the open channel flow into full flow in the soil pipes.

Subsurface water flow can be expressed by $Q_s = A v_a$, where Q_s is the subsurface water flow, A is the flow section area, and v_a a is the mean velocity of subsurface water flow. According to the experimental results, this equation suggests that the reason for the abrupt increase in subsurface water discharge shown in Figure 10(a) (i.e., the concave curvilinear correlation) derived not from an increase in flow section area (A) as the shallow groundwater level rose, but from an increase in the mean flow velocity (v_a) resulting from an increase in pipe flow. That is, the increase in the mean flow velocity (v_a) ultimately depended on the increase in the subsurface water flow velocity from the soil matrix into the drainage networks typical in soil pipes. Accordingly, subsurface water discharge abruptly increased with the increase in pipe discharge under the partly full depth condition in soil pipes.

There is no information that can confirm whether these open channel flows actually occur at any head slopes. However, the concave curvilinear correlations in Figure 10 must disclose the occurrence of partly full depth condition in soil pipes or drainage networks causing the open channel flow.

3. 2. 4 Subsurface water discharge regime

Table 4 shows the subsurface water discharge regime from the head hollow of the Jozankei Watershed :

(1) The drainage capacities of the soil pipes had a small effect on subsurface water discharge during low flows, and subsurface water discharge shows linear correlations to the hydraulic head gradient ($a = 1$ in eq. (2)). Matrix flow contributed chiefly to subsurface water discharge and DARCY's law elucidates the subsurface water discharge regime.

(2) Pipe flow intensively affected the subsurface water discharge regime during runoff events.

    1) In the high drainage capacity of the soil pipes (or drainege networks), the flow via the soil pipes shows hydraulic property as the open channel flow (the partly full depth condition). The increase in pipe discharge with the rising of the hydraulic head gradient of subsurface water flow created the abrupt increase in subsurface water discharge (the concave curvilinear correlation ; $a > 1$ in eq. (2)).

    2) In the low drainage capacity of the soil pipes (or pipe networks), the flow via soil pipes

Table 4　Modes of subsurface discharge at the valley head of the Jozankei Watershed.

	During small flow	During storm runoff	
Dominant pathways of subsurface flows	Matrix	Pipe	
Drainage capacities of pipes	Mostly unrelate	Large	Small
Dominant flows	Matrix flow	Open-channel flow	Pipe flow
Equation	Darcy	?	Manning Darcy- Weisbach
Coefficient "a" in Eq.(2)	a=1	a>1	a<1
Correlation curves shown in Fig.10			

shows the hydraulic property as being full of water in soil pipes (the full flow condition), indicating the reduction of the increasing ratio of pipe discharge with the rising of the hydraulic head gradient of subsurface water flow. The increasing ratio of subsurface water discharge also decreased with the rising of the hydraulic head gradient of subsurface water flow (the convex curvilinear correlation : $a < 1$ in eq. (2)).

(3)　The various curvilinear correlations during the snowmelt season, shown in Figure 10, indicate that the drainage capacities of soil pipes (or drainage networks) changed at every runoff event. This changeable drainage capacity of soil pipes, accompanied with their expansion, retrenchment, and closing, is often induced in slopes, so that various subsurface water discharge regimes appear in the slopes of head waters.

(4)　An abrupt formation of a shallow groundwater level, destroying the steady state hydraulic condition at slopes during heavy rain, provided insufficient pipe flow to the subsurface drainage (i.e., the low drainage capacity of soil pipes). If the drainage capacity of soil pipes is not restored by the contribution of the other soil pipes to the subsurface drain or by subsurface hydraulic erosion, it is impossible to drain subsurface water in slopes through soil pipes in a sufficient amount and rate. Accordingly, if more rain is supplied to the slopes, generation of saturated overland flow or sediment movement in subsurface portions can release the subsurface hydraulic pressure in the slopes. That is, changes in the drainage capacity of soil pipes are closely related with the mechanism of overland flow generation and sediment production at the slopes of headwaters.

4.　Coarse-grained sediment production

4. 1　Dynamics on sediment yield initiation

In order to provide a physical understanding of both piping with coarse-grained sediment discharge and the mechanism of subsurface hydraulic erosion, theoretical equations regarding the hydraulic agent of coarse-grained sediment discharge at slopes are given below.

4.1.1 Seepage force and hydraulic gradient

DUNNE (1980) described how spring sapping and seepage erosion such as piping primarily caused soil movement through the agent of subsurface water flow, and the change in seepage force was an important index for describing the erosion by subsurface water flow.

Seepage force of subsurface water flow affecting a unit volume of soil under the steady state hydraulic condition is given by CEDERGREN (1977) as :

$$F_{sf} = \rho_w g i \tag{5}$$

where F_{sf} is the seepage force of subsurface water flow, ρ_w is the subsurface water flow density, g is the gravitational acceleration, and i is the hydraulic gradient. Since $\rho_w g$ in eq. (5) indicates the unit weight of subsurface water flow, F_{sf} is modified for unit length of soils as

$$F_{sf} = \rho_w A g i = A \gamma_w i \tag{6}$$

where A is the flow section area, γ_w is the unit volumetric weight of subsurface water flow that has a narrow range in variation under normal air temperature ($\gamma_w = 1$ (tf·m^{-3}) $= 1$ (gf·cm^{-3})). Thus, the seepage force depends on the change in the hydraulic head which reveals the primary significance for sediment movement by subsurface water flow. YASUHARA *et al.* (1984) reported that the hydraulic gradient during a storm was larger than that before the storm at a valley head of a hillslope, and they discussed the possibility of pipes forming through the subsurface sediment movement as seepage force changes. In addition, SAKURA *et al.* (1987) conducted that the instantaneous vertical ascending hydraulic gradient to a slope surface ranged between 0.5 and 1.0 for the flotation of sand particles and that sandy soils liquified when hydraulic gradients exceeded 1.0.

Saturated subsurface water flow flux in soils is expressed as

$$q = K_s i \tag{7}$$

where q is the subsurface water flow flux in saturated soils and K_s is the saturated hydraulic conductivity of soils. Eqs. (5), (6), and (7) indicate that an increase in the subsurface water flow flux with a rising of the hydraulic gradient induces sediment movement through the increment of seepage force that influences slope soils.

On the other hand, on account of the various hydraulic gradients and flow directions of subsurface water flow in slopes during storms, the direction of subsurface water flow is an essential element in the sediment movement caused by piping as well as the change in the hydraulic head gradient (IVERSON and MAJOR, 1986 ; HOWARD and MACLANE, 1988 ; REID and IVERSON, 1992). That is, if the hydraulic head of saturated subsurface water flow is sufficient for liquefaction and if the direction of flow that can transport coarse-grained particles from slopes is ascending enough to a slope surface, there is a large possibility that piping will be initiated in slopes.

The dynamics of the sediment movement caused by liquefaction or by shear destruction are arranged in the following sections with consideration of the changes in the hydraulic gradient and the direction of subsurface water flow.

4.1.2 Liquefaction and seepage force

Critical conditions for piping initiation at a slope which is composed of cohesionless, isotoropic, and homogenous sand is given by ZASLAVSKY and KASSIFE (1965) for a case in which the saturated subsurface water flow is ascending perpendicular to a slope surface :

$$i_n = \frac{\rho_s - \rho_w}{\rho_w} (1-n) \cos\theta \frac{1}{a_1} \tag{8}$$
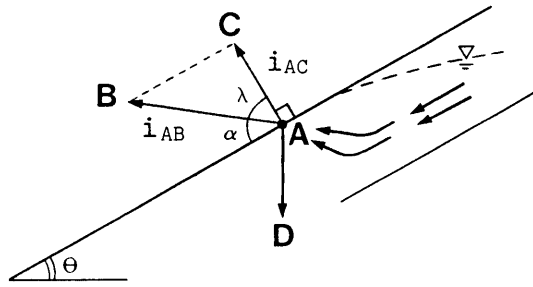
Fig. 19　Schematic illustration of saturated subsurface flow, seepage force, and gravitational force affecting a clod on a slope.

where i_n is the vertical ascending hydraulic gradient of saturated subsurface water flow to the slope surface, ρ_s is the density of sand, n is the porosity, θ is the slope inclination, and a_l is the shape coefficient of soil particles which is usually negligible (i.e., $a_l = 1$) from experimental evidence. If piping results from liquefaction, eq. (8) is adequate for analyzing the relationship between piping and liquefaction originating in cohesionless soils. Eq. (8), however, is applicable only to piping caused by the vertical subsurface water flow to a slope surface. As previously described, the direction of subsurface water flow varies at slopes, so that the effect of the direction of subsurface water flow on liquefaction has to be combined into eq. (8).

Figure 19 shows the schematic conditions of saturated subsurface water flow, seepage force, and gravitational force affected on a soil clod at a slope with an infinite length, the inclination θ, and the conditions for an isotropic and homogeneous soil layer. The following assumptions are made for the subsurface water flow agent affecting point A in Figure 19 : Slope soils at the site of piping initiation are saturated with subsurface water, and not overland flow but saturated subsurface water flow causes all sediment discharges that accompany pipe formation. When the vertical ascending subsurface water flow seeps from the subsurface to point A and seepage force acts on a soil clod at point A, vector AC exhibits the seepage force. The combination of AC and AD (gravitational force of the soil clod) provides the seepage force that removes the clod by liquefaction. If the direction of the combined force is parallel to a slope, then the situation indicates a critical condition for piping initiation, and just a slight ascending direction of subsurface water flow will rapidly create piping. The hydraulic gradient of this critical subsurface water flow in Eq. (8) is modified for piping caused by liquefaction as follows :

$$i_{AC} = \frac{\rho_s - \rho_w}{\rho_w}(1 - n)\cos\theta \tag{9}$$

where i_{AC} is the critical hydraulic gradient perpendicular to a slope surface resulting in eq. (8).

In contrast, the vector AB indicates the seepage force of all directions of subsurface water flow affecting a clod at point A. The critical condition of piping initiation by such a flow, therefore, is that the combined force of AB and AD is parallel to a slope surface. That is, the condition is given from eq. (9) by :

$$i_{AB} = i_{AC}\sin^{-1}\alpha = \frac{\rho_s - \rho_w}{\rho_w}(1 - n)\frac{\cos\theta}{\sin\alpha} \tag{10}$$

where i_{AB} is the critical hydraulic gradient for any direction of subsurface water flow and α is the

angle between the direction of the slope surface and subsurface water flow (positive for ascending direction to the slope). Even though the hydraulic gradient is large, the condition of $\alpha \lesssim 0°$ (parallel to and descending the slope surface) adds a descending force to the sediment, which increases the submerged weight of the soil. This indicates that sediment removal outside a slope by piping is impossible in this situation. Thus, α in eq. (10) ranges from the ascending to vertical directions to a slope surface ($0° < \alpha \leq 90° + \theta$). This fact demonstrates the applicability of eq. (10) to piping occurring in a cohesionless soil.

KOHNO *et al.* (1987) studied the critical hydraulic gradient of cohesive soils under the one-dimensional vertical flow condition, and they obtained :

$$i_{cr} = \frac{\rho_s - \rho_w}{\rho_w}(1-n) + \frac{2c}{r_p \rho_w g} \tag{11}$$

where i_{cr} is the critical hydraulic gradient, c is the cohesion of a soil, and r_p is the radius of a circle when seepage force acts on a circular cross-section of the soil. Eq. (11) is in equilibrium with eq. (8) under $\theta = 0$ and a cohesionless soil. Eq. (11), therefore, supplies important information on piping caused by one-dimensional saturated subsurface water flow in cohesive soils.

4.1.3 Shear destruction and seepage force

When subsurface water flow seeps from a soil surface slowly, shear destruction in the soil precedes liquefaction of the soil (IVERSON and MAJOR, 1986). In this case, the critical condition of sediment movement caused by shear destruction at a slope composed of an isotoropic and homogeneous sand is given by the following equation :

$$i_c = \frac{\rho_s - \rho_w}{\rho_w}(1-n)\frac{\sin(\phi - \theta)}{\sin(\lambda + \phi)} \tag{12}$$

where ϕ is the angle of internal friction of a porous medium, and λ is the angle between the normal direction to a slope surface and flow directions. In eq. (12), the qualification of $\theta \geq \phi$ and $0° \leq \lambda + \phi \leq 180°$ derives $i \leq 0$ under the situation of $90° \leq \lambda \leq 180° - \phi$. This shows the descending subsurface water flow to a slope surface at a steep slope whose angle is larger than the internal friction, and indicates that the slope is being destabilized and a landslide may instantaneously occur. Piping does not necessarily always take place in the case of descending subsurface water flow to slope surfaces. Accordingly, eq. (12) is not applicable to piping at a steep slope composed of sediments of $\theta \geq \phi$. That is, the confirmation of $\theta < \phi$ and $-\theta \leq \lambda \leq 90°$ in eq. (12) is indispensable for the analysis of piping caused by shear destruction.

In addition, taking into account the balance of torque acting on soil, KOCHEL *et al.* (1985) improved the critical condition of sediment movement caused by shear destruction with negligible surface flow :

$$i_c = \frac{C_1}{C_2}\frac{\rho_s - \rho_w}{\rho_w}\frac{\sin(\phi - \theta)}{\cos(\theta + \nu - \phi)} \tag{13}$$

where C_1 and C_2 are the coefficients for soil particle shape and packing, and ν is the angle between horizontal direction and flow direction. The complete evaluation of C_1/C_2 is impossible owing to the heterogeneity of soils on slopes. Eq. (13) is, therefore, inapplicable to the analysis in this study.

4.2 Analysis of coarse-grained sediment yield with piping

4.2.1 Numerical analysis using the Finite Element Method

In order to understand the unsteady two-dimensional hydraulics in an isotropic and homogeneous slope, the Finite Element Method (FEM) was applied to quantify the changes in the

hydraulic gradient and flux of subsurface water flow at a slope (see Fig. 4 and Photo 5) where a soil pipe and a depression were created during a storm.

The slope was first divided into many parts with small triangles in the FEM. The average value of the hydraulic heads and fluxes of subsurface water flow, calculated for each apex, were expressed at the gravitational center of the individual triangles. Rainfall intensities of 10 min intervals during a storm event (24 to 26 September, 1988) were inserted to the FEM calculation. Slope inclination (45°), horizontal distance (15 m), and permeable soil depth (5 m), corresponding to the location of the depression shown in Figure 4 and in YAMAGUCHI (1963), were used in the FEM calculation. The effect of the three-dimensional concentration of subsurface water flow was negligible because of the topographical smoothness at the slope surface. Eq. (7) derived the flux of subsurface water flow based on the hydraulic conductivity of saturated and unsaturated flows. The average saturation hydraulic conductivity of soils, calculated both from the four samples in the head floor shown in Table 3 and the other four samples at the depression shown in Table 5 and in 4.2.2, was applied in the FEM calculation.

The following equation (BRUTSAERT, 1968 ; TANI, 1982) expresses the unsaturation hydraulic conductivity based on a saturation hydraulic conductivity (K_s) and the moisture characteristics curve (C2-50) shown in Figure 5 as :

$$K = K_s M_e^{\beta} \tag{14}$$

where K is the unsaturated hydraulic conductivity, and M_e is the effective moisture content given by :

$$M_e = (\theta_a - \theta_r)(\theta_s - \theta_r)^{-1} \tag{15}$$

where θ_a is the practical soil moisture content, θ_r is the field capacity, and θ_s is the saturated water content equal to the porosity. In addition, β is given by :

$$\beta = \theta_a \phi^{-1} \tag{16}$$

where ϕ is the pressure head of subsurface water flow.

Neither the changes in the hydraulics of subsurface water flow with the enlargement of soil pipes nor the physical characteristics of soils such as heterogeneity, the angle of internal friction, and soil cohesion, were combined into the FEM calculation. The boundary conditions were described as follows : The fact that the perennial flow was produced at the bottom of the slope in the Kitadani Watershed established a shallow groundwater table at the lower end of the model slope. Subsurface water flow from the model slope was impeded to flow out toward the opposite site of the model slope without passing through under the stream, owing to the emergence of subsurface water flow from the opposite facing slope. Thus, subsurface water flow from the model slope was drained completely in the stream in the Kitadani Watershed. The rainfall supplied to the model slope did not flow out to the other slopes beyond the drainage divide on the ridge. Additionally, the cone penetration test completely delineated the boundary between the regolith zone and the basement rock at $N_{10} = 40$. Thus, the bottom of the model slope reached the basement rock that acted as an impermeable zone for quick subsurface water discharges.

Figure 20 shows the temporal variation in the hydraulic gradient (a) at the foot of the slope where piping was initiated, and the hydrographs of the valley head drain (b) measured at the W 2-weir and the Kitadani Watershed (c) measured at the W1-weir (see Fig. 3). The data on the hydrographs of (b) and (c) were obtained from the Tokyo University Forest in Aichi. The hydraulic gradient (a) increased gradually from 0.03 to 0.05 rise·h⁻¹ with the storm on 25

Table 5   Saturated hydraulic conductivity, critical hydraulic gradient obtained by liquefaction experiments, and type of liquefaction.

Sample name	Saturated hydraulic conductivity (ms^{-1})	Critical hydraulic gradient	Type of Liquefaction
Toyoura sand	1.68×10^{-4}	1.01	Boiling
Corresponding slope			
Depression 1(V)	2.30×10^{-5}	〈 1.03 / 1.11	Tunneling / Boiling
Depression 1(L)	2.30×10^{-5}	1.14	Tunneling
Depression 2(L)	5.95×10^{-5}	1.31	Tunneling
Depression 3(L)	5.95×10^{-5}	1.52	Tunneling
Pipe 1(L)	2.11×10^{-5}	1.42	Heaving
Pipe 2(L)	3.67×10^{-6}	1.42	Heaving
Pipe 3(V)	6.43×10^{-8}	—	—
Akatsu watershed			
Head floor (V)	8.86×10^{-5}	—	—
Side slope 1(V)	1.16×10^{-4}	—	—
Side slope 2(V)	1.90×10^{-4}	—	—
Side slope 3(V)	3.67×10^{-5}	1.73	Heaving
Crest slope (V)	6.30×10^{-5}	1.10	Tunneling

— marks mean that liquefaction of samples did not occur with a hydraulic gradient below 2.0.
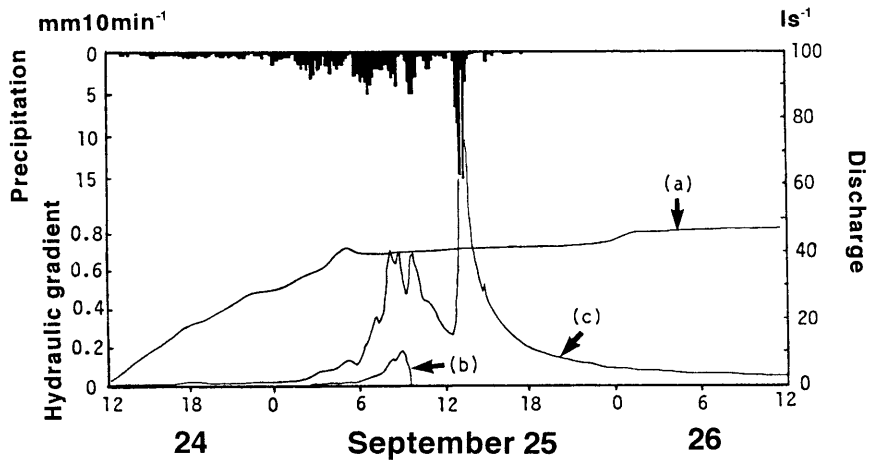
Fig. 20   Hydraulic gradient at the soil pipe calculated by numerical analysis (a), and hydrographs in the valley head (b) and the Kitadani watershed (c).

September, but, it rose suddenly from 0.6 to 0.8 (0.2 rise·h⁻¹) from 4 : 00 to 5 : 00 and formed a peak at about 0.8 at 5 : 00. The hydraulic gradient then decreased after the peak ranging between 0.7 and 0.8 regardless of the change in rainfall intensity. The maximum hydraulic gradient near the

(A) Hydraulic gradient　　(B) Flow flux

...... Water table
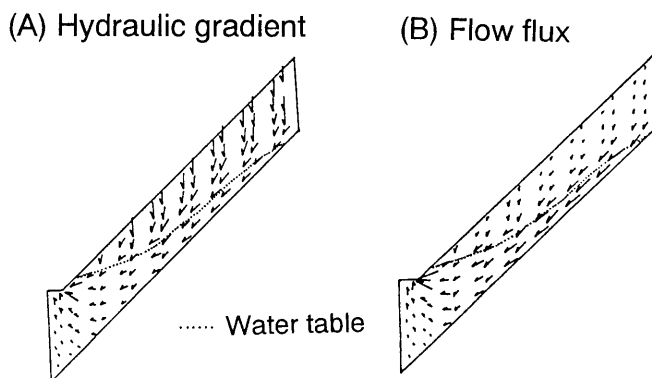
Fig. 21　Hydraulic gradient and flux of subsurface flow in the model slope when hydraulic gradient shown in Fig. 20 represented the first peak.

soil pipe was at least about 0.8 in the two-dimensional model slope of 45° in inclination, 15 m in length, and 5 m in regolith thickness. One reason for the gradual rising of the hydraulic gradient on 26 September may be the no program on the pressure release of subsurface water flow associated with pipe formation.

In contrast, the stream flow (b) from the valley head drain measured by the W2-weir decreased suddenly at 10 : 00 on 25 September. This interruption of flow measurement signifies that sediment yield from the soil pipe and its deposition in the W2-weir interrupted the continuous measurement of stream flow at around 10 : 00. The lack of deposition of sediment enabled the continuous measurement of stream flow at the W1-weir.

Figure 21 shows the spatial distribution of both the hydraulic gradient and flux of subsurface water flow at the model slope at 6 : 00 on 25 September, 1988, calculated by the FEM. The shallow groundwater table expanded gradually with the continuity of rainfall, eventually reaching the upper portion of the slope at the peak in the hydraulic gradient. While the hydraulic gradient (A) exhibited a larger value in the unsaturated zone at the upper portion of the slope, the directions were almost all vertically descending. The hydraulic gradient at the downslope became parallel or ascending to the slope surface. A relatively large hydraulic gradient of saturated subsurface water flow, corresponding to the peak in the hydraulic gradient in Figure 20, appeared at the boundary between the down slope end of the slope surface and the head floor.

Subsurface water flow fluxes (B) had low intensity and the descending directions in the unsaturated zone at the upper slope, but, saturated subsurface water flow with high intensity of flux dominated below the water table. At the downslope, subsurface water flow in an ascending direction and with a high intensity of flux occurred, and the concentration of the flow was simultaneously promoted at the foot of the slope with the formation of a knick point. The ascending flow established the most upward direction with an angle of 72° at the peak in the hydraulic gradient shown in Figure 20. Consequently, these subsurface water flows exhibited at the down slope end must have initiated piping and created the soil pipe.

4.2.2　Experiment on liquefaction of granitic soils

A liquefaction experiment under one-dimensional steady state hydraulic conditions disclosed the true values of the hydraulic gradient to cause piping in undisturbed soil samples of 100 cm³

soil cores, collected either near the soil pipe below the depression or in the Akatsu Watershed (see Fig. 3).

Figure 22 schematically shows the experimental equipment which enabled the hydraulic gradient to be measured when piping began in the soil samples. The 100 cm³ soil cores filled with the samples were installed at the end of the equipment. The saturation hydraulic conductivity of the paper filter was 1.0×10^{-3} m·s⁻¹ which was larger than the conductivity of the samples. The change in the position of a tank with a constant water level in the tank derived the hydraulic gradient under the quasi-steady-state hydraulic condition (0.1 rise·h⁻¹ in the hydraulic gradient) from :

$$i = \Delta h l_S^{-1} \tag{17}$$

where Δh is the hydraulic head difference between the surface of the samples and the water level in the tank, and l_S is the thickness of the samples.

Critical hydraulic gradients (CHG) to cause sediment movement in this study were calculated from eq. (17) through visual observations of the removal of soil particles and/or clods. In general, during a liquefaction experiment, the abrupt changes in water discharge from the surface of a sample supply the CHG under the gradual change in the hydraulic head. This is because the hydraulic conductivity of the sample becomes larger as fine-grained particles are removed and resultant water discharge from the surface of the sample increases. The measurement of water discharge from the sample is, therefore, more accurate for the soil particle movement than the visual determination of piping initiation. In many cases in liquefaction experiments, a suspension of very fine-grained particles, indicating piping initiation, occurs before the hydraulic gradient reaches its critical value. However, in this study, the time when sand-sized particles or soil clods actually and obviously began to move was recognized as the piping initiation. Thus, the values of the CHG introduced here are likely to be larger than those in usual cases because of the no attention to removal of fine-grained particles.

Table 5 shows the experimental results for the soils in the corresponding watershed and the Toyoura standard sand which was used as the control. The parentheses after the sample names indicate the samples collected vertically (V) and laterally (L) at each soil profile. The samples termed as "depression 1 to 3", "pipes 1 and 2", pipe 3, "head floor", "side slopes 1 and 2", "side slope 3", and "crest slope" were collected at the upper small scar of the depression (0.5 m deep), the side wall of the soil pipe outlet (0.3 m deep), the bottom of the soil pipe outlet, and the head floor (1 m deep), the surface of the side slope, 0.2 m deep of the side slope, and 0.3 m deep on the ridge in the Akatsu Watershed, respectively (see Figs. 3 and 4 and Photo 5 for the locations of sampling). The
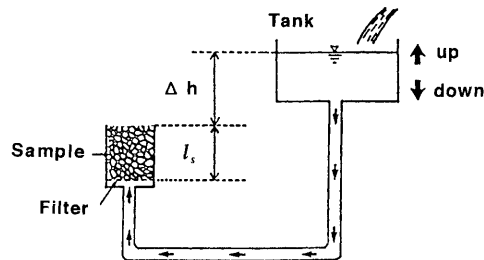

Fig. 22   Schematic illustration of an apparatus used in the liquefaction experiment.

- symbols in Table 5 indicate that liquefaction was not induced at a hydraulic gradient below 2.0.

All the CHGs registered values higher than 1.0 with the various types of piping. In the Toyoura sand, boiling occurred at the hydraulic gradient of 1.0 and the sample liquefied completely. Tunneling was induced in the sample of the depression 1 (V) at the hydraulic gradient of approximately 1.0 ; however, it liquefied completely with the boiling after the further ascent of the hydraulic gradient. This phenomenon demonstrates that two types of liquefaction were present in one sample. The samples at the depression maintained lower CHGs than those near the soil pipe outlet (Pipes 1 to 3) and they tended to create the tunneling. The low hydraulic conductivity was represented and the heaving was created in the samples of Pipe 1 and 2 at the hydraulic gradient of 1.42. The samples at the side slope in the Akatsu Watershed seemed to have relatively high hydraulic conductivity and CHGs. The sample at the crest slope in the Akatsu Watershed caused tunneling at the hydraulic gradient of 1.10 with low hydraulic conductivity.

4.3 Mechanism of coarse-grained sediment discharge

4.3.1 Sediment movement by liquefaction for cohesionless soils

The mean values of the physical properties of the slope soils in the Akatsu Watershed are $\rho_s g = 2.58$ $(tf \cdot m^{-3})$ and $n = 0.38$ (see Table 2). when $\rho_{wg} = 1.0$ (tf·m^{-3}), eq. (10) is modified as

$$i_{AB} = 0.98 \cos\theta \cdot \sin^{-1}\alpha \tag{18}$$

Accordingly, subsurface water flow causes liquefaction for the cohesionless soils in this granodiolite region at the values exceeding i_{AB} in eq. (18). That is, eq. (18) reveals the relationship between the direction of subsurface water flow (α) and the piping initiation by liquefaction in the cohesionless soils under the slope inclination θ.

Figure 23 shows the relationship between the direction and the CHG of subsurface water flow for the cohesionless soils, derived from eq. (18). At the same α, the gentle slopes require a larger hydraulic gradient to cause piping by liquefaction than the steep slopes. when subsurface water flow had a vertical ascending direction ($\alpha = 90°$ for $\theta = 0°$, $\alpha = 120°$ for $\theta = 30°$, $\alpha = 135°$ for $\theta = 45°$, and $\alpha = 150°$ for $\theta = 60°$), the CHGs were a constant 0.98 for each slope inclination. Figure 23 indicates that the slope inclination of 45° and the maximum hydraulic gradient of 0.8, which were calculated by the FEM, require $60° \leqq \alpha \leqq 120°$ for the sediment discharge by liquefaction. In contrast, Figure 21 shows $\alpha = 72°$ at the timing of a maximum hydraulic gradient calculated at the downslope end where piping initiated. This suggests a satisfying of the condition needed for piping initiation by liquefaction (it needs $i = 0.73$ for $\alpha = 72°$). That is, when there was no cohesion in the slope soil of the Kitadani Watershed, the maximum hydraulic gradient of 0.8 and the direction of subsurface water flow of 72° were sufficient to cause the piping triggered by liquefaction.

4.3.2 Sediment movement by shear destruction for cohesionless soils

According to IVERSON and MAJOR (1986), shear destruction must cause piping at a smaller hydraulic gradient before reaching the CHG to produce liquefaction. Thus, the relationship between shear destruction and sediment movement is examined in the following part.

OSAKA et al. (1992) proposed the following equation for the granodiolitic soils measured in the Akatsu experimental forest of Tokyo University :

$$\phi' = 29.6 + 9.20 \, ln(N_c) \tag{19}$$

where ϕ' is the internal friction angle of the soils inferred from the N_c-value, ln is the natural logarithm, and N_c is the number of beating which needs to penetrate the cone to 10 cm deep ($=$

Fig. 23 Relationships between the direction and critical hydraulic gradient of saturated subsurface flow in case of cohesionless soil according to Eq.(18).

N_{10}), supplied from the cone penetration test. The penetration resistance of the soils at the head floor and side slope in the Akatsu Watershed was in the range $1 \leq N_{10} \leq 5$ (see Table 2). Eq. (19), therefore, supplies the internal friction angle of $29.6° \leq \phi \leq 44.4°$ for the valley head soils around the Akatsu Watershed.

Eq. (12) provides the relationship between shear destruction and the CHG with the parameter θ under the condition of $30° \leq \phi \leq 45°$. Under $\rho_s g = 2.58$ (tf·m^{-3}) and $\rho_w g = 1.0$ (tf·m^{-3}), eq. (12) transforms λ into $\lambda = 90° - \alpha$ and is modified as

$$i = 0.98 \frac{\sin(\phi - \theta)}{\sin(90° - \alpha + \phi)} \tag{20}$$

Eq. (20) represents the relationship between i and α in shear destruction as shown in Figure 24, where "M.V." indicates the maximum value of the hydraulic gradient calculated by the FEM. Independently of the ϕ-values, i decreased with an increase in θ at the same α. If the slope inclination was large, a small hydraulic gradient was required for shear destruction occurring in the same direction as subsurface water flow. The peaks in both α ($=72°$) and i ($=0.8$) evaluated from the FEM exceeded the threshold for shear destruction for every combination of ϕ and θ. The hydraulic gradient by the FEM was particularly higher than this threshold at steeper slopes such as $\theta \geq 30°$. Thus, slow subsurface water discharge near the site of the piping initiation may have induced the initial sediment discharge caused by shear destruction before liquefaction. If shear destruction was responsible for piping, the sediment discharge occurring on 24 September should also be considered as well as sediment production caused by liquefaction on 25 September.

4.3.3 Effect of soil cohesion on the critical hydraulic gradient in the liquefaction experiment

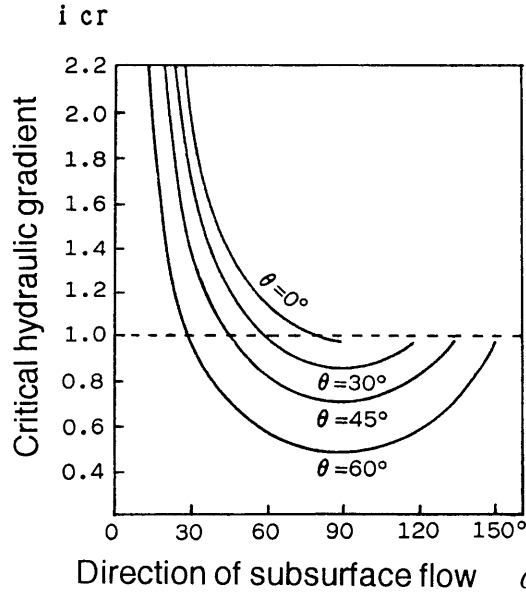In the relationship between the cohesion of the soil and the CHG, the condition of $\theta = 0°$, $\alpha =$
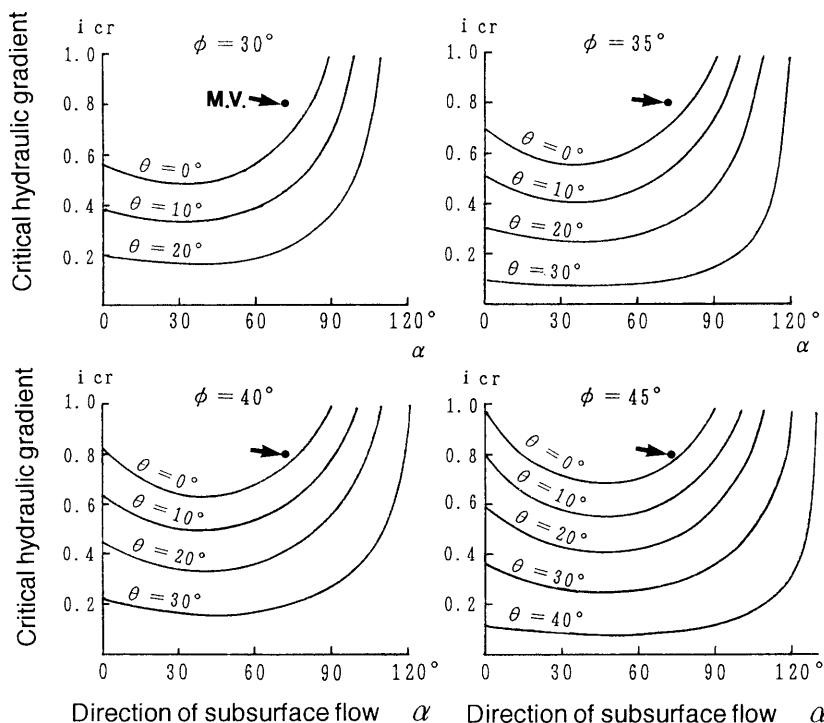
Fig. 24　Relationship between the direction and critical hydraulic gradient of saturated subsurface flow in case of cohesionless soil according to Eq.(12). "M.V." in the figure indicates the combination of maximum value of hydraulic gradient and flow direction calculated by numerical analysis.

$90°$, $\rho_s g = 2.58$ (tf·m^{-3}), and $\rho_w g = 1.0$ (tf·m^{-3}) modifies eq. (11) into

$$i = 0.98 + 2cr^{-1} \tag{21}$$

The liquefaction experiment satisfies the limits for liquefaction (i.e., under the vertical ascending flow condition, which is indicated by IVERSON and MAJOR (1986) and eq. (21)). Thus, eq. (21) identifies sufficiently the piping mechanism in the liquefaction experiment.

Figure 25 shows the relationship between i_c for the ambient soil of the Kitadani Watershed and r with the parameter c based on eq. (21). When the cohesion is negligible as a sand (i.e., $c=0$), all soil particles can move individually at $i_c=0.98$ for the corresponding samples at the study site, implying that boiling can occur under this condition. When the CHG is around 1.5, the radius of a soil pipe becomes larger with an increase in the cohesion of the soil, meaning that heaving can occur in cohesive soils. That is, sediment movement in cohesive soils at small CHGs requires a large failure region, and soils are extensively removed just like a clod.

The differences in liquefaction styles such as boiling, tunneling, and heaving shown in Table 5 results from the heterogeneity and cohesion of the soil samples. That is, when hydraulic gradient reached the critical value, boiling could be instantaneously created in cohesionless soils such as Toyoura sand by the liquefaction of individual soil particles. In the heterogeneous samples, water selectively and intensively passes through the permeable (and less cohesive) zone in the samples with the rising of the hydraulic gradient. Thus, tunneling must have been induced

i cr
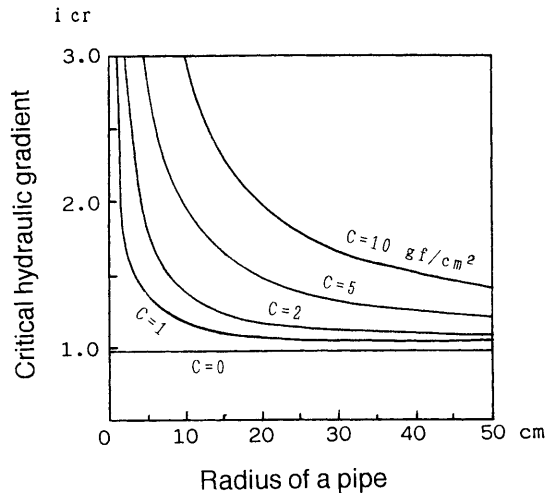
Fig. 25   Relationship between the radius of soil pipe and critical hydraulic gradient for different values of soil cohesion from eq.(11).

at the permeable and cohesionless zones in the samples by liquefaction. In addition, since cohesive soils require a larger radius of failure region by seepage force at the hydraulic gradient of 1.5, which was beyond the radius of the soil core of 0.025 m, heaving must have been induced in the samples.

TANAKA et al. (1984) reported that the ratio (K_0/K_s) constructed by the saturation hydraulic conductivity of soils (K_s) and the filter (K_0) used in experiments affected the type of seepage failure. That is, tunneling and boiling were induced at $K_0/K_s > 15$ and $1 < K_0/K_s < 5$, respectively. In the present liquefaction experiment, K_0 is the saturation hydraulic conductivity of the paper filter $(1.0 \times 10^{-3} \text{m} \cdot \text{s}^{-1})$. Thus, all samples excluding the samples in $K_s = 10^{-1} \text{m} \cdot \text{s}^{-1}$ shown in Table 5 are under the condition of $K_0/K_s > 15$. This indicates that tunneling occurs in the experiment. However, three types of liquefaction, such as boiling, tunneling, and heaving, occurred in the samples. This was not always consistent with the description by TANAKA et al. (1984). This fact supports that the cohesion and heterogeneity of samples provide the difference in the liquefaction style rather than the relation between the saturated hydraulic conductivity of samples and filters. Despite the extensive dependence of soil samples on the cohesion and heterogeneity of the liquefaction style, these physical properties of soils were ignored for measuring K_s by TANAKA et al. (1984). Thus, the results in TANAKA et al. (1984) can not be applied to interpret the sediment movement indicated here.

4.4   Topographic change and forest devastation by piping

Figure 20 represents the gradual rising of the hydraulic gradient with rainfall, and the abrupt increase in the hydraulic gradient appeared prior to its peak. There is no useful evidence for understanding the cause of piping ; that is, the piping initiation depended on shear destruction at the smaller hydraulic gradient indicated by IVERSON and MAJOR (1986) or on liquefaction with an abrupt increase in the hydraulic gradient exceeding the CHG. At any rate, the maximum hydraulic gradient obtained by the FEM showed a sufficient value to remove the soil particles or clods by liquefaction. Accordingly, liquefaction with the ascending change in subsurface water

flow direction and with the abrupt increase in the hydraulic gradient ($i = 0.8$, at 6 : 00 on 25 September) or shear destruction on 24 September, at the foot of the slope, must have initiated sediment discharge with piping. Sediment discharge likely continued until a decrease in the hydraulic gradient or the change in subsurface water flow to the descending direction, and the sediment entirely buried weir-W2 at about 10 : 00 on 25 September, subsequently interrupting the stream flow measurement there.

In addition, the observation and the results shown in Table 5 and Figure 25 strongly indicate that the large and small CHGs were required for the soil near the soil pipe outlet and in the depression, respectively. The hydraulic gradient, therefore, seemed to have been large at the piping initiation. Since the soil pipe enlarged with the progression of piping into the sandy (less cohesive) soil in the depression, which showed small CHGs in the liquefaction experiment, a larger hydraulic gradient was not required for the pipe expansion. The area of piping expanded optionally in the slope soil during the storm with the change in the hydraulic gradient and the direction of subsurface water flow.

As described in Chapter 2, forest devastation resulting from the formation of a depression with piping also occurred in September 1989, in which the rainfall amount was similar to the storm episode in September 1988. Accordingly, these sediment discharges from slopes must sometimes be repeated during heavy rains and bring about subsurface hydraulic erosion as progressive failure at slopes. Moreover, topographic changes at slopes derives the forest devastation.

The depression by piping often characterizes the topography of slopes as rills and gullies, so that not only the denudation process by overland flow but also seepage force of subsurface water flow is involved with sediment removal from slopes as the initial process of rill and gully formation. Furthermore, since stream flow generation and piping occur at the same sites, sediment movement with subsurface hydraulic erosion makes a significant contribution to hillslope evolution through the upstream migration of the site of stream flow generation.

The magnitude of the hydraulic gradient and the direction of subsurface water flow are important factors affecting piping, and the cohesion of slope soils and the area on which seepage force acts significantly affect the formation and enlargement of soil pipes as sediment is removed from slopes. However, the mechanism of piping has not been explicated completely by liquefaction experiments. That is, there is still debate regarding which of the following two theories explain cause of piping :

① The gradual change in hydraulic gradient on 24 September, 1988 (according to the theory proposed by IVERSON and MAJOR, 1986)

② The exceeding CHG or the abrupt rising of the hydraulic gradient prior to its peak on 25 September, 1988

The reason for remaining above two theories depends certainly on no observation data on the temporal variations in subsurface water discharge and sediment yield, and on the little quantitative comprehension of the relationship between subsurface water flow and sediment yield in head slopes.

For a more quantitative understanding of the relationship between subsurface water discharge and sediment yield, the author has attempted to analyze the process of fine-grained sediment production in subsurface water flow, which is easy to measure the temporal variation.

5 Fine-grained sediment production

The previous chapters revealed the following information about subsurface water discharge and coarse-grained sediment in head slopes : (1) Water via soil pipes contributes intensively to the subsurface water discharge regime at a head slope during storms (Chapter 3), and (2) coarse-grained sediment discharge results in piping accompanied with creating a soil pipe at a head slope (Chapter 4).

Most sediment discharges from slopes resulting from the agent of subsurface water flow, therefore, must be produced through preferential flow pathways typical in soil pipes. In this chapter, in order to understand the effect of soil pipes on subsurface sediment movement, the author analyzes the process of fine-grained sediment discharge passing chiefly through soil pipes.

5.1 Pipe flow and fine-grained sediment yield

Figure 26 shows the relationships among the hydraulic head gradient $i_{(W1)}$, subsurface water discharge, and fine-grained sediment yield during the rising limb of the storm hydrograph on 27 May and 16 September 1994, when the shallow groundwater levels in well W1 were completely measured without any interruption caused by problems with data loggers.

Subsurface water discharge tended to show concave curvilinear correlations between 0.25 and 0.39 of the hydraulic head gradient on 27 May and between 0.36 and 0.45 on 16 September. On 16 September, overland flow was initiated in the rill running between well W1 and the spring when the correlation line changed convexly near 0.45.

Fine-grained sediment reached peaks at 21 : 00 on 27 May and at 11 : 00 on 16 September, and both peak times coincided well with the gradient changes in concave correlation lines as shown in Figures 10, 16 b, and 17. Almost no gradient changes in the more concave curvilinear correlation were observed after the sediment peaks. That is, as will be described in Chapter 6, no sediment discharge during the snowmelt created the concave curvilinear correlation in the $i_{(W1)}$ Q_l relation, showing the indistinct alteration of the gradient (see Fig. 10). In contrast, sediment production during the storms provided a notable gradient change in the $i_{(W1)}$ Q_l relation.

The concave curvilinear correlation of subsurface drainage with the hydraulic head gradient, as described in Chapter 3, corresponds to an optimum drainage condition where preferential flow networks, including soil pipes, drain subsurface water from the head hollow. Therefore, the
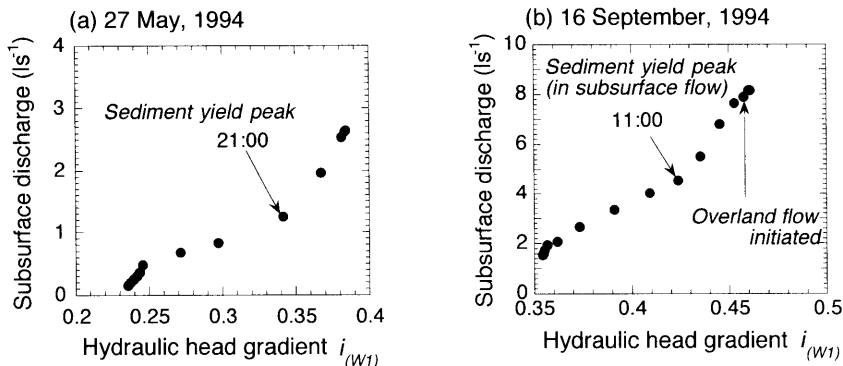

Fig. 26 Relationship among hydraulic head gradient, subsurface discharge and fine-grained sediment on (a) 27 May and (b) 16 September in 1994.

sediment peak preceding the peak in subsurface water discharge affects the sudden increase in the subsurface drainage capacity of the head hollow during the rising limb of the hydrograph, and interacts with the subsurface water flow system in the head hollow between well W1 and the spring.

Consequently, the fine particles occurring between well W1 and the spring affected the sediment peak at the spring, resulting from subsurface hydraulic erosion caused by preferential flows (including pipe flow). Thus, the main origin of the fine particles was possibly the site between well W1 and the spring. Since the particles measured after the sediment peaks scarcely affected an increase in the drainage capacity of the head hollow soil between well W1 and the spring, these sediments came not from the site between well W1 and the spring but from another subsurface portion of the valley head.

Preferential flows cause sediment discharge during storm runoffs as well as the indicated macro-pores for sediment and solute transport in subsurface water flow (e.g., PILGRIM and HUFF, 1983 ; TSUBOYAMA *et al.*, 1994). Thus, the rise of the seepage flow velocity from the soil matrix to the soil pipes must have led to the concave curvilinear correlations in the $i_{(W1)}$ Q_t relation described in Chapter 3. Many fine particles produced before the sediment peak originated from the head hollow soil between well W1 and the spring, and the seepage force of subsurface water flow (which has the same mechanism as piping) must have transported the fine particles from the soil matrix into the macro pores (i.e., preferential flow pathways). Then, the pipe flow transported this sediment to the spring after an extensive flushing of the soil particles from the walls of the soil pipes.

5.2 Relationship between fine-grained sediment and rate of change in subsurface water discharge

Although the fine-grained sediment discharge from the head hollow poorly correlated with the subsurface water discharge, the concentration and flux of fine-grained sediment obviously increased as subsurface water discharge increased at the initiation of the storm runoffs. Thus, some physical mechanisms must appear in the relationship between the subsurface water discharge and fine-grained sediment production.

The rate of change in discharge (dQ/dt, where d is differential, Q is stream discharge, and t is time) is an important parameter for describing suspended sediment yield following road construction and logging in a second order drainage basin. Hydrograph characteristics, such as dQ/dt, aid the explanation of the variability of observed suspended sediment concentration (ANDERSON and POTTS, 1987). Sediment yield during the early period of storm discharge results from the rapid rising of the sapping force associated with subsurface water flow acceleration (NAMIKI *et al.*, 1993). Therefore, the correlations between the rate of change in subsurface water discharge ($l \cdot s^{-2}$) and the changes in Fg.S.C and Fg.S. Flux offer useful information for understanding more fully the fine-grained sediment discharge in subsurface water flow, because the rate of change in subsurface water discharge is a function of subsurface water flow velocity (that is, $dQ/dt = dA v/dt$, where A is the flow section area and v is the flow velocity), and because the effect of dv/dt on subsurface hydraulic erosion is supported physically by one of NEWTON's laws ($F = m dv/dt$, where F is the body force, m is the body mass, and dv/dt is the acceleration).

In addition, the extended BERNOULLI theorem derives the following equation for the unsteady flow condition :

$$-\partial(v^2/2g+Z+P/\rho_w g)/\partial x=1/g\,\partial v/\partial t \tag{22}$$

where x is the distance along a flow line, g is the gravitational acceleration, Z is the potential head, P is the pressure, and $v^2/2g$ and $P/\rho_w g$ indicate the velocity head (kinetic energy) and the pressure head, respectively. Eq. (22) reveals that the change in the unit volume of flow energy is proportional to the acceleration of the flow. However, the precise measurement of subsurface water flow velocity is often difficult in the field, due to the complex routes of subsurface water flow. Accordingly, dv/dt is not usually applied to analyze sediment production, and dQ/dt is preferable for indicating erosion force caused by subsurface water flow because measurement of subsurface water discharge is easier than that of subsurface water velocity.

In contrast, the analysis used the stream power recommended by Bagnold (1960) gives the following useful equation for sediment production :

$$\Omega=\rho_w ghSWV=\rho_w gQS \tag{23}$$

where Ω is the stream power, h is the flow depth, S is the energy gradient, W is the flow width, V is the average flow velocity, and Q is the stream discharge. However, as shown in Figures 11 and 12, the fine-grained sediment discharge did not depend entirely on the change in subsurface water discharge, and clockwise hysteresis loops occurred in the relationship between sediment yield and subsurface water discharge. In addition, as will be described in Chapter 6, almost no fine-grained sediment discharge was generated during snowmelt even though subsurface water discharge was more than that during storms. Consequently, not only the stream power in eq. (23) but also the soil mobility expressed by the effective stream power (Bagnold, 1966) and the effect of energy gradient under unsteady flow conditions are the most significant parameters for describing fine-grained sediment discharge in subsurface water flow.

Owing to the variation in slope topography or flow pathways, the critical stream power as the threshold related to sediment removal involves various values for each storm (Ikeda, 1981). In addition, the acceleration term is commonly included in S in eq. (23) under the unsteady flow conditions. Thus, the function composed of subsurface water discharge and energy gradient under steady flow conditions rarely explicates the actual process of sediment discharge in drainage basins where an abrupt change in subsurface water discharge usually occurs. A one-dimensional function based on subsurface water discharge such as eq. (23) may be inappropriate for describing the mechanism of sediment production with piping.

Consequently, the rate of change in subsurface water discharge associated with the subsurface water flow velocity (dQ_s/dt ; where Q_s is subsurface water discharge) is an adequate parameter to explain the relationship between Fg.S.C., Fg.S. Flux, and subsurface water discharge under unsteady flow condition.

Figure 27 shows the results for the two cases of 22 October 1993 and 16 September 1994. Positive and negative values in the rate of change in subsurface water discharge occur during the rising and falling limbs of the hydrograph, respectively. The ascending ($dQ_s/dt \cdot d/dt > 0$) and receding ($dQ_s/dt \cdot d/dt < 0$) portions of the change in dQ_s/dt during the rising limb appear to be in the acceleratory (concave hydrograph) and deceleratory (convex hydrograph) rising limbs, respectively. In both cases, the initial changes in Fg.S.C., were consistent with the initial rises in the rate of change in subsurface water discharge.

The maximum value of Fg.S.C. on 22 October 1993 mostly corresponded with the fourth (and largest) peak in the rate of change in subsurface water discharge, but this correlation diminished
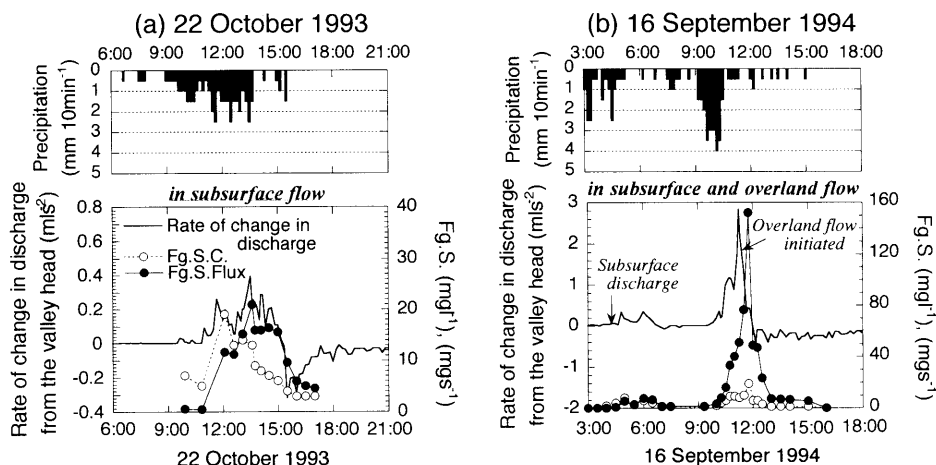
Fig. 27　Rate of change in subsurface discharge, changes in concentration (Fg.S.C.) and flux (Fg.S.Flux) of fine-grained sediment on (a) 22 October 1933 and (b) 16 September, 1994.

thereafter. In both cases, the changes in Fg.S. Flux correlated precisely with the variations in the rate of change in subsurface water discharge. These facts reveal that the erosion process of subsurface water flow, associated with the rate of change in subsurface water discharge, created the changes in Fg.S. Flux during the storms.

Figure 28 shows the relationships between the rate of change in subsurface water discharge, Fg.S.C., and Fg.S. Flux during the rising limb of the hydrograph (including both the acceleratory and deceleratory rising limbs, see Fig. 31 and below for the definition of terms) on 22 October, 1993 and 16 September, 1994. The linear correlation coefficient (r) of Fg.S.C. was 0.52 and 0.66 on 22 October and 16 September, respectively. In contrast, the correlation coefficient of Fg.S. Flux was 0.88 and 0.91 on 22 October, 1993 and 16 September, 1994, respectively. Accordingly, for understanding the physical aspects of fine-grained sediment discharge in subsurface water flow from the head hollow, the Fg.S. Flux is a better indicator of sediment yield process than the Fg.S.C.

Table 6 shows the linear correlation coefficients for the relationship between the rate of change in subsurface water discharge and the Fg.S. Flux during the rising limb in the eight observed storms. The minimum value of the linear correlation coefficient was 0.88 on 22 October, 1993. Consequently, at least during the rising limb of a storm hydrograph, erosion processes associated with the rate of change in subsurface water discharge lead to changes in Fg.S. Flux. If the Fg.S. Flux during the deceleratory rising limb ($dQ_s/dt \cdot d/dt < 0$, which shows a convex hydrograph, see Fig. 31) is ignored, the correlation coefficients in Figure 28(b) and Table 6 are modified to 0.96 and 0.97 for the storms on 22 October, 1993 and 16 September, 1994, respectively. That is, the Fg.S.Flux during the deceleratory rising limb is distributed in the upper part above the linear correlation line for every storm as shown in Figure 28(b). Thus, in principle, the linear correlation is applicable during the acceleratory rising limb of the hydrograph ($dQ_s/dt \cdot d/dt \geq 0$; which shows the concave hydrograph, see Fig. 31).

By rearranging the results in Figure 28 b and Table 6, the following equation can be used to respect the process of fine-grained sediment discharge in subsurface water flow for the ac-

Table 6   Linear correlation coefficient for the relationship between rate of change in subsurface discharge and fine-grained sediment flux during the rising limb of the hydrograph, coefficient ε in Eq. (24), and initial subsurface discharge prior to the storms.

Storm	Linear correlation coefficient	ε (gsl^{-1})	Initial discharge (ls^{-1})
30 Sep. 1993	0.93	0.007	20.99
22 Oct. 1993	0.88	0.005	73.48
27 May 1994	0.94	0.115	20.98
16 Sep. 1994	0.91	0.031	19.32
23 Sep. 1994	0.95	0.205	8.18
30 Sep. 1994	0.99	0.126	7.28
5 Oct. 1994	0.98	0.115	3.92
19 Nov.1994	0.94	0.110	29.60
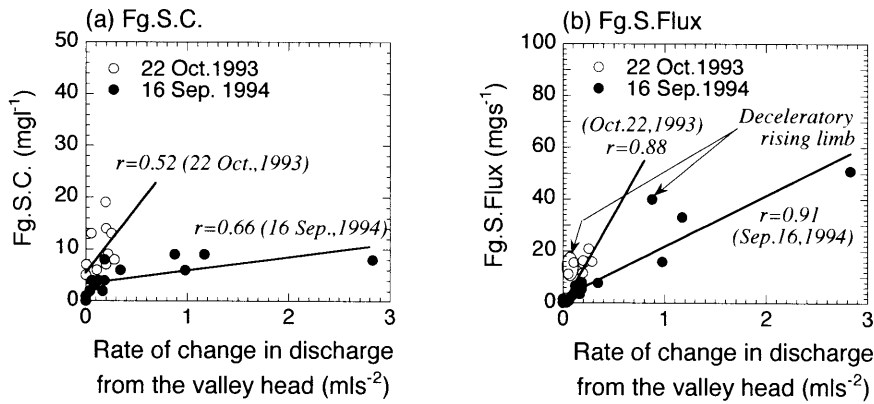
Fig. 28   Relationship between rate of change in subsurface discharge and (a) fine-grained sediment concentration and (b) flux during the rising limb of the hydrograph on 22 Oct., 1993 and 16 Sep., 1994.

celeratory rising limb of the hydrograph at which subsurface hydraulic erosion occurs and both the production and transport of fine-grained sediment are caused :

$$S = \varepsilon \{dQ_s/dt - (dQ_s/dt)_0\} \tag{24}$$

where S is the Fg.S. Flux, ε is a coefficient, Q_s is subsurface water discharge (flow rate), dQ_s/dt indicates the rate of change in subsurface water discharge, and $(dQ_s/dt)_0$ is the threshold value to produce fine-grained sediment.

In addition, dQ_s/dt is expressed by :

$$dQ_s/dt = dAv/dt = Adv/dt + vdA/dt \tag{25}$$

where A is the flow section area of subsurface water flow. CHOLEY et al. (1984) indicated that wash load flowed down with the same velocity as stream flow. This may suggest that eqs. (24) and (25) indicate that the seepage force acting on soils causes fine-grained sediment production and consequently fine-grained sediment is subjected to the acceleration corresponding to dv/dt. The kinetic equation for the volume of subsurface drainage is expressed by

$$F_{sf} = \rho_w A dv/dt \tag{26}$$

Eqs. (25) and (26) gives

$$dQ_s/dt = F_{sf}/\rho_w + vdA/dt \quad \text{or} \quad F_{sf} = \rho_w(dQ_s/dt - vdA/dt) \tag{27}$$

Thus, the rate of change in subsurface water discharge (dQ_s/dt) shows the linear correlation with the seepage force acting on fine-grained sediment under the condition influenced by vdA/dt.

If the Fg.S. Flux is proportional to seepage force beyond the threshold value (i.e., $dQ_s/dt > (dQ_s/dt)_0$) and under the sufficient sediment availability, and besides it is represented from $S = u\,F_{sf}$ (where u is the coefficient [S]), eq. (24) is modified as

$$F_{sf} = \varepsilon/u \cdot \{dQ_s/dt - (dQ_s/dt)_0\} \tag{28}$$

and combining eqs. (27) and (28) derives

$$(dQ_s/dt)_0 = vdA/dt \tag{29}$$

That is, $(dQ_s/dt)_0$ depends eventually on subsurface water flow velocity and the rate of change in flow section area (dA/dt) : this may describe a term associated with the hydraulic boundary of the laminar and turbulent flows (critical Reynolds number) under unsteady flow condition. Anyway, the problem is that the assumption of $S = u\,F_{sf}$ should be certified : the relationship between Fg.S. Flux and seepage force must be obtained in future.

In addition, the equation combined by eqs. (27) and (28) shows that the dimension of ε is [KSM^{-3}], which is also shown from eq. (24). This indicates that ε is inversely proportional to the volume of water flow (i.e., [M^3]). Table 6 and Figure 29 show the relationship between ε and initial subsurface water discharge (Q_i) prior to the storm runoffs. Coefficient ε is inversely correlated with Q_i and exhibits rare seasonal variation. Therefor, the initial condition of fine-grained sediment production associated with subsurface water discharge affects ε on account of the different gradient of the correlation lines (Fig. 28(b)), providing more evidence that the change in flow section area strongly affects sediment production. The small water flow section area prior to the storms, which is one of the suggestive indicators to consider the antecedent soil moisture condition in the head hollow, created a lot of fine-grained sediment discharge even though the same magnitude of rainfall occurred. This indicates that an unsaturated area in slope soils plays an important role in the mode of fine-grained sediment discharge in subsurface water flow. Fine-grained sediment, therefore, tends to be low when the soil moisture content prior to a storm is high.

Fine-grained sediment discharge can be characterized as follows : Subsurface water discharge with storms intensively promotes a large amount of fine-grained sediment production under dry antecedent conditions of the soil moisture at slopes. That is, an increase in dQ_s/dt with the rising of seepage force creates subsurface hydraulic erosion with erosive sediment discharge from unsaturated zones during the acceleratory rising limb of the hydrograph.

5.3 Clockwise hysteresis loop and the origin of sediment

The clockwise hysteresis loops in the relationship between subsurface water discharge and fine-grained sediment production have long been explained for the sediment discharge in mountainous streams as follows :

1) Lack of sediment during the falling stage of stream flow owing to the preceding sediment transport during the rising stage (a theorem for sediment availability proposed by WALLING and WEBB, 1982).

2) Supply of sediment from the riparian zone during the rising stage associated with a rain-splash and overland flow.

3) Even though stream discharge during the rising and falling stages is the same, the

transportation forces of stream flow are different because of the difference in energy gradients of the stream flow during the respective stages.

4) Even though the water levels during the rising stage and the falling stage are the same, the stream discharge is different owing to the difference in the energy gradient of stream flow. Thus, stream discharge, calculated from the water level-discharge relationship, includes some unreliable errors for the rising and falling stages in storm runoffs.

Reason 1) for the creation of clockwise hysteresis loops is inapplicable because fine-grained sediment must have been sufficiently supplied from the head hollow soil during the observation period. Reason 2) has no relation to fine-grained sediment discharge in subsurface water flow. Additionally, the other reasons involve only a qualitative indication for the sediment discharge and offer only an ambiguous explanation for clockwise hysteresis loops owing to the insufficient consideration of the mechanism, process, and origin of sediment production.

This study revealed that fine-grained sediment discharge in subsurface water flow depended on the change in seepage force shown in eqs. (24) and (27). Accordingly, based on the change in seepage force affecting the fine-grained sediment, the author will now examine why clock-wise hysteresis loops are created in the relationship between subsurface water discharge and fine-grained sediment production.

If the supply and availability of fine-grained sediment is ignored, "erosion (or production)" and "transport" must primarily characterize the processes of fine-grained sediment yield in subsurface water flow : The relationship between "erosion (or production)" and "transport" determines the modes of fine-grained sediment yield in subsurface water flow. The term "erosion (or production)" in this study is applied not in the broad sense that includes particle transport in subsurface water, but simply to the phenomenon by which soil particles are removed from the sediment. Thus, in this study, the process of fine-grained sediment discharge is defined as follows : "After the extensive flushing of soil particles from the matrix into subsurface pathways, the particles are transported by subsurface water flow, and then sediment discharge eventually occurs at the spring". According to this definition, the interaction between "erosion (or production)" and "transport" operates on the process of fine-grained sediment discharge under an initial condition associated with sediment supply. The fact that fine-grained sediment was measured at the spring outlet indicates that the sediment had been eroded and produced according to Eq. (24) and had been transported rapidly via the subsurface pathways (i.e., soil macro-pores) without being trapped in drainage networks in the sedimentary soil.

SAKAMOTO et al. (1993 a) argued that, being beyond 0.1 l·s^{-1}, the stream flows in the Jozankei Watershed and an adjacent drainage (6.0 ha in area) enabled the transport of fine-grained sediments up to 20 mg·s^{-1} regardless of the change in stream flow velocity. Fine-grained sediment discharge in subsurface water flow ranged from a maximum of 20 mg·s^{-1} for usual storms to at least about 50 mg·s^{-1} for the storm on 16 September, 1994 when overland flow was generated on the head hollow. Table 7 exhibits that most of the subsurface water discharge prior to the storms exceeded 0.1 l·s^{-1}. Furthermore, even if the initial subsurface water discharge prior to the storm was below 0.1 l·s^{-1}, Figure 11 indicats that subsurface water discharge had already exceeded 0.1 l·s^{-1} when sediment production was taking place. Fine-grained sediment discharge depends mostly on the open channel subsurface water flow via soil pipes as described in Section 1 of this Chapter. When the sediment transportation capacity of the open channel subsurface water flow
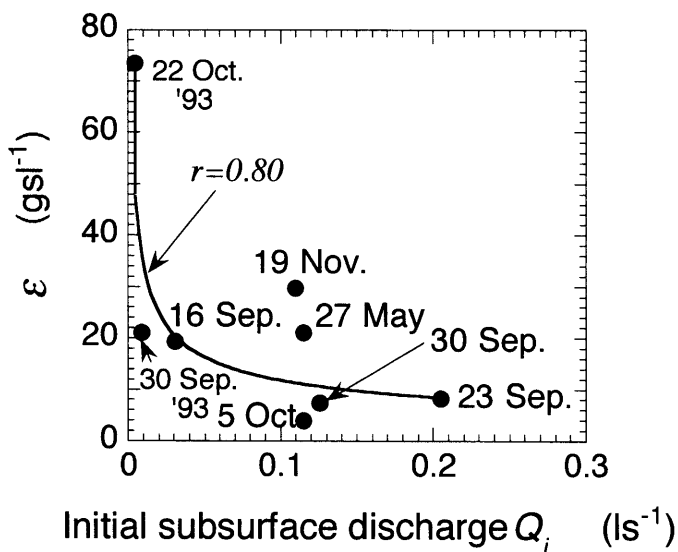
Fig. 29　Coefficient ε distribution associated with initial subsurface discharge prior to the
storms.

in the head slopes followed the results in SAKAMOTO *et al.* (1993a), most subsurface water dis-
charges had already maintained the transportation capacity that enabled them tocarry the
maximum amount of fine-grained sediment during the low flow prior to the storm.

Figure 30 shows a conceptual illustration of the erosion and transport of fine-grained
sediment. Subsurface water flow associated with soil pipes eroded and simultaneously trans-
ported fine-grained sediment in soils under an optimum condition for sediment transport, and
thereafter only the transportation force of subsurface water flow created sediment discharge at
the spring.

Accordingly, the possible clockwise hysteresis loops in the relationship between subsurface
water discharge and fine-grained sediment yield are summarized in Figure 31, based on the
aspects on "erosion (or production)" and "transport". Changes in Fg.S. Flux resulting from
subsurface hydraulic erosion are caused during the acceleratory rising limb of the hydrograph
(between A and B in Fig. 31 (a), (b)) which is chiefly observed at the initial stage of storm runoffs.
Thus, during the initial rising limb of the hydrograph, subsurface hydraulic erosion produces
fine-grained sediment particles and subsurface water flow transports them. That is, "erosion (or
production)" and "transport" of fine-grained sediment simultaneously occur in the head hollow
during the acceleratory rising limb, and intensive sediment production arises from the spring,
with increasing subsurface water discharge (see AB Fig. 31 (c)). Since the peak in fine-grained
sediment is affected by the subsurface water flow system between well W1 and the spring (see Fig.
26), the sediment forming the peak chiefly originates from the subsurface portion near well W1.
Accordingly, the production of fine-grained sediment prior to the sediment peak (between A and
B shown in Fig. 31 c) should come mostly from the lower part of the hollow between well W1 and
the spring.

However, because of the reduced erosion (or production) force of subsurface water flow
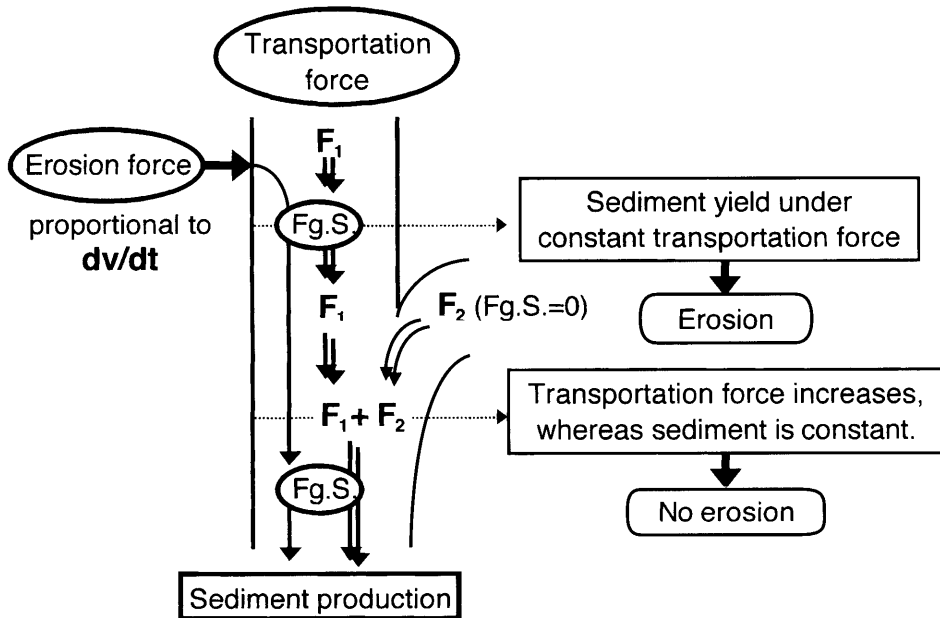
Fig. 30 Conceptual illustration of the erosion and transport of fine-grained sediment.

resulting from decreased dQ_s/dt during the deceleratory rising limb (between B and C, see Figs. 31 (a), (b)), the transport of fine-grained sediment must be more important than the erosion (or production) and likely occurred more during increased subsurface water discharge than during the initial acceleratory rising limb. Since gradient changes into the more concave correlation were hardly observed after the sediment peak (see Fig. 26), fine-grained sediment measured after the sediment peak scarcely affected the subsurface water flow system between well W1 and the spring. That is, fine-grained sediment measured during the deceleratory rising limb (Fig. 31 (b), (c)) originated from the upper subsurface portion of the hollow above well W1, and the sediment may have come with a time lag to dQ_s/dt measured at the spring.

During the falling limb, negative dQ_s/dt (Fig. 31 (b)) in the any subsurface portion of the head hollow caused no erosion (or production) of fine-grained sediment. Only transport, accompanied with decreased subsurface water discharge, released the residual sediment in the hollow. Consequently, the clockwise hysteresis loop appears in the process of fine-grained sediment discharge in subsurface water flow (Fig. 31 (c)).

5.4 Role of head slopes for different categories in drainage basins

Figure 32 and Table 7 show the relative importance of subsurface yields to total basin yields for fine-grained sediment discharge. The drainage area contribution to the spring corresponds to 55% of the total drainage area. Thus, if the ratio exceeds the 55% in Figure 32, water and sediment discharge from the valley head greatly affect those from the total drainage.

Water discharge from the valley head contributed considerably to stream discharge during the falling limb of the stream hydrograph (Fig. 32). When saturated overland flow was initiated on 16 September, 1994, water discharge from the valley head affected the total discharge from the drainage as soon as the stream discharge formed the peak. In contrast, the effect of the

(a) Hydrograph and change in S.S.Flux

Subsurface discharge

Deceleratory rising limb
Acceleratory rising limb
C Falling limb
B
A
D
S.S.Flux

Time
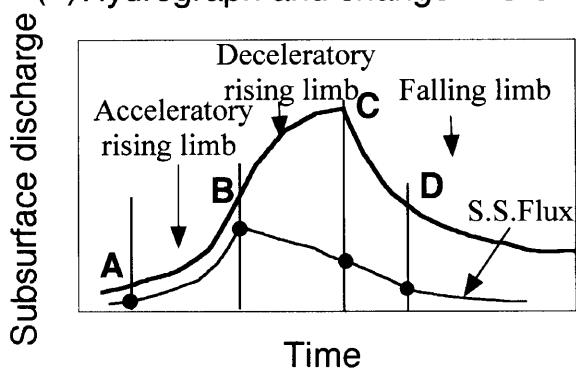
(b) Change in S.S.Flux with *dQs/dt*

S.S.Flux

Falling limb *(only Transport)*
Deceleratory rising limb *(mainly Transport)*
B
D **C**
A
Acceleratory lising limb *(Erosion + Transport)*

-　**0**　**+**

Rate of change in discharge (*dQs/dt*)

(c) Change in S.S.Flux with *Qs*

S.S.Flux

Acceleratory lising limb *(Erosion∓Transport)*
Deceleratory rising limb *(mainly Transport)*
B
C
A
D Falling limb *(only Transport)*
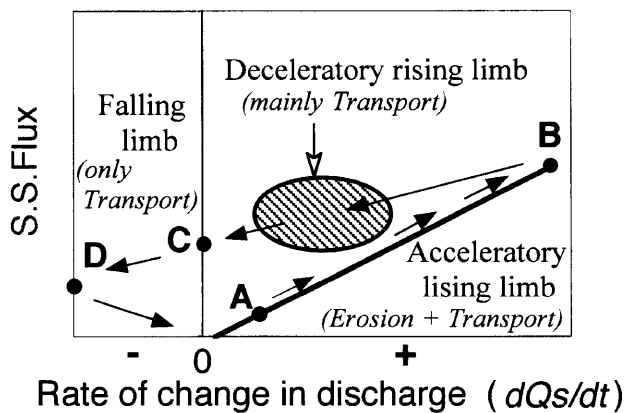
Subsurface discharge (*Qs*)
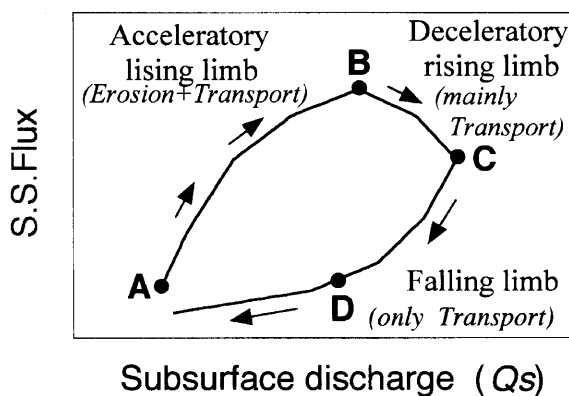
Fig. 31　Conceputal model to explain the clockwise hysteresis loop in the relationship between subsurface discharge and fine-grained sediment.

fine-grained sediment discharge from the valley head on the total sediment discharge from the drainage appeared during the rising limb of the stream hydrograph.

Additionally, fine-grained sediment discharge in subsurface water flow (Fig. 32(a)) contributed to total sediment discharge and exceeded 10% during the falling limb of the stream hydrograph. However, the ratio of Fg.S. Flux was at most 13.5% in the case of subsurface water discharge (Fig. 32(a), Tab. 7 and rarely exceeded 18% even in the case of overland flow initiation (Fig. 32(b), Tab. 7).

In comparison with both the drainage area contributing to the spring (55%) and the ratio of water discharge from the valley head which exceeded 55% during the falling limb of the stream hydrograph, the small effect on sediment yield from the total drainage occurs in the yield from the

Table 7   Maximum ratio of sediment yields in subsurface flow from the valley head to total drainage yield.

Storm	Maximum ratio (%)	Notes
30 Sep. 1993	0.003	Low Q_i
22 Oct. 1993	13.50	Fig.35a, low
27 May 1994	—	No data on fine-grained sediment discharge in stream flow
16 Sep. 1994	18.00	Fig.35b, Overland flow generated
23 Sep. 1994	5.39	Large Q_i
30 Sep. 1994	4.00	Middle Q_i
5 Oct. 1994	0.43	Middle Q_i
19 Nov.1994	12.07	Middle Q_i
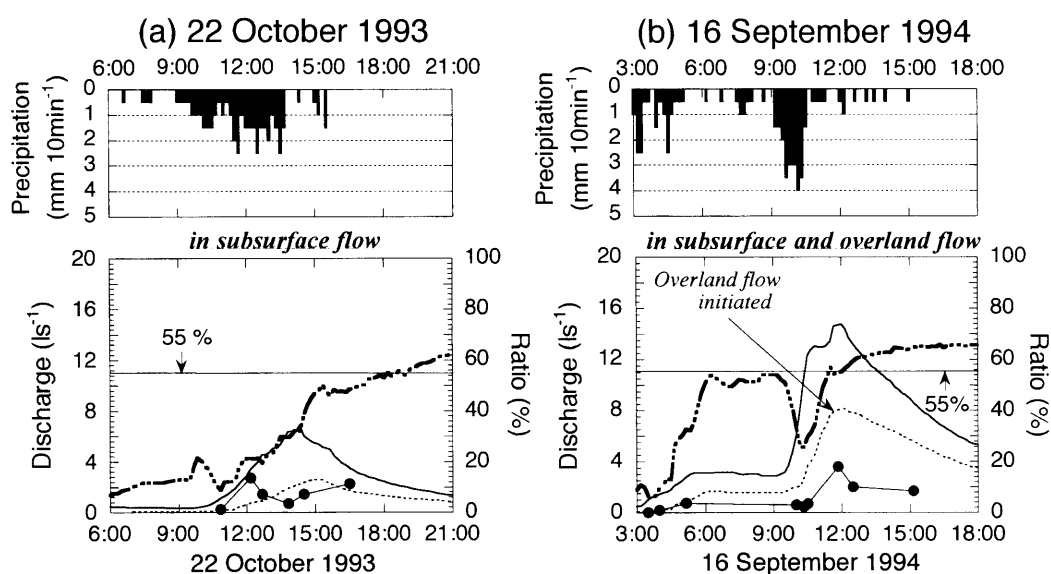
Fig. 32   Relative importance of subsurface yield to total drainage yields of water and sediment discharge on (a) 22 October, 1993 and (b) 16 September, 1994.

valley head. Accordingly, more than 80% of Fg.S. Flux from the Jozankei Watershed originates from the stream bed and banks in these typical storms. However, in comparison with fine-grained sediment for unit drainage area, the ratio of fine-grained sediment discharge from the valley head to that from the total drainage was a maximum of 24.3% for subsurface water discharge alone and a maximum of 32.4% for overland flow generation. If the stream bank is integrated into the drainage area calculation for subsurface water flow, the subsurface drain occupies about 99.5 per cent of total drainage area. Therefore, the ratio of sediment discharge considering this total subsurface drain must be larger than that considering only the valley head. Except for the sediment supply caused by rain-splash, the rate of change in stream discharge also explains the changes in Fg.S. Flux in the stream of the Jozankei Watershed (TERAJIMA et al., 1996) during the acceleratory rising limb of the stream hydrograph. From the aspect of sediment discharge caused by water flow, fine-grained sediment discharges in subsurface water and stream flow may be created fundamentally by the similar mechanism in the aspect of water flow agent depending on the rate of change in discharge.

6　Relationship between subsurface water discharge and sediment yield in subsurface hydraulic erosion

As described in Chapters 2 to 5, the erosion and transport processes of subsurface water flow intensively interact with sediment discharge in the head waters. These hydrogeomorphic processes obviously affect the forest devastation, valley formation, slope evolution, and turbid water discharge caused by subsurface hydraulic erosion. Research on the watershed management and land utilization phases will seek to investigate thoroughly the characteristics and interrelation of subsurface water flow and sediment yield and to understand the effect of subsurface hydraulic erosion on topographic change in forests.

Individual studies on water discharge and sediment movement have been conducted previouly. For instance, the recent development of interdisciplinary knowledge in hillslope hydrology has provided information on water movement in hillslopes (KIRKBY, 1978), and observations and experiments have led to an understanding of rainfall-runoff mechanism in hillslopes. The integration of hillslope hydrology with topographic diversity, such as variations in drainage networks or in valley head configurations, has recently emphasized the importance of hydrogeomorphic processes in valley development (BEVEN and KIRKBY, 1993).

Most watershed studies on sediment movement do not address the interaction between water discharge and sediment yield. Instead, these investigations have focused on such issues as sediment budgets and the mechanism of debris flows and shallow landslides (JSEC, 1992). This may be because the interactive processes of hydrology and sediment movement, which dictate the hydraulic conditions that generate sediment discharge and changes in the hydraulic condition resulting from sediment yield, are difficult to quantify in terms of hydrogeomorphic processes in headwaters.

In Section 1 of this chapter, the author discusses measurement of shallow groundwater, subsurface water discharge, and suspended sediment yield from the valley head of the Jozankei Watershed and considers the interactive processes of subsurface water flow agents and subsurface soil movement in the valley head. In addition, subsurfacehydraulic erosion resulting from subsurface water discharge and sediment yield under unsteady hydraulic conditions led to forest

devastation and valley development, so the effect of sediment yield with subsurface water discharge on geomorphic process in the drainage is considered in Section 2. On the basis of the above results, the effect of subsurface hydraulic erosion on the drainage environment is described in Section 3, and the technical evolution of both measures for priventing slope devastation and the management of water quality is discussed in Section 4.

6.1 Interaction between subsurface water discharge and fine-grained sediment yield

6.1.1 Hydraulic head gradient and subsurface water discharge from the head hollow during a thaw season

The thaw season is a sufficient time interval to evaluate hydrological processes in the valley head because of the extended wet soil moisture conditions. Thus, melt water discharge from 18 March to 13 May, 1944 was examined to analyze the interaction between subsurface water discharge and fine-grained sediment yield.

Figure 9 shows that melt water generated the maximum groundwater level on 16 April and a similar peak on 5 May. An easy analysis of the relation between subsurface water discharge and the shallow groundwater level for the same time periods is possible as shown in Chapter 2. Four strong repeated patterns of melt water discharge are shown in Figure 9 : (1) from 16 to 18 April, (2) from 21 to 23 April, (3) from 27 to 29 April, (4) and after 2 May. Details of subsurface water movement and fine-grained sediment yield during these four melt water discharge episodes provide information about the interaction between subsurface hydrology and soil movement.

Figure 33 shows the relationship between subsurface water discharge and the hydraulic head gradient of shallow groundwater in the head hollow during the rising limb of the hydrograph. Most data from 21 to 23 April and 27 to 29 April exhibited a linear or slightly concave curvilinear correlation. On 16 April, a greater concave curvilinear deviation from the linear correlation was observed. However, the data from 17 April and from 10 to 12 May exhibited a convex curvilinear correlation compared to the more linear correlation of the data for 21 to 23 April and 27 to 29 April. The ratio of subsurface water discharge to hydraulic head gradient increased from 18 : 00 to 20 : 00 on 21 April and remained constant through 29 April. After 10 May, groundwater levels declined
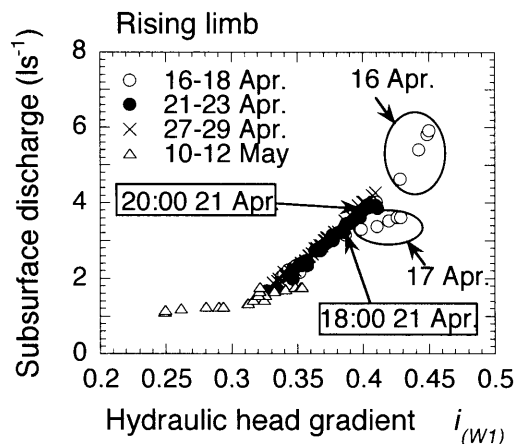
Fig. 33   Relationship between subsurface water discharge and hydraulic head gradient in the head hollow during the rising limb of meltwater discharge in 1994

Table 8 Fine-grained sediment concentration (Fg.S.C.) during the initial snow melt season in 1994.

Day	18 March	19-21	22	22-31	1 April	2-11
Time	0,6,12,18 h	0,6,12,18 h	0,6 h	14 h	14 h	14 h
Number of Samples	12	12	2	10	1	10
Fg.S.C (mgl^{-1})	0	0	0	0	6	0
Notes on Fg.S.C. value	mixed four samples	for each sample	for each sample	for each sample	for one sample	for each sample
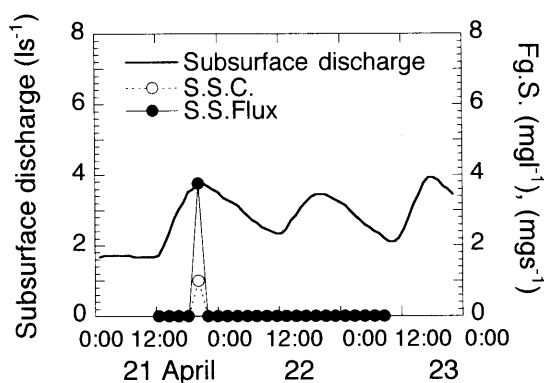
Fig. 34 Subsurface discharge and fine-grained sediment yield from the valley head during the meltwater discharge in 1994.

sharply because of reduced melt water supply and the subsurface water discharge was lower for the same hydraulic heads compared to April. These results indicate a wide ranging subsurface water discharge from the valley head for the same hydraulic head gradient and changes in drainage capacity of the soil occurred in the specific period during the melt water season.

6.1.2 Fine-grained sediment discharge with thaw and storms

Table 8 shows fine-grained sediment concentration during the initial thaw season from 18 March to 11 April in 1994. The shallow groundwater level in well W1 during the period was not recorded because of a snow avalanche and subsequent data logger troubles. Water sampling was conducted only once a day, at 14 : 00, from 22 March to 11 April because the rate of change in subsurface water discharge shown in eq. (24) was sufficient to understand fine-grained sediment discharge in subsurface water flow and was likely to be the highest in the early afternoon. Fine-grained sediment (6 mg·l^{-1}) at the outlet from the spring was generated when the melt water discharge was initiated on 1 April (about 0.022 l·s^{-1} of constant base flow from 18 to 31 March and 0.77 l·s^{-1} of peak flow at 23 : 00 on 1 April). No fine-grained sediment occurred that until 11 April.

Figure 34 shows subsurface water discharge and fine-grained sediment yield from the hollow from 21 to 23 April in 1994. Bed load material and fine-grained sediment in the subsurface water flow were not produced by the spring from 12 April to 13 May except in one case at 20 : 00 on 21 April. Although the maximum subsurface water discharge was generated on 16 April (see Fig. 3), no fine-grained sediment was produced on that day. It is possible that the two-hour collection intervals of subsurface water discharge might have yielded an incomplete record of fine-grained

sediment. However, the infrequent production of fine-grained sediment during the melt water discharge in 1994 indicates that this is a stochastic process. Only 2 out of 119 samples (1.7 per cent of samples) collected between 1 April and 13 May contained measurable sediment. On 1 April, a sample containing $6 \, mg \cdot l^{-1}$ was collected during snowmelt. On 21 April, a small sediment pulse ($1 \, mg \cdot l^{-1}$) was produced during a small peak in the snowmelt hydrograph. At the time of this small sediment discharge, the relationship between discharge and hydraulic head shifted noticeably.

During 1995, there was no sediment discharge measured during the melt season in the 148 samples collected between 22 March and 22 April (unfortunately no records of groundwater were available because of problems with the data logger). Sediment initiation, like that for 1 April shown in Table 9, could not be observed during the melt period in 1995 because melt water discharge had already begun before 22 March when sample collection was initiated.

In any case, fine-grained sediment in subsurface water flow with melt water is produced quite sporadically. There are two reasons for this : 1) dQ_s/dt in eq. (24) of melt water discharge is usually smaller than that of storms (a maximum of $0.11 \, ml \cdot s^{-2}$), 2) regardless of the sufficient sediment transportation capacity of subsurface water flow during the snow melt, ε in eq. (24) is extremely small because initial subsurface water discharge prior to the storm (Q_i) during the snow melt ($1 \sim 1.5 \, l \cdot s^{-1}$, see Tab. 6) is more than during storms. That is, sediment discharge shown in Figure 34 was attributed not to the erosive agent resulting from the changes in dQ_s/dt, but to some antecedent factors that cause sediment removal.

The sediment discharge on 21 April shown in Figure 34 recorded barely 1 mg at 20 : 00 (equals to $1.43 \, cm^3 \cdot sec^{-1}$, $86 \, cm^3 \cdot min^{-1}$, or $5000 \, cm^3 \cdot hr^{-1}$) ; however, the time of sediment discharge initiation (20 : 00 in Fig. 34) precisely coincided with the time of an increase in drainage capacity of the head hollow soil (from 18 : 00 to 20 : 00 in Fig. 33). Hence, fine-grained sediment discharge seemed to relate to an increase in drainage capacity of the head hollow soil, that is, may have been influenced the subsurface drainage system in the head hollow.

Figure 35 shows subsurface water discharge, fine-grained sediment yield, and the hydraulic head gradient (head gradient is only for the rising limb of the storm hydrograph) for storms on 27 May and 16 September, 1994. The 27 May storm flow peak was less than many of the earlier melt water episodes. No storms occurred from 13 to 27 May. Subsurface water discharge increased more on 27 May than during the snow-melt period from 10 to 12 May and fine-grained sediment began to discharge after 17 : 00 on 27 May, forming two discharge peaks : one at 18 : 00 and another from 21 : 00 to 22 : 00 (Fig. 35(a)). Although we have no fine-grained sediment data between 17 : 00 and 18 : 00 due to the one-hour collection interval for subsurface water discharge, the first sediment peak may actually have occurred between 17 : 00 and 18 : 00 because of the increase in drainage capacity measured from 17 : 00 to 18 : 00. Although subsurface water discharge exhibited a linear or slightly convex curvilinear correlation before 17 : 00, it abruptly increased from 17 : 00 to 18 : 00 and from 21 : 00 to 22 : 00 (Fig. 35(b)). Gradient changes in the correlation line from convex to concave (Fig. 35(b)) clearly appeared from 17 : 00 to 18 : 00 and at 21 : 00 when fine-grained sediment began to discharge or peak ; that is, the peak in fine-grained sediment discharge might provide a sudden increase in subsurface water discharge.

More detailed (15-minute interval) changes in subsurface water discharge, fine-grained sediment yield, and the hydraulic head gradient (hydraulic head is only for the rising limb) are
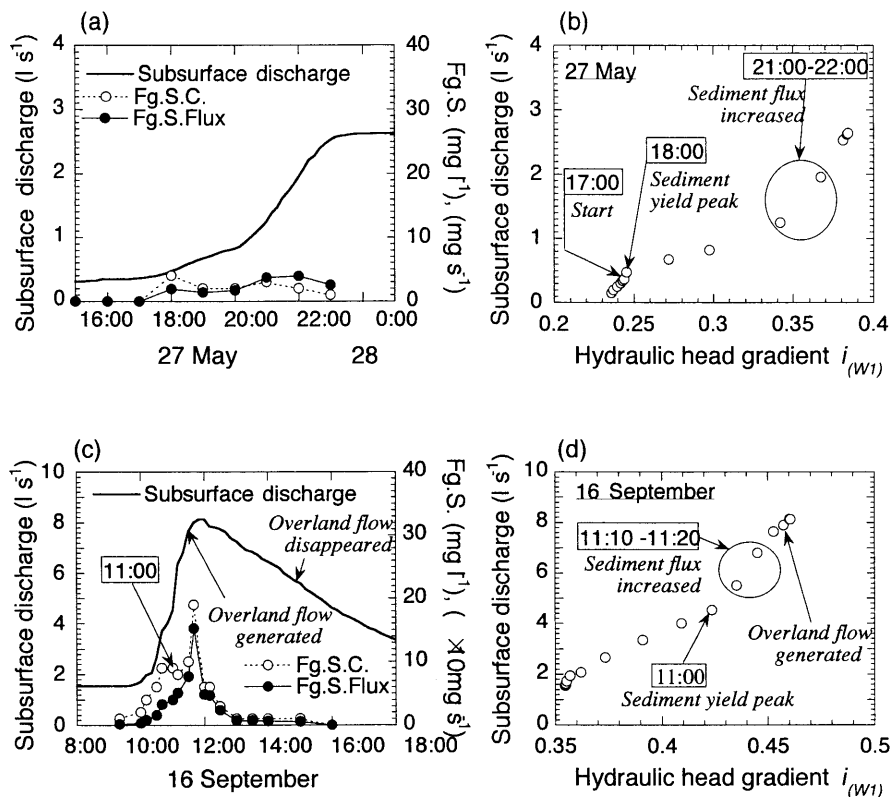
Fig. 35　Charges in (a), (c) subsurface discharge and fine-grained sediment and (b), (d) the relationship among hydraulic head gradient of subsurface flow, subsurface discharge and fine-grained sediment.

presented for a larger autumn storm on 16 September 1994 (Fig. 35 (c), (d)). No bed load material was generated during the storm. The sediment peak occurred at 11 : 00 and preceded peak subsurface water discharge.

Subsurface water discharge exhibits a concave curvilinear correlation from 11 : 00 to 11 : 20, but, it abruptly changes to a convex curvilinear shape after 11 : 20 (Fig. 35 (d)). Pipe flow was discharged at the surface in the area near well W1 at 11 : 40 and the saturation overland flow was generated simultaneously between well W1 and the spring when the gradient of the correlation line changed from concave to convex (also at 11 : 40). The earlier change in gradient in the correlation line from convex to concave (at 11 : 00) clearly appeared when fine-grained sediment discharge peaked. The peak concentration and flux of fine-grained sediment appeared to affect the sudden increase in subsurface water discharge during the 16 September storm as was the case during the 27 May storm (Fig. 35 (b)). Thus, interaction between changes in subsurface water discharge and subsurface soil movement may commonly occur during storm runoffs.

The following conclusions can be drawn from the results in Chapter 5 and the data from the thaw season :

(1)　Subsurface water discharge concerns fine-grained sediment yield during the storm, and simultaneously,

(2) Fine-grained sediment yield affects also the changes in mode of subsurface water discharge during both snow melt and storms.

Consequently, regardless of the origin of runoff (by melt water or storms), subsurface water discharge and fine-grained sediment removal interact with each other in the head hollow.

6.1.3 Change in the drainage capacity of a slope soil and fine-grained sediment yield

Changes in drainage capacity of the sedimentary soil in the hollow (shown in Fig. 33) resulting from macro-pore volume variation directly affects subsurface water discharge. The linear or slightly concave curvilinear correlation of subsurface drainage with hydraulic head gradient corresponds to an optimum drainage condition where preferential flow networks, including soil pipes, drain subsurface water from the hollow. The convex curvilinear correlation corresponds to conditions of insufficient drainage capacity of the soil. These two types of drainage conditions are shown in plots of subsurface water discharge versus hydraulic head gradient for various snow-melt periods in the hollow as well as during the May and September 1994 rain storms. Subsurface soil movement and enlargement of preferential flow passes may provide these changes in the drainage capacity of the sedimentary soil.

Figure 36 shows the qualitative relations among drainage capacity of the soil, fine-grained sediment discharge in subsurface water flow, and forms of sediment movement in the hollow (*in italics*) from 16 April to 27 May, 1994.

(1) 16 to 18 April : Since the drainage capacity of the sedimentary soil in the hollow declined between 16 and 17 April, subsurface water discharge decreased on 17 April even though the hydraulic head gradient was the same as on 16 April. Although stream power (BAGNOLD, 1960), calculated from subsurface water discharge and hydraulic head gradient, was maximum on 16 April, no fine-grained sediment was generated via the spring. These results reveal that an obstruction of sediment discharge occurred in the hollow ; that is, *clogging* of preferential flow paths with fine-grained sediment caused the decrease in soil drainage capacity between 16 and 17 April. During such wet conditions in the melt water season, the interactive zone of the macro pores and the macro pore network is believed to expand (TSUBOYAMA *et al.*, 1994). The measured decrease in soil drainage capacity caused both a decrease in subsurface water
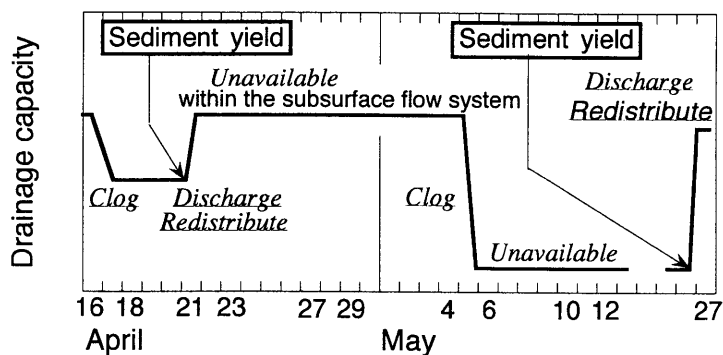

Fig. 36 Relationship among the drainage capacity of the sedimentary soil, fine-grained sediment discharge in subsurface flow, and forms of subsurface sediment movement in the hollow during the meltwater discharge and subsequent storm runoff in 1994.

discharge and a rise in the shallow groundwater level in well W1.

(2) 21 to 23 April : On 21 April, a small discharge in fine-grained sediment was noted at the spring outlet. Subsurface water discharge subsequently increased from 18 : 00 to 22 : 00 with the increase in drainage capacity. This increase in drainage capacity was the result of both sediment *discharge* and subsequent *redistribution* of fine-grained sediment n the hollow.

(3) 23 April to 4 May : Drainage capacity remained relatively constant from 23 April to 4 May, because subsurface ater discharge, which is related to hydraulic head gradient, also varied very little. No fine-grained sediment was generated from 23 April to 4 May. Therefore, sediment supply was unavailable within the subsurface water flow system of the hollow and *clogging* of the preferential flow paths with fine-grained sediment or *discharge* and *redistribution* of fine-grained sediment during this period was negligible.

(4) After 4 May : Between 4 and 6 May, the drainage capacity of the soil declined abruptly. This decline coincided with a decrease in subsurface water discharge after 5 May with the same hydraulic head gradient as before 4 May (when discharge was higher). This low drainage capacity continued until 12 May, and no fine-grained sediment was generated from 6 to 12 May. *Clogging* of the subsurface drainage system with fine-grained sediment may have occurred on 5 May to instigate this decrease in drainage capacity of the sedimentary soil. This low drainage capacity increased again during the storm runoff on 27 May, accompanied by fine-grained sediment *discharge* and *redistribution*.

6.1.4 Implication of subsurface water discharge and fine-grained sediment yield

Fine-grained sediment flux in the subsurface water flow generated during the rising limb of the storm hydrograph was correlated precisely ($r = 0.88$ to 0.99) with the rate of change in subsurface water discharge. This relationship was developed for the rising limb of the hydrograph where subsurface hydraulic erosion is likely initiated.

Figure 37 shows the conceptual relationship between subsurface water discharge and fine-grained sediment yield from the valley head, based on the results of this study. According to eq. (24), fine-grained sediment moves without impediment in drainage networks in the sedimentary soil when subsurface water discharge increases during storm runoff. This sediment is transported out through the spring without being trapped in soil macro pores when the subsurface water flow is able to carry the fine-grained particles from the subsurface to the seepage outlet of the hollow (in case of $\varepsilon > 0$ and $dQ_s/dt > (dQ_s/dt)_0$). That is, *discharge* and *redistribution* of the fine-grained particles occur in the sedimentary soil, and the drainage capacity increases with the enlargement of the pore volume.

Since much subsurface water flow is generated during melt water discharge, the transportation force of subsurface water flow is sufficient for the production of fine-grained sediment due to the larger stream power than the cases of storm runoff on 27 May. If subsurface hydraulic erosion in the valley head occurs according to eq. (24), fine-grained sediment would be expected to flow out through the spring. However, subsurface water discharge associated with melt water rarely produces fine-grained sediment (i.e., when $\varepsilon = 0$ and $dQ_s/dt \leqq (dQ_s/dt)_0$) because of *clogging* due to fine-grained particles in the sedimentary soil which decrease the permeability and drainage capacity of the soil. The clogging due to fine-grained particles consequently causes the shallow groundwater level to rise. On the other hand, the lack of fine-grained sediment discharge indicates that fine-grained particles are not available under the wet soil conditions because they
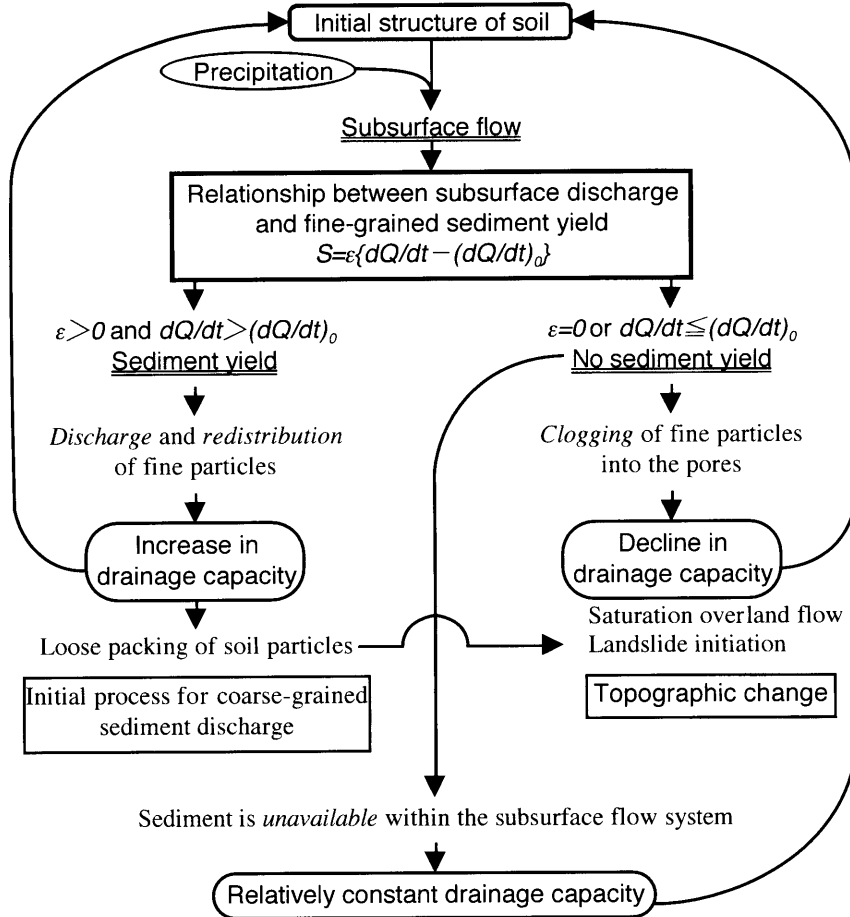
Fig. 37   Interaction between subsurface water dsicharge and fine-grained sediment yield.

are probably immobile or are bound by the cohesive forces of the sediment. Thus, the drainage capacity of the soil in the valley head was relatively constant.

Periodic clogging with fine-grained particles terminates fine-grained sediment discharge. The lower drainage capacity of the soil continues to cause the shallow groundwater level to rise and saturation over land flow is consequently generated in the hollow. Furthermore, the decline in drainage capacity may initiate shallow landslides due to increased hydraulic gradients and pore water pressures (BLONG and DUNKERLEY, 1976 ; TSUKAMOTO et al., 1982).

The phenomena described in Figure 37 do not always take place independently ; they are often interrelated, since *discharge, redistribution,* and *clogging* due to fine-grained particles sometimes arise simultaneously in the valley head.

6.2 Subsurface hydraulic erosion and topographic change

6.2.1 Significance of coarse- and fine-grained sediment discharges for topographic changes

Eq. (24) involves no data for coarse-grained sediment discharge in subsurface water flow. The following items, however, are essential for understanding fine-grained sediment discharge in subsurface water flow under the unsteady hydraulic condition as described in Chapter 5 : 1) The

temporal variation in subsurface water flow velocity (i.e., acceleration) controls strictly the fine-grained sediment removal, and 2) If the temporal variation in flow section area is combined into the discussion related to fine-grained sediment discharge in subsurface water flow, the rate of change in subsurface water discharge is an indispensable parameter to understand subsurface hydraulic erosion.

Eq. (6) is modified :

$$F_{sf}=\rho_{n}gA\left(-dh/dx\right) \tag{30}$$

where h is the hydraulic head of subsurface water flow and x is the downslope distance. The $-dh/dx$ indicates the hydraulic gradient with the change in shallow groundwater level toward downslopes. Combining eq. (26) with eq. (30) induces :

$$(-dh/dx)=1/g \cdot dv/dt \tag{31}$$

Although the velocity head (kinetic energy term) in the BERNOULLI theorem under unsteady hydraulic conditions (see eq. (22)) is ignored in eq. (32), eq. (32) indicates that the hydraulic gradient is in proportion to the acceleration of subsurface water flow, and consequently that the increases in the acceleration provides the increase in seepage force that is proportional to the hydraulic gradient $(-dh/dx)$.

Accordingly, the following view explains the coarse-grained sediment discharge : The piping created on 25 September 1988 shown in Figure 20 must have resulted not in "shear destruction with the slow rising of hydraulic gradient on 24 September (based on eq. (12))" but in "liquefaction caused by the expanding seepage force increasing with the rising of acceleration of subsurface water flow (based on eq. (9))". In contrast, coarse-grained sediment discharge may be created during the acceleratory rising limb of the hydrograph $(dv/dt \cdot d/dt > 0)$ as well as the erosion of fine-grained sediment during the acceleratory rising limb (that is, coarse-grained sediment discharge possibly depended on $-dh/dx \cdot d/dt$ in Eq. (32)). In other words, the liquefaction in the slope of the Kitadani watershed was encouraged by the abrupt rising of the hydraulic gradient prior to its peak at 5 : 00 on 25 September 1988 (see Fig. 20), being supported both from the time that the cohesionless sediment buried the weir-W2 (at 10 : 00 on 25 September) and from the substantial sediment discharge observed at the time.

Landslides caused by shear destruction resulting from subsurface water flow parallel to a slope have chiefly been examined in studies which dealt with mass movement by subsurface water flow. The safety factor constructed by the ratio of shear force to soil resistance has commonly been employed to solve the numerous problems regarding slope instability, without involving the process of shallow landslide under unsteady hydraulic conditions. However, the results of this study indicate that liquefaction of part of the sediment (the spouting of individual soil particles or clods out of slopes) is created by 1) an increase in the acceleration (seepage force) of subsurface water flow as the hydraulic gradient rises, 2) fine-grained sediment erosion during the acceleratory rising limb of the hydrograph $(dv/dt \cdot d/dt > 0)$ with an abrupt rise in the hydraulic gradient $(-dh/dx \cdot d/dt > 0)$, and 3) the ascending changes in direction of subsurface water flow. Hence, piping triggers sediment removal from the subsurface portion of slopes. This conclusion is supported by KOBASHI (1993), who found that landslides were often initiated not by shear destruction, but by the piping of slopes.

6.2.2 Effect of subsurface hydraulic erosion on geomorphic processes at slopes

Sediment movement, such as landslides, usually occurs during a heavy rain under the
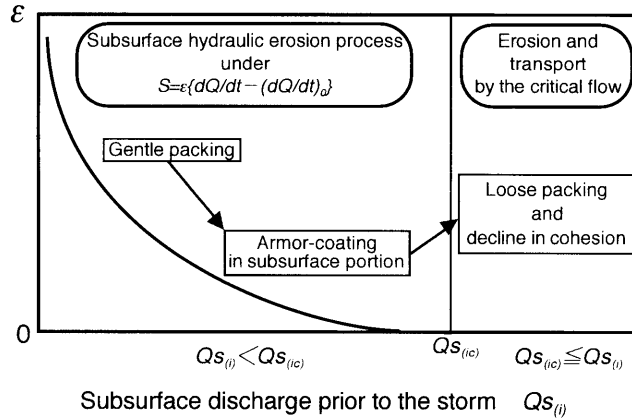
Fig. 38   Conceptual model of the effect of initial subsurface discharge prior to the storm on sediment discharge in subsurface water flow. $Qs_{(i)}$: Subsurface water discharge prior to storm runoff ; $Qs_{(ic)}$: Critical subsurface water discharge for sediment production under steady hydraulic conditions.

sufficient soil moisture content following a previous rainfall events as during the rainy season. This fact seems to contradict the statement that "Fine-grained sediment discharge is rarely promoted by a wet condition of the soil" in Figure 29. The rate of change in subsurface water discharge (dQ_s/dt) and initial subsurface water discharge prior to storms (Q_i) at the landslide initiation, possibly have much larger values during the rainy season than during the ordinary rainfalls that are dealt with in this study. Few rainfall events during the study periods exhibited dQ_s/dt and Q_i representing the critical situation for landslide initiation, so that sediment discharge under such conditions was likely not observed in this study.

Figure 38 shows the conceptual model related to the effect of $Qs_{(i)}$ on sediment discharge in subsurface water flow. If $Qs_{(i)}$ is previously over the critical subsurface water discharge $(Qs_{(ic)})$ for creating sediment movement, sediment discharge depends on the critical tractive force (τ_c) or critical hydraulic gradient (i_c) without being affected by dQ_s/dt because of unconditional erosion. These situations are summarized below :

(1) at $Qs_{(i)} < Qs_{(ic)}$: Sediment discharge is explicated by Eq. (24) expressing the sediment removal under unsteady hydraulic conditions. The soil structure of the slopes controls fine-grained sediment discharge as follows : 1) When $Qs_{(i)}$ is small under the dry antecedent soil moisture condition, loose packing of soil particles may enable fine-grained sediment erosion, and 2) When $Qs_{(i)}$ is optimum for the wet antecedent soil moisture condition, very little fine-grained sediment discharge may be produced by the effect of the armor coating or cohesion of sediment.

(2) at $Qs_{(i)} \geqq Qs_{(ic)}$ ($Qs_{(i)}$ is more than the discharge needed to create τ_c or i_c) : Sediment discharge depends on the changes in τ_c or i_c under the corresponding hydraulic property, and the sediment is produced through the lost equilibrium between erosion force and soil resistance. These phases of sediment discharge disclose that sediment production occurs mostly under static criticality and that a different mechanism of sediment movement opposite to condition (1) exists in the process of subsurface hydraulic erosion.

Subsurface hydraulic erosion caused by liquefaction resulting from changes in dQ_s/dt and the critical velocity of subsurface water flow has to be considered sufficiently to quantify the

slope evolution and topographic change in valleys. This consideration contributes to the quantitative comprehension of the forest devastation with sediment removal in drainages, such as landslides, mud and debris flows, and rill and gully formation.

In future, the universal application of eq. (12) to sediment movement should be validated : that is, whether eq. (24) is applicable or not to coarse-grained sediment discharge and to sediment discharge in slopes underlying different topographies, geology, and vegetation. Additionally, the relationship between the universal application of eq. (24) and the concept shown in Figure 38 should also be verified. More information on the characteristics of subsurface water discharge from slopes needs to be obtained to completely disclose the relationship between flow generation and sediment movement in various areas. The theories based on the critical hydraulic values for sediment movement under steady hydraulic conditions may not be sufficient to quantify the hydrogeomorphic processes in drainages where drastic changes in subsurface water discharge are promoted under unsteady hydraulic conditions. This is because the flow energy is proportional to the acceleration of flow as shown in eq. (22), and the energy gradient expressed in eq. (23) usually involves a term of unsteady hydraulic condition (i.e., acceleration). Accordingly, when sediment movement at slopes is examined, the interactions of subsurface hydraulic erosion and topographic change should be described by elucidating the relationship between changes in flow energy and soil resistance under unsteady hydraulic conditions.

6.3 Influences of subsurface hydraulic erosion on the drainage environment

Figure 39 shows the impact of subsurface water discharge and sediment yield from the valley head on head water hydrology and environment in temperate and humid regions.

Rainfall infiltrates mostly into soil ; consequently, subsurface water discharge is one of the main agents for erosion. Sediment discharge caused by piping is one of the most important processes in watershed hydrology, shallow landslides, and debris flow. It produces sediment that often triggers fine-grained sediment discharge, and turbid water is simultaneously supplied into streams. Furthermore, sediment discharge resulting from piping induces the topographic changes, such as slope depressions or rill and gully formation at valley heads, and subsequently shifts the area of stream flow generation upslope leading eventually to valley development. Vegetational destruction and the change in conditions of forest soil caused by fallen trees, root excavation, and soil loss ultimately bring about the forest devastation.

In contrast, subsurface water discharge creates fine-grained sediment flushing as the initial process of subsurface hydraulic erosion. This fine-grained sediment flows down mostly as turbid water, and affects the downstream environment through the destraction of fluvial ecosystem, and lake or marsh reclamation. The removal and transport of fine-grained particles at head slopes promotes the physical weathering of slope materials, which affects, directly and indirectly, the consequent coarse-grained sediment discharge.

Numerous studies have long focused on "the agent of overland flow as the enlargement process of rills and gullies or sheet wash erosion" and "the mechanism of shallow landslide by shear destruction". However, this study indicates that the effect of subsurface water flow agents on hydraulic and geomorphic processes in drainages must be integrated sufficiently into the studies on forest hydrology when the forest conservation with sediment movement at slopes is examined, for the following reasons : ① Subsurface water flow is the most significant and dominant agent in head water hydrology and geomorphology, ② Subsurface water flows via soil

Fig. 39   Impact of subsurface water discharge and sediment yield from a valley head on head water hydrology and environment.

pipes or forming soil pipes are indispensable for head water hydrology and geomorphology during heavy rains, and they are the main agents involved in sediment movement in head slopes of humid region, and ③ Topographic changes in valley heads are often caused by piping.

6.4   Technical problems for erosion control and creating water quality

Figure 40 shows the methodology for controlling subsurface water discharge and sediment yield in head waters, based on the forest management that aims at both water and soil conservation. The goal of "sediment control in head waters and restraint of turbid water discharge" is indispensable for watershed conservation and management. In other words, "no liquefaction of soil in head slopes caused by subsurface water flow" ahould be allowed. Consequently, the following two aspects are essential for examining forest utilization :

(1)   Keeping the value of dQ_s/dt in eq. (24) small : That is, watershed management for keeping

Precipitation

↓

Infiltration
Percolation

↓

Subsurface discharge

↓

Piping → Initial stage of subsurface hydraulic erosion

↓

Coarse-grained sediment discharge ← Physical weathering — Fine-grained sediment discharge

Shallow landslide Debris flow — Origin → Turbid water discharge

When large amount of discharge was created

Surface depression Rill and gully formation

Tree fall Root excavation Soil loss

Destruction of fluvial ecosystem

Lake and marsh reclamation

Upward shift in stream flow generated area

Valley development

Interaction

Forest devastation

Changes in watershed environment

(Objective) Control of sediment movement and turbid water discharge

Restraint of liquefaction

(Method) Decline in dQ_s/dt — Restraint of sudden rise in subsurface water discharge

Decline in ε in Eq.(24) — Maintenance of soil moisture content

(Means) Increase in water storage capacity of soil ← Forest

(Example) Litter cover

(Result) Development of A or A$_0$ Horizons — Canopy

Water chemistry

Increase in infiltration capacity
Litter flow
Restraint of rain-splash erosion
Mitigation of freezing and thawing of soil

Restraint of evaporation Rainfall interception

Erosion restraint

Maintenance of soil moisture content at the forest floor

Thick soil layer

Change in style of sediment movement
Decrease in frequency of sediment movement

Growing environment for understory vegetation and trees

Forest soil conservation

Manifestation of the water and soil conservation functions

Fig. 40　Control of subsurface water discharge and sediment yield in head basins based on the aspect of forest management.

small values of dQ_s/dt during storms and for creating gentle runoffs from slopes.

(2)　Keeping the value of ε in eq. (24) small : That is, watershed management for keeping wet soil conditions and much subsurface water discharge during low flows. Consequently, the flow from the spring is conserved.

　　An increase in the infiltration capacity of soils through the artificial coating of the land

surface in forests is the most effective measure for fundamental treatment as "increase in water storage capacity of slope soils". However, an increase in the water storage capacity of soils through the more spontaneous functions provides temporal, spatial, and economic benefits. Forests are common in humid regions, so that the following is effective for the forest soil conservation : Maintaining and developing forest soils contains organic matter typified by A_0 and A-horizons, and increasing the permeability and water storage capacity of the soils. Litter layers play a major role in natural erosion control because they directly cover slope surfaces, which is expected to create a litter flow (LEE and SHIBANO, 1990), restrain a rain-splash on slopes, mitigate frost and melt in soils (TERAJIMA, 1994), and reduce the tractive force of flow due to an increase in the roughness of slope surfaces (KITAHARA and JANG, 1994). Subsequently, depending on the soil thickness on slopes, changes in the mode of sediment movement occur (ONDA, 1989), and the reduced sediment movement contributes eventually to forest soil conservation.

In addition, the litter layers make subsurface water discharge increase by hindering evaporation from the soil surface and help to maintain the soil moisture content during dry periods (TERAJIMA et al., 1993). Moreover, the litter layers regulate infiltration of rainwater into soils, and keep about 5% of the annual precipitation (HERVEY and PARTRIC, 1965). TERAJIMA et al. (1993) and TERAJIMA (1994) investigated the effects of typical litter covers in Hokkaido, such as Mizunara oak (Qerucus mongolica Fischer et Turcz.), Todo fir (Abies sachalinensis (Fr. Schmid.) Masters), and Japanese larch (Larix Kaempferi (Lamb.) Carriere), on hydrological processes on forest floors, and indicated that 1) the litter of broad-leaved trees, such as Mizunara oak, was adequate to promote infiltration into and restrain evaporation from soils, and 2) the litters of Japanese larch were optimum for controlling frost and melt of soils as well as the litter of Mizunara oak. That is, the litters of broad-leaved trees play important rolls in water and soil conservation on forest floors.

At any rate, the litter cover supplies the desirable soil moisture conditions for water and soil conservation on the forest floor and develops the growing environment for understory vegetation and trees. It is also favorable for germination, and is thus indispensable for the creation and maintenance of the forest for succeeding generations.

Once forests are established on slopes, litter would be absolutely supplied to land surfaces. Thus, in order to control the erosion caused by water flow in head slopes and to sustain the most desirable type of water management in head waters based on natural processes, the A_0 and A-horizons must be long maintained through the spontaneous deposition and decomposition of litter on forest floors.

To improve the water quality conservation and erosion control by creating a more favorable environment on forest floors, the author makes the followings suggestion : Assume that the recently required function of forests, erosion control, is associated with the improvement of water storage of forest soils. In addition, assume the function for the water quality conservation is related to turbid water discharge, a supply of iron ions regarding the growth of the sea plants such as tangles, and the organic matter (carbon) removal from the aspect on the green-house effect, as well as ordinary chemical component discharge. Based on these views, litter layers play an important roll in turbid water flushing, iron ion supply, carbon component behavior, and the improvement of water storage capacity, because litter layers are organic matter which contain many macro-pores, and they are the origin of corrosive matter that decompose into fulbo-acid that contains $-COOH$ and $-C=O$ species that react easily with metal ions (MATSUNAGA, 1993).

Accordingly, the maintenance and/or positive utilization of litter layers is essential for improving the environmental conservation function of forests in future.

Litter cover on slopes may itself be insufficient as a technical material for the forest conservation to improve the above functions. This is because a lot of litter is removed from forest floors when overland flow is generated where there is no understory vegetation, as typically occurs in Hinoki cypress (*Chamaecyparis obtusa* (Sieb. et Zucc.) Endlicher) forests (OIKAWA, 1977 ; YOSHIMURA *et al.*, 1982 ; and SAKAI *et al.*, 1987). Another suggestion is that, instead of litter, artificial soil should be used to keep a favorable environment for water and soil conservation in forests. Artificial soils as the organic materials have to be made for rain water absorption, storage, and quality conservation. Thus, artificial soils that retain organic matter are desirable to use for covering forest floors. Artificial soils are already applied to the beds of trees lining streets, promenades and lawns in parks, and on erosive areas such as climbing routes.

The application of tree chips to the pavement of promenades seems to be one of the best ways to examine artificial soils. The cover of land surface with the artificial soils which are made of tree chips contributes to the soil conservation and simultaneously acts as natural permeable pavement. In addition, the flushing effect of the artificial soils is useful for the bio-remediation that is recently gaining notice in soil physics and chemical hydrology, from the aspect of holding organic materials containing numerous effective pores.

What kind of the forest management is desirable to create the ideal water and sediment discharge for the human life and ecological conservation ? The answer to this question requires a multi-disciplinary approach covering not only geomorphology, hydrology, and erosion control but also soil physics, ecology, fisheries, and social science. Moreover, there must be an understanding of the mechanism of sediment production and water quality creation. In order to gain a holistic picture of the function of forests affecting the watershed management from the mountains to the rivers to the sea, cooperative multi-disciplinary research activities, are essential to solve the problems on the basis of water flow as a common factor affecting the watershed environment.

Closing remarks

In the past few decade, Japan has been increasingly urbanizing. The urbanized zones are expanding to plateaus and hills and also to mountainous areas. Until a few decades ago, forests were utilized as places for the production for woody fuels and building materials, and of food procurement by the collection and capture of wild plants and animals. However, people are increasingly viewing forests as spaces related closely to their urban lives and recreation.

The water and soil conservation of forests, such as the preservation of water resources and the mitigation of floods and disasters by sediment movement, has been indispensable for improving urban living condition. The recent sudden urbanization and increase in population require forests to play greater roles in water management, disaster prevention, and environmental conservation. Moreover, the utilization of forests for recreation is growing at a rapid pace. Thus, not only water management, disaster prevention, and environment conservation but also the more direct applications, such as a recreational use through the preparation of forest parks, are required for manifesting the public functions of forests.

At the same time, though, human impacts produce the negative loads for water and soil conservation of forests. Environmental changes in and around forested watersheds mean that

forests must adapt to new circumstances, making them more vulnerable to hydrogeomorphic phenomena such as floods, landslides, debris flows, and turbid water discharges. This study had an objective to technical procedure to make display effectively the functions of the water and soil conservation of forests, and was assigned to model fundamentally forest devastation with subsurface hydraulic erosion and turbid water discharge from forests. Thus, integrating the results from this study into the relationship between water and sediment discharge in the water cycle will be useful for obtaining more information on desirable watershed management. In addition, understanding the discharge process of turbid water will give us significant information on the effect of water purification in forests on fluvial and coastal ecosystems. In this sense, this study should provide useful information for forest hydrology, geomorphology, and engineering.

References

ANDERSON, B. and POTTS, D.F. (1987) : Suspended sediment and turbidity following road construction and logging in Western Montana. *Water Res. Bull.*, **23**, 681–690.

ASANO, S., SHINDO, S., SAKURA, Y. and NISHIO, K. (1993) : Mechanism of storm runoff in a small watershed in granitic mountain : Contribution of side slope and valley head to storm runoff. *Bull. Tokyo Univ. Forests*, **90**, 183–210 (in Japanese with English abstract and captions).

BAGNOLD, R.A. (1960) : Sediment discharge and stream power, A preliminary announcement. *U.S.G. S. Circular*, **421**, 1–23.

BAGNOLD, R.A. (1966) : An approach to the sediment transport problem from general physics. *U.S. G.S. Prof. Paper*, 422–I.

BEVEN, K. and GERMANN, P. (1982) : Macropores and water flow in soils. *Water Res. Res.*, **18**, 1311–1325.

BEVEN, K. and KIRKBY, M.J. (1993) : *Channel Network Hydrology.* John Wiley and Sons, 310 pp, New York.

BLONG, R.J. and DUNKERLEY, D.L. (1976) : Landslides in the Razorback area, New South Wales, Australia. *Geogr. Annu.*, **58A**, 139–147.

BRUTSAERT, W. (1968) : The permeability of a porous medium determined from certain probability laws for pore-size distribution. *Water Res. Res.*, **4**, 425–434.

CEDERGREN, H.R. (1977) : *Seepage, Drainage and Flow Nets, 2nd ed.*, John Wiley and Sons, New York, 534 pp.

CHOLEY, R.J., SCHUMM, S.A. and SUGDEN, D.E. (1984) : *Geomorphology.* Methuen & Co. Ltd., London, 605 pp.

DIETRICH, W.E. and DUNNE, T. (1993) : The channel head. *Channel network hydrology*, edited by BEVEN, K. and KIRKBY, M.J., 175–219. John Wiley & Sons, New York.

DUNNE, T. and BLACK, R.D. (1970) : An experimental investigation of runoff production in permeable soils. *Water Res. Res.*, **6**, 478–490.

DUNNE, T. (1980) : Formation and controls of channel networks. *Progress in Physical Geography*, **4**, 211–239.

EGASHIRA, S. and ASHIDA, K. (1981) : The productive areas and transporting processes of wash load in mountainous drainage basins. *Reprinted from Annu. Disaster Prev. Res. Inst., Kyoto Univ.*, **24**, B-2, 239–250 (in Japanese with English abstract and captions).

GARLAND, G. and HUMPHREY, B. (1992) : Field measurement of discharge and sediment yield from a soil pipe in the Natal Drakensberg, South Africa. *Zeitschrift fur Geomorphologie*, **36**, 15-23.

Geological Survey of Hokkaido (1980) : Geology and Resources of Hokkaido, Japan, Part 1, Geology of Hokkaido. 113 pp (in Japanese).

HELVEY, J.D. and PARTRIC, J.H. (1965) : Canopy and litter interception of rainfall by hardwoods of Eastern United States, *Water Res. Res.*, **1**, 193-206.

HIGGINS, C.G. and COATES, D.R. (1990) : *in Groundwater Geomorphology, The role of subsurface water in Earth-surface processes and landforms.* The Geological Soc. Ammer., Special paper, 252, 368 pp.

HOWARD, A.D. and McLANE, C.F (1988) : Erosion of cohesionless sediment by groundwater seepage. *Water Res. Res.*, **24**, 1659-1674.

IKEDA, H. (1981) : Experiments on the transport of fine gravel in 4 meter wide flume (1), Effect of threshold stream power on sediment transport rate. *Bull. Environ. Res. Ctr. Univ. Tsukuba*, **5**, 35-49 (in Japanese with English abstract and captions).

IVERSON, R.M. and MAJOR, J.J. (1986) : Groundwater seepage vectors and the potential for hillslope failure and debris flow mobilization. *Water Res. Res.*, **22**, 1543-1548.

Japanese Erosion Control Society, (1992) : Soil erosion control, No. 3, *Sediment movement on slopes.* Sankaido, 357 pp, Tokyo (in Japanese).

JONES, A.A. (1971) : Soil piping and stream channel initiation. *Water Res. Res.*, **7**, 602-610.

JONES, A.A. (1978) : Soil pipe networks : Distribution and discharge. *Cambria*, **5**, 1-21.

JONES, A.A. (1987) : The effect of soil piping on contributing areas and erosion patterns. *Earth Surface Processes and Landforms*, **12**, 229-248.

KIRKBY, M.J. (1978) : *Hillslope Hydrology*, 330 pp. John Wiley and Sons, New York.

KITAHARA, H., SHIMIZU, A. and MASHIMA, Y. (1988) : Characteristics of pipe flow in a subsurface soil layer of a gentle hill side. *J. Jpn. For. Soc.*, **70**, 318-323 (in Japanese with English abstract and captions).

KITAHARA, H. (1989) : Characteristics of pipe flow in a subsurface soil layer on a gentle slope (II), Hydraulic properties of pipes. *J. Jpn. For. Soc.*, **71**, 317-322 (in Japanese with English abstract and captions).

KITAHARA, H. (1992) : Characteristics of pipe flow in the forest soil. *J. Jpn. Soc. Hydrol. & Water Res.*, **5**, 15-25 (in Japanese).

KITAHARA, H. and NAKAI, Y. (1992) : Relationship of pipe flow to stream flow in a first order watershed. *J. Jpn. For. Soc.*, **74**, 49-54 (in Japanese).

KITAHARA, H., SIDLE, R.C., TERAJIMA, T. and NAKAI, Y. (1992) : Hydraulic experiments of saturated throughflow with an artificial soil pipe. *Trans. Jpn. For. Soc.*, **103**, 589-591 (in Japanese with English title).

KITAHARA, H., TERAJIMA, T. and NAKAI, Y. (1994) : Ratio of pipe flow to through flow discharge. *J. Jpn. For. Soc.*, **76**, 10-17 (in Japanese with English abstract and captions).

KITAHARA, H. and ZHANG, H. (1994) : Hydraulic experiments on erosion control function of forest in Huangtu Plateau, China (II), Relationship between the amount of vegetation cover and coefficient of roughness. *Trans. Jpn. For. Soc.*, **105**, 587-590 (in Japanese with English title).

KOBASHI, S. (1993) : *Mountain Conservation*, p 135-141. Buneido, Tokyo (in Japanese).

KOCHEL, R.C., HOWARD, A.D. and McLANE, C.F. (1985) : Channel networks developed by groundwater

sapping in fine-grained sediments. Analogs to some Martian Valleys, in WOLDENBERG, M. J. (ed.), *Models in Geomorphology,* Allen and Unwin, Boston, 313–341.

KOHNO, I., NISHIGAKI, M. and TAKESHITA, Y. (1987) : Levee failure caused by seepage and preventive measures. *Natural Disaster Science,* **9,** 55–76.

KURASHIGE, Y. (1985) : Mode of sediment supply in the Bankei River catchment, Hokkaido, Japan. *Trans. Jpn. Geomorphol. Union,* **6,** 45–64 (in Japanese with English abstract and captions).

LEE, H and SHIBANO, H (1990) : Hydraulic characteristics of storm water flowing through litter layer. *J. Jpn. For. Soc.,* **72,** 223–229.

MATSUNAGA, K. (1993) : *The sea is killed when the forest disappears,* Ecological linkage between land and ocean. 194 pp, Kodansha, Tokyo (in Japanese).

NAKAI, Y. (1970) : On the granites in the Mikawa district, Aichi Prefecture, central Japan. *Earth Science,* **24,** 139–145 (in Japanese with English abstract).

NAMIKI, K., YUI, S., ONODERA, S., SHINDO, S. and TERASHIMA, H. (1993) : Experimental study of sediment yield mechanism in storm-runoff process on a hill slope. IAMAP-IAHS'93 Joint International meeting, *Concepts and Methodology in Hydrogeomorphology,* Abstracts of Accepted Papers, p 8.

NEWSON, M. (1976) : Soil piping in upland Wales ; A call for more information. *Cambria,* **1,** 33–39.

OIKAWA, O. (1977) : The surface movement of soil and organic matter in a *Chanaecyparis obtusa* stand. *J. Jpn. For. Soc.,* **59,** 153–158 (in Japanese with English abstract and captions).

OKUNISHI, K., SAITO, T. and SONODA, E. (1993) : Origin of characteristics microtopographical features at the headwaters of the Otani River basin, Shiga Prefecture, Japan. *Annuals Disas. Prev. Res. Inst., Kyoto Univ.,* **36,** 207–218 (in Japanese with English abstract and captions).

ONDA, Y. (1989) : Influence of water storage capacity in regolith zone on runoff characteristics and slope failure on granite hills in Aichi, Japan. *Trans. Jpn. Geomorphol. Union,* **10,** 13–26 (in Japanese with English abstract and captions).

ONDA, Y. (1994) : Seepage erosion and its implication to the formation of amphitheatre valley heads, A case study at Obara, Japan. *Earth Surface processes and Landforms,* **19,** 627–640.

OSAKA, O., TAMURA, T., KUBOTA, J. and TSUKAMOTO, Y. (1992) : Process study of the soil stratification on watershed granite slope. *J. Jpn. Erosion Control Soc.,* **45,** 3–12 (in Japanese with English abstract and captions).

PIERSON, T.C. (1983) : Soil pipes and slope stability. *Quarterly Journal of Engineering Geology, London,* **16,** 1–11.

PILGRIM, D.H. and HUFF, D.D. (1983) : Suspended sediment in rapid subsurface stormflow on a large field plot. *Earth Surface Processes and Landforms,* **8,** 451–463.

REID, M.E. and IVERSON, R.M. (1992) : Gravity-driven groundwater flow and slope potential 2. Effects of slope morphology, material properties, and hydraulic heterogeneity. *Water Res. Res.,* **28,** 939–950.

SAKAI, M., INOUE, K. and IWAKAWA, Y. (1987) : Mixture content of large organic matter in soil (III), Mixture content of leaf in soil related to the slope position in *Chamaecyparis obtusa* stand. *Trans. Jpn. For. Soc.,* **98,** 193–196 (in Japanese with English title).

SAKAMOTO, T., NAKAI, Y. and KITAHARA, H. (1992) : Measurement of suspended sediment in small mountain watershed. *Trans. Meeting of Hokkaido Branch of Jpn. For. Soc.,* **40,** 190–192 (in Japanese with English title).

SAKAMOTO, T., NAKAI, Y., KITAHARA, H. and TERAJIMA, T. (1993 a) : Measurement of suspended sediment in small mountain watersheds, II, A change during floods. *Trans. Meeting of Hokkaido Branch of Jpn. For. Soc.*, **41**, 145-147 (in Japanese).

SAKAMOTO, T., NAKAI, Y., KITAHARA, H. and TERAJIMA, T. (1993 b) : Suspended sediment in small mountain watershed. *Trans. Jpn. For. Soc.*, **104**, 753-754 (in Japanese).

SAKAMOTO, T., NAKAI, Y. and TERAJIMA, T. (1994) : Measurement of suspended sediment in small mountain watersheds, III, Discharge during a thaw. *Trans. Meeting of Hokkaido Branch of Jpn. For. Soc.*, **42**, 190-192 (in Japanese).

SAKAMOTO, T., TERAJIMA, T, NAKAI, Y., KITAMURA, K. and SHIRAI, T. (1996) : Measurement of suspended sediment in small mountain watershed, (IV) ; Influence of a pool upstream of a construction for erosion control. *Trans. Meeting of Hokkaido Branch of Jpn. For. Soc.*, **44**, 37-39 (in Japanese with English title).

SAKURA, Y., MOCHIZUKI, M. and KAWASAKI, I. (1987) : Experimental studies on valley headward erosion due to groundwater flow. *Geophysical Bull. Hokkaido Univ.*, **49**, 229-239 (in Japanese with English abstract and captions).

SASSA, K. (1984) : Monitoring of a crystalline schist landslide. Compressive creep affected by "underground erosion". *Proc. Tnt. Symp. Landslide*, Toront, Canada, 179-184.

SATO, A. (1987) : *Environmental engineering in water*. Environmental conservation based on the aspect of suspended matter. 247 pp, Gihoudo, Tokyo (in Japanese).

SHINDO, S. and SAKAI, H. (1983) : Hydrological response in hillslope hollows *(2)* ; Characteristics of pipe flow. *Landslide and subsurface water flow behavior at hillslopes*. A special study on a natural disasters funded by a Grant in Aid for Scientific Research from the Min. Edu., Sci., and Cul. Japan, in 1982. S. Shindo-ed., 50-51 (in Japanese).

SHINDO, S. (1983, 1984) : *Landslide and subsurface water flow behavior at hillslopes, Nos. 1 and 2* ; A special study on natural disasters funded by a Grant in Aid for Scientific Research from the Min. Edu., Sci., and Cul. Japan, in 1982 and 1983 (in Japanese).

SIDLE, R.C. and SWANSTON, D.N. (1986) : Groundwater dynamics in unstable zero-order basins of coastal Alaska. *Eos Trans. AGU*, p 956.

SIDLE, R.C., KITAHARA, H., TERAJIMA, T. and NAKAI, Y. (1995) : Experimental studies on the effects of pipeflow on throughflow partitioning. *J. Hydrol.*, **165**, 207-219.

SWANSON, M., KONDOLF, G.M. and BOISON, P.J. (1989) : An example of rapid gully initiation and extension by subsurface erosion. Coastal San Mateo Country, California. *Geomorphology*, **2**, 393-403.

TAMURA, T. (1987) : Landform-soil features of the humid temperate hills. *Pedorogist*, **31**, 136-146 (in Japanese with English title).

TANAKA, S. (1956) : On the mechanism of the sand-slope-failure in case of heavy rain. *J. Jpn. Erosion Control Eng.*, **22**, 3-9 (in Japanese with English abstract and captions).

TANAKA, T., SAKURAI, K. and OKAYAMA, T. (1990) : An observation for shallow groundwater level at a steep slope in head waters. *Abstracts for the annual meeting of Jpn. Soc. Hydrol. & Water Resour. in 1990*, 212-215 (in Japanese).

TANAKA, T., KIRA, H. and HASEGAWA, T. (1984) : Seepage failure of an one-layered sand column (without a loaded filter), Experimental study on the failure of a piece-wise homogeneous sand column caused by a vertically upward seepage flow (I). *Trans. JSIDRE*, **110**, 87-99 (in

Japanese with English abstract and captions).

TANI, M. (1982) : The properties of a water-table rise produced by a one-dimensional, vertical, unsaturated flow. *J. Jpn. For. Soc.*, **64**, 409–418 (in Japanese with English abstract and captions).

TERAJIMA, T. and MOROTO, K. (1990) : Stream flow generation in a small watershed in granitic mountains. *Trans. Jpn. Geomorphol. Union*, **11**, 75–96 (in Japanese with English abstract and captions).

TERAJIMA, T., KITAHARA, H. and NAKAI, Y. (1993) : Effect of litter cover on the process of water movement in the vicinity of ground surface, a consideration used the lysimeter. *Trans. of Hokkaido Branch, Jpn. For. Soc.*, **41**, 151–153 (in Japanese with English title).

TERAJIMA, T. (1994) : Role of litter cover on the mitigation of the freezing and thawing of soil. *Northern Forestry ("Hoppou Ringyou" in Japanese)*, **46**, 41–44 (in Japanese).

TERAJIMA, T., SAKAMOTO, T., NAKAI, Y., KITAMURA, K. and SHIRAI, T. (1996) : Diversity of suspended sediment yield in a forested head basin. *Trans. Meeting of Hokkaido Branch of Jpn. For. Soc.*, **44**, 40–43 (in Japanese with English title).

TSUBOYAMA, Y., SIDLE, R.C., NOGUCHI, S. and HOSODA, I. (1994) : Flow and solute transport through the soil matrix and macropores of a hillslope segment. *Water Res. Res.*, **30**, 879–890.

TSUKAMOTO, Y. (1973) : Study on the growth of stream channel (I), Relationship between stream channel growth and landslides occurring during heavy storm. *J. Jpn. Erosion Control Eng.*, **87**, 4–13 (in Japanese with English title).

TSUKAMOTO, Y., OTA, T. and NOGUCHI, H. (1982) : Hydrological and geomorphological studies of debris slides on forested hillslopes in Japan. *IAHS. Publ.*, **137**, Wallingford, 89–98.

TSUKAMOTO, Y. and OTA, T. (1985) : Introduction to forest works for water management. *Water science*, **158**, 28–61 (in Japanese).

TSUKAMOTO, Y., MINEMATSU, H. and TANGE, I. (1988) : Soil pipes developing at the slope regolith. *Studies in Hakyuchi Experimental Forest*, **6**, 268–280 (in Japanese).

WALLING, D.E. (1974) : Suspended sediment and solid yields from a small catchment prior to urbanization. In *Fluvial processes in instrumented watershed, Institute of British Geographers Special Publ.*, **6**, 169–192.

WALLING, D.E. and WEBB, B.W. (1982) : Sediment availability and the prediction of storm-period sediment yields. Recent developments in the explanation and prediction of erosion and sediment yield, *IAHS Publ.*, **137**, 327–337.

YAMAGUCHI, I. (1963) : Fundamental studies on the groundwater flow phenomena at the water source zone. *Bull. Tokyo Univ. Forests*, No. 58 (in Japanese with English title and abstract).

YASUHARA, M., MARUI, A., YASUIKE, S. and SUZUKI, Y. (1992) : An experimental study on the behavior of infiltration water in soils with a macropore. *Hydrology*, **22**, 3–15 (in Japanese with English abstract and captions).

YOSHIMURA, K., AKAI, T., MANABE, I., AIBA, Y., SUGIURA, K., ISHII, H. and HONJO, N. (1982) : Flowing drift of litter, soil and others under artificial rainfall in Hinoki stands (VI, Difference of movement of litter and surface soil between Sugi and Hinoki stand. *Trans. Jpn. For. Soc.*, **93**, 347–348 (in Japanese with English abstract and captions).

ZASLAVSKY, D. and KASSIFE, G. (1965) : Theoretical formulation of piping mechanism in cohesive soils. *Geotechnique*, **15**, 305–316.

斜面における浅層地下水および土砂の流出特性と
地下侵食機構に関する研究

寺　嶋　智　巳[1]

摘　　要

わが国のように湿潤な気候下にあり山地の多くが森林に覆われている地域では，斜面に供給された降水のほとんどが地下に浸透し，土地改変等の人為作用がない限り地表流が発生することは希である。そのため，斜面に供給された降水の大部分は地下を経由して河川へ流出することになり，この流動・流出過程において崩壊，土石流，地表面の陥没，リル・ガリーの形成といった土砂流出に起因する地形変化あるいは河川の水質形成などが行われる。このように，斜面の地下水流出は地形プロセスに大きく影響するため，「水循環と地形変化の相互作用」を検討して森林の有する水土保全機能の定量的解明を行う場合には，まず第一に，斜面における地下水流の挙動とその作用による土砂流出（地下侵食）の関係を十分に検討しなければならない。本研究では，流域管理技術に資するための基礎的資料とする目的から，森林流域谷頭部斜面での水流出の主要形態である浅層地下水とその地下水の流出に起因する土砂の流出プロセスの定量的解明と相互作用の検討を行い，浅層地下水流による侵食機構を明らかにすることを試みた。

第1章では，森林流域谷頭部を研究対象として扱うことの意義を示した後，流域または斜面における浅層地下水と土砂の流出に関する研究の紹介を行い，研究対象地および観測・解析方法について記述した。

第2章では，斜面からの浅層地下水流出とそれによる土砂流出の実態を記述した。まず，札幌市定山渓の1次谷流域谷頭堆積地を対象として，地下水位およびそこからの浅層地下水流出量を計測した。その結果，土砂の侵食が発生するような洪水流出時ではパイプを媒介とした浅層地下水流出が支配的であることを明らかにした。また，愛知県瀬戸市の北谷流域谷頭部で生じた粗粒土砂の流出と林地の荒廃を記述し，パイピングにより土砂流出が生じたことについて言及した。さらに，札幌市の定山渓流域谷頭部における浅層地下水と細粒土砂の流出実態を記述し，細粒土砂流出量のピークが浅層地下水流出量のピークに先行して現れ，浅層地下水流出量と土砂流出量の変動が一致しないことを明らかにした。

第3章では，斜面での浅層地下水の流出メカニズムを明らかにするため，パイプ流出に関する室内実験を行った。その結果，パイプを経由して流出してくる水が斜面での浅層地下水流出に大きく影響しており，その流出形態はパイプの排水能力の大小により決定されていることを明らかにした。そして，土砂流出が発生するような出水時にはパイプを経由してくる地下水流が流出の主成分を占めることがわかった。

第4章では，粗粒土砂流出に及ぼす浅層地下水の作用を明らかにするため，まず，浅層地下水流出に伴う土砂移動の発生に関する力学的条件を整理するとともに，浅層地下水流出に伴う土砂移動に関する理論式を紹介・提示した。

　次に，有限要素法を用いて，パイピングに伴う粗粒土砂の流出発生時における斜面内の浅層地下水の動水勾配を計算した。さらに，流動化実験により実際に平面において流動化による土砂移動が生じるときの動水勾配（限界動水勾配）を算出した。そして，数値実験および流動化実験で得られたデータ，実際の水文観測データ，上記理論式とを対応させて粗粒土砂の流出機構を検討した。その結果，セン断破壊や流動化により粗粒土砂の移動が発生する可能性，および粘着力の差による土砂移動形態の違い，などを説明した。

　第5章では，谷頭部斜面における細粒土砂流出の観測結果から，地下侵食機構を明らかにすることを試みた。その結果，加速度的増水過程では，地下水流出水量変化率と細粒土砂フラックスの関係が一次近似できることを明らかにした。この結果を用いて，浅層地下水流出と細粒土砂流出の関係において時計回りのヒステリシスが生じる原因を明らかにした。

　第6章では，浅層地下水流出と細粒土砂流出の相互作用を検討した。その結果，細粒土砂の流出と谷頭部斜面土層の排水能力の変動が非常によく一致し，細粒土砂が浅層地下水流により生産されるばかりではなく，細粒土砂流出自体が谷頭部の浅層地下水流出システムに大きく影響してくるという相互作用があることを明らかにした。

　また，浅層地下水と細粒土砂の流出の関係から，地形変化に直接結びつく粗粒土砂流出について検討した。ここでは，浅層地下水流の動水勾配と加速度が比例することを示し，粗粒土砂の移動が「動水勾配が増加して加速度が大きくなり浸出水力（侵食力）が増大して生じる」と判断した。そのため，パイピングによる粗粒土砂の移動が動水勾配の急増に伴う流動化により発生した可能性があることを指摘した。

　さらに，地下侵食による土砂流出が流域環境の変化に及ぼす影響について考察するとともに，侵食抑制や水質形成に対する技術的アイデアについて私見を述べた。